

GROWTH OF GROUP II-VI QUANTUM DOTS (CdTeSe) IN GLASS STUDIED
THROUGH OPTICAL ABSORPTION AND RAMAN SPECTROSCOPIES



by

Mehmet Kemalettin Torun

Submitted to Graduate School of Natural and Applied Sciences
in Partial Fulfillment of the Requirements
for the Degree of Doctor of Philosophy in
Physics

Yeditepe University

2017

GROWTH OF GROUP II-VI QUANTUM DOTS (CdTeSe) IN GLASS STUDIED
THROUGH OPTICAL ABSORPTION AND RAMAN SPECTROSCOPIES

APPROVED BY:

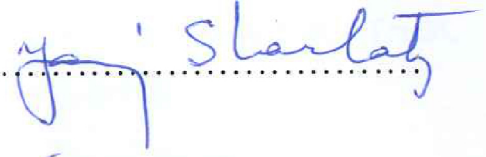
Prof. Dr. Ahmet Turan İnce
(Thesis Supervisor)


.....

Prof. Dr. Mehmet Hikmet Yükselici


.....

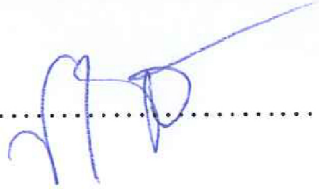
Prof. Dr. Yani Skarlatos


.....

Assoc. Prof. Dr. Şerife İpek Karaaslan


.....

Assoc. Prof. Dr. Vildan Üstoğlu Ünal


.....

DATE OF APPROVAL: / / 2017

ACKNOWLEDGEMENTS

I would like to thank my Ph.D. supervisor Prof. Dr. Ahmet T. INCE for his great patience, guidance and support without which the completion of this work would have been impossible.

Prof. Dr. M. Hikmet Yükselici, without his advice, support and all the days and nights of study, I could not manage to finish this work.

In addition to all, I would like to thank my grand jury, for the questions and advices they gave me during my thesis defence, Prof. Dr. Yani Skarlatos, Assoc. Prof. Dr. Şerife İpek Karaaslan, Assoc. Prof. Dr. Vildan Üstoğlu Ünal.

Asist Prof. Dr. Ercüment Akat, I will never forget your contributionson physics and mathematics during the Ph.D. courses we had together. Thank you.

All my family for their continued support. Natali Arakelyan Torun, Ada Mirel Torun, Sevin Torun, Behice Gül Torun, Silva Arakelyan and Harutyun Arakelyan.

My colleagues F. Melda Patan Alper, Ekrem Sınır, thank you all my friends.

This thesis is dedicated to my daughter Ada Mirel Torun

ABSTRACT

GROWTH OF GROUP II-VI QUANTUM DOTS (CdTeSe) IN GLASS STUDIED THROUGH OPTICAL ABSORPTION AND RAMAN SPECTROSCOPIES

The sample composition and physics of quantum dots embedded in matrices is of fundamental importance in the properties and tailoring of nanodevices that are increasingly being integrated into information technology, electronic, magnetic, mechanical and biological systems.

Quantum dots embedded in glass have a very long shelf life because they are inside a constrained medium. Nanoparticles in liquids are inside a free medium in which they can easily migrate and so join up with nearby nanoparticles to form larger colloids; this causes a limit on their shelf- life.

A study of the growth of group II-VI quantum dots in glass studied through optical absorption and Raman spectroscopies will be carried out.

The embedded quantum dots under investigation are Cd-Te-S, which have a variety of compositions of Te/S ratios as: $\text{CdTe}_x\text{S}_{1-x}$ where $0 < x < 1$. These compositions and percent impurities will be determined using Raman spectroscopy techniques. The modification of the sample composition with heat treatment will be investigated in order to examine the physics of particle migration and to tailor the composition.

Nanoparticles embedded in matrices with a smaller dielectric constant and a larger energy gap cause the exciton binding energy to increase much more than in normal low dimensional system. This causes enhanced optical effects that will be studied in this work.

In the study of the growth of $\text{CdTe}_{1-x}\text{Se}$ nanocrystals in zinc-containing boraxilicate glass, it has been observed that the penetration of zinc into the nanocrystalline structure, during thermal growth has been neglected in the literature, considering the work done so far.

In this thesis study, the amount of zinc in the nanocrystal structure was determined by Raman spectroscopy and optical permeability spectroscopy. It was discussed how the electronic forbidden energy bandgap and Raman symmetry change due to nanocrystalline information, how the red and blue shifts in Raman type are related to phonon encircling and stretching.

ÖZET

GROWTH OF GROUP II-VI QUANTUM DOTS (CdTeSe) IN GLASS STUDIED THROUGH OPTICAL ABSORPTION AND RAMAN SPECTROSCOPIES

Matrislere yerleştirilen kuantum noktalarının örnek kompozisyonu ve fiziği, bilgi teknolojisi, elektronik, manyetik, mekanik ve biyolojik sistemlerle gittikçe daha çok içiçe hale gelen nanodrevrelerin özelliklerinde ve yapılarında temel önem taşımaktadır.

Cam içine yerleştirilen kuantum noktaları, kısıtlı bir ortam içinde olduklarından ötürü çok uzun bir raf ömrüne sahiptirler. Sıvılardaki nanoparçacıklar, kolayca taşınabildikleri ve böylece daha büyük kolloidler oluşturdukları ve yakındaki nanoparçacıklar ile birleşebileceği serbest bir ortam içerisindedir. Bu onların kullanım ömrü üzerinde bir sınır oluşturur. Camda optik soğurma ve Raman spektroskopileri ile incelenen grup II-VI kuantum noktalarının büyümesi üzerine bir araştırma yapılacaktır.

İncelenen kuantum noktaları, Cd-Te-S olup Te/S oranlarında çeşitli kompozisyonlara sahiptir: $CdTe_xS_{1-x}$. ($0 < x < 1$) Bu bileşimler ve oransal safsızlıklar Raman spektroskopi teknikleri kullanılarak belirlenecektir. Örnek kompozisyonunun ısı ile modifikasyonu, parçacık göçünün fiziksel araştırması ve kompozisyonun uyarlanması için incelenecektir.

Daha küçük bir yalıtkanlık sabiti ve daha büyük bir enerji boşluğuna sahip matrisler içine gömülmüş nanoparçacıklar eksiton bağlanma enerjisinin normal düşük boyutlu sistemden çok daha fazla artmasına neden olur. Bu, ise gelişmiş optik etkilere neden olur. Geliştirilmiş optik etkiler bu çalışmada incelenecektir.

Çinko içeren borasilikat cam içinde $CdTe_{1-x}Se$ nanokristallerinin büyütülmesi çalışmalarında, çinkonun ısı ile büyüme sırasında nanokristal yapının içine işlemesi için literatürde bugüne kadar yapılan çalışmalar gözönüne alındığında ihmal edildiği görülmektedir. Bu tez çalışmasında Raman spektroskopisi ve optik geçirgenlik spektroskopisi ile nanokristal yapı içindeki çinko miktarı belirlenmiş olup, elektronik yasak enerji kuşak aralığının ve Raman kiplerinin nanokristalin bileşimine bağlı olarak nasıl değiştiği, Raman kiplerindeki kırmızıya ve maviye kaymaların fonon kuşatması ve gerilemeyle nasıl ilişkili olduğu tartışılmıştır.

TABLE OF CONTENTS

ACKNOWLEDGEMENTS.....	iii
ABSTRACT.....	iv
ÖZET	v
LIST OF FIGURES	viii
1. INTRODUCTION.....	1
2. THEORY	4
2.1. QUANTUM SIZE EFFECT	4
2.2. EFFECTIVE MASS MODEL.....	5
2.3. QUANTUM DOT IN A SPHERICAL BOX.....	13
2.4. GROWTH OF QUANTUM DOTS	16
2.5. ABSORPTION SPECTROSCOPY	17
2.6. URBACH DISORDER	20
2.7. RAMAN SPECTROSCOPY	21
3. MATERIALS AND METHODS	26
3.1. PREPARING SAMPLES.....	26
3.1.1. Heat Treatment Procedure, Quenching.....	30
3.2. ANALYSING SAMPLES	33
3.2.1. Raman Spectroscopy.....	33
3.2.2. Absorption Spectroscopy.....	34
4. RESULTS AND DISCUSSION.....	36
4.1. RESULTS	36
4.1.1. Numerical Solutions for Finite Well Using Matlab Programme	36
4.1.2. Raman Spectroscopy Results.....	38
4.1.3. Absorption Spectroscopy Results	53
4.2. DISCUSSION	69
4.2.1. Phonon Confinement	69
4.2.2. Raman Scattering.....	71
5. CONCLUSION	75

REFERENCES77

APPENDIX A..... 84

APPENDIX B.....90

APPENDIX C..... 92

APPENDIX D.....93

APPENDIX E.....94

APPENDIX F.....95

APPENDIX G.....96

APPENDIX H.....98

APPENDIX I.....99



LIST OF FIGURES

Figure 2.1. Bohr radius	4
Figure 2.2. Density of electron states as a function of dimension.	7
Figure 2.3. Bandgap difference between nanomaterial and bulk material.	7
Figure 2.4. Finite square well, width a , depth V	8
Figure 2.5. Wave functions for Infinite and Finite potential wells repectively.	13
Figure 2.6. Optical absorption spectra for as received colour glass filter doped with CdTe (1), melted (2) and heat treated (3). Oriel Model 70310 serial no 176 monochromator is used to obtain absorption spectroscopy data.	18
Figure 2.7. A denotes Absorbance, I_0 is the reference value of the media, I is the transmitted value after the sample in the equation above.	19
Figure 3.1. RG 830 Plate.	26
Figure 3.2. Wooden rail for cutting the width of the sample glass.	27
Figure 3.3. Close view of wooden rail and the glass sample fitted inside.	27
Figure 3.4. Buehler wafering blade used to cut the sample.	27
Figure 3.5. Buehler Diamond Disc.	28
Figure 3.6. Glass cutting system.	28
Figure 3.7. Close view of glass cutting system.	29
Figure 3.8. After slicing the plate glass RG830.	29
Figure 3.9. Prepared sample in furnace	31
Figure 3.10. Calibration notes for thermocouple	31
Figure 3.11. Calibration notes.	32
Figure 4.1. Energy levels for a particle in a potential well. Energy plotted against a (nm) for $V = 0.5$ (eV)	37
Figure 4.2. CdTe QD's as received sample excited at 30 mW with an average 10 measurements.	39
Figure 4.3. CdTe QD's as received sample excited at 30 mW with an average 20 measurements.	39
Figure 4.4. CdTe QD's as received sample excited at 150 mW with an average 10 measurements.	40

Figure 4.5. CdTe QD's as received sample excited at 150 mW with an average 20 measurements.....	41
Figure 4.6. CdTe QD's melted sample excited at 30 mW with an average 10 measurements.	41
Figure 4.7. CdTe QD's melted sample excited at 30 mW with an average 20 measurements.	42
Figure 4.8. CdTe QD's melted sample excited at 150 mW with an average 10 measurements.	42
Figure 4.9. CdTe QD's melted sample excited at 150 mW with an average of 20 measurements.....	43
Figure 4.10. CdTe QD's heat treated sample excited at 30 mW with an average of 10 measurements.....	44
Figure 4.11. CdTe QD's heat treated sample excited at 30 mW with an average of 20 measurements.....	44
Figure 4.12. CdTe QD's heat treated sample excited at 150 mW with an average of 10 measurements.....	45
Figure 4.13. CdTe QD's heat treated sample excited at 150 mW with an average 20 of measurements.....	45
Figure 4.14. CdTe QD's heat treated sample at 600 °C for two hours, excited at 150 mW..	46
Figure 4.15. CdTe QD's heat treated sample at 600 °C for 10 hours, excited at 150 mW ...	48
Figure 4.16. $(OD \times hv)^2$ plotted versus photon energy hv to find bandgap energy.	54
Figure 4.17. Optical absorption using Tauc plot for heat treated sample.	57
Figure 4.18. Urbach energy for heat treated sample.	58
Figure 4.19. Optical absorption by using Tauc plot for melted sample.....	58
Figure 4.20. Urbach energy for melted sample	59
Figure 4.21. Optical Absorption heat treated at 600 °C for 6 hours, thickness of 0.46 mm.	60
Figure 4.22. Optical absorption using Tauc plot heat treated for 6 hours at 600 °C.	60
Figure 4.23. Urbach energy heat treated at 600 °C for 6 hours.....	61
Figure 4.24. Optical absorption heat treated at 600 °C for 8 hours, thickness of 0.62mm. .	61
Figure 4.25. Optical absorption using Tauc plot heat treated at 600 °C for 8 hours, thickness of 0.62mm.....	62
Figure 4.26. Urbach energy heat treated at 600 °C for 8 hours.....	62

Figure 4.27. Optical absorption heat treated at 600 °C for 10 hours, thickness of 0.34 mm.
.....63

Figure 4.28. Optical absorption using Tauc plot for heat treated at 600 °C for 10 hours. ...63

Figure 4.29. Urbach energy heat treated at 600 °C for 10 hours.....64

Figure 4.30. Optical absorption heat treated at 600 °C for 12 hours thickness of 0.67mm..64

Figure 4.31. Optical absorption using Tauc plot heat treated at 600 °C for 12 hours.....65



LIST OF TABLES

Table 2.1. Quantum confined structure vs Bulk structure	6
Table 2.2. Fundamental vibrational frequencies.....	23
Table 4.1. Calculations of energy levels for a particle in a potential well. Energy listed against a (nm).....	37
Table 4.2. CdTe Quantum Dots excited by Argon laser at 514.5 nm with a power of 30 mW average of 10 measurements.....	50
Table 4.3. CdTe Quantum Dots excited by Argon laser at 514.5 nm with a power of 30 mW average of 20 measurements.....	50
Table 4.4. CdTe Quantum Dots excited by Argon laser at 514.5 nm with a power of 150 mW average of 10 measurements.....	51
Table 4.5. CdTe Quantum Dots excited by Argon laser at 514.5 nm with a power of 150 mW average 20 measurement.....	51
Table 4.6. CdTe Quantum Dots excited by Argon laser at 514.5 nm with a power of 150 mW average of 20 measurements.....	51
Table 4.7. Fundamental modes in Raman spectra	73
Table 5.1. Optical transmission measurements	75

LIST OF SYMBOLS/ABBREVIATIONS

A	Absorbance
a^*	Critical radius
au	Arbitrary unit
E	Energy
E_g	Bandgap
E_u	Urbach Energy
eV	Electron volt
h	Planck's constant
IR	Infrared
I_0	Reference value
L	Angular momentum
L	Thickness of the sample
LO	Longitudinal optical phonon frequency
LO_i^B	Longitudinal optical phonon frequency bulk
m^*	Effective mass
OD	Optical Density
P_i	Raman modes
R	Average radius of quantum dot
RG	Red and black glasses, infrared transmitting
V	Volume
V	Potential
0D	Zero Dimension
1D	One Dimensional
2D	Two Dimensional
3D	Three Dimensional
γ	Grüneisen parameter
ϵ	Dielectric constant
λ	Wavelength

ν	Frequency
Φ	Dimension
ψ	Wave function
ΔG_c	Free energy
ΔG_a	Activation energy
$\Delta\omega$	Strain on glass host
$\Delta\omega^c$	Phonon confinement



1. INTRODUCTION

The sample composition and physics of quantum dots embedded in solids is of fundamental importance in the properties and tailoring of nanodevices that are increasingly being integrated into information technology, electronic, magnetic, mechanical and biological systems [1-5]. Conceptual foundations of nano technology began with the famous speech of Richard Feynman “ There is a plenty of room at the bottom” in 1959. His speech is about control and manipulation of atoms. 15 years after his speech, in 1974 Norio Taniguchi defined the term nanotechnology in his paper ion-sputter machining[6]. In 1977 Dr. K. Eric Drexler originated molecular nanotechnology concepts at MIT and in 1986 his book ‘Engines of Creation: The coming era of nanotechnology’ published [7]. Drexler discussed about possibilities, dangers and hopes about nanotechnology in the future. The first quantum dots were discovered by Alexei Ekimov in a glass matrix and the solutions by Louis E. Brus. From then on quantum dots are investigated for semi conductors in different media. First carbon nanotubes were discovered by S. Iijima in 1991 [8]. A few years later than 1999 first Nano Medicine book was published by Robert A. Freitas Jr. [9]. Using quantum dots in biological systems is quiet dangerous for now. Unfortunately, most of the quantum dots are toxic, shelf life for CdTe quantum dots are very important for different applications, the most common nanoparticles used in medication is cadmium teluride because its quantum confinement regime covers the entire optical spectrum [10]. Cadmium ions were the main reason for cytotoxicity, because they are able to bind to thiol groups on critical molecules in the mitochondria and cause enough stress and damage to cause significant cell death [11,12]. Nanoparticles in liquids are inside a free medium in which they can easily migrate and so join up with nearby nanoparticles to form larger colloids; this causes a limit on their shelf-life. Using nanoparticles for semiconductors long shelf life is required for stability. The importance of the solid matrix comes from the quantum dots embedded in glass having a very long shelf-life because they are inside a constrained medium. When the size of bulk semiconductor is reduced to nanometer scales, the crystal gains new optical and electronic properties. Energy levels are quantized as in atoms and the energy difference between successive levels widens with the inverse of the size squared [13-21]. As mentioned in the definition, semiconductors have an energy bandgap due to the interaction of electrons and holes. These bands are called “conduction” and “valence bands”. The energy bandgap is

located between conduction and valence bands. It is also called the forbidden band. The size of the energy gap determines whether the medium is an insulator, a conductor or a semiconductor. In this study, Schott optical filter glass RG 830 (Red and Black glasses, IR transmitting) is used. It is a well known commercial optical filter containing CdTe. To obtain CdTe nanocrystals, heat treatment procedure is applied to RG 830 optical filter. Outlines of the heat treatment procedure is RG 830 optical filter sliced to dimensions of 10mmx10mmx10mm. These samples were melted at 1100°C for 15 min and quenched rapidly to room temperature by using an air blower, then treated at 400°C for two hours to avoid internal stress, protect and prepare the sample for the final thickness and long term heat treatment. The samples were then treated at 600°C for 6 hours, 8 hours, 10 hours, 12 hours and 24 hours to grow different sizes of CdTe nanocrystals [22]. This procedure will be explained in detail in the experimental methods section which also includes metrology science. Prepared CdTe nanocrystal in zinc-containing glass matrix is investigated by Raman spectroscopy and absorption spectroscopy for understanding the characterization of the CdTe quantum dots. Spectroscopy is a branch of science which investigates light. When the light hits any kind of matter, there will be an interaction between the light and matter. Light can be reflected, absorbed, scattered or transmitted through the matter during this situation. The wavelength of the light and the type of the material affects this interaction and this is the main purpose of spectroscopy measurements. In Raman spectroscopy scattered light is examined in detail. Scattering is a form of reflection, but due to the irregularities of the surface, the light that hits the surface is reflected as scattered. The scattered light gives information about the materials on the surface of the medium. Raman spectroscopy is used to define CdTe nanocrystal using Green Argon laser of 514.5 nm wavelength as excitation source. Secondly, absorption spectroscopy is used. Visible light lies in the wavelength range 380-700 nm, a halogen lamp which covers all the visible wavelength range is used as a visible light source. Prepared samples are located between the light source and monochromator respectively. When the light is absorbed by the media, valence electrons are excited from their ground states to higher energy levels. The Gaussian peak in each absorption spectrum results from the lowest electron hole pair transitions in CdTe nanocrystals embedded in zinc-containing glass matrix. By plotting the Absorption Coefficient vs Energy graph, bandgap energy can be found. The radii of quantum dots are examined with two different methods. The first method is the effective mass model in strong confinement limit [23] and the second method is numerical solutions to Schrödinger's

equation. To use the effective mass model first of all the band structure must be well reviewed. As a result of this study the defect levels below bandgap are discussed by Urbach tail method [24,25]. Briefly Urbach tail is related with amorphous materials and related to localized states at the band edges.



2. THEORY

2.1. QUANTUM SIZE EFFECT

When the physical dimensions decrease to the nanometer scale, the quantum size effect becomes significant. A quantum dot is a semiconductor whose excitons are confined in three dimensions [26]. An exciton is a bound electron-hole pair which are attracted to each other by Coulomb force. In a bulk semiconductor, an electron-hole pair is bound within a Bohr exciton radius. If the electrons and holes are squeezed below Bohr radius then the semiconductor's properties will change. For further information starting from Bohr model of hydrogen atom is described with a scheme below.

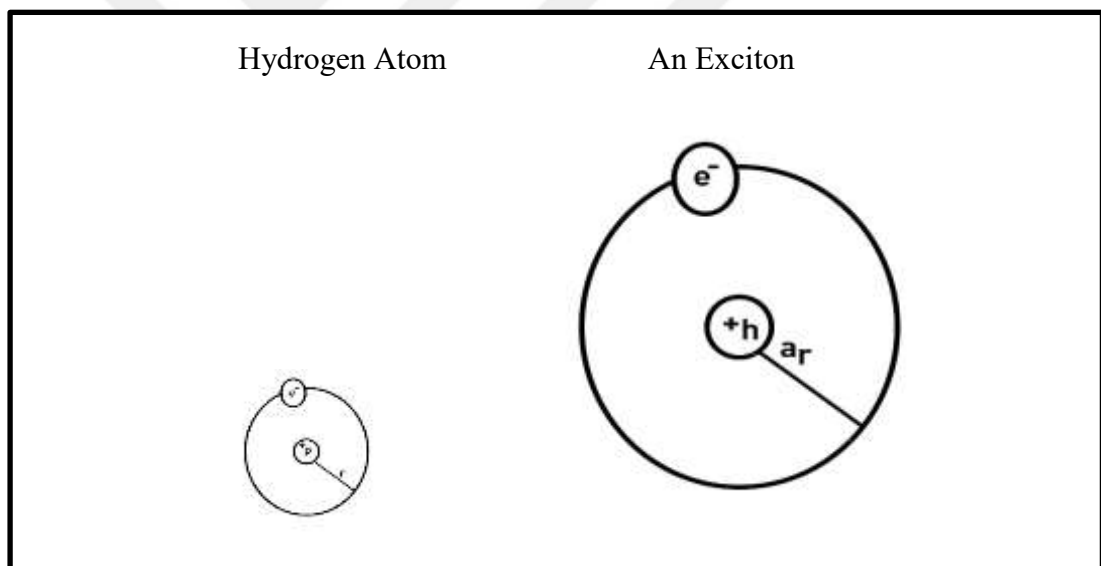


Figure 2.1. Bohr radius

In Bohr model angular momentum L ,

$$L = mvr_n = n \frac{h}{2\pi} \quad n = 1, 2, 3, \dots, \quad (2.1)$$

Bohr radius

$$a_r = \frac{n^2 h^2 \epsilon_0}{\pi m Z e^2} = \frac{n^2}{Z} r_1 \quad (2.2)$$

$$r_1 = 0.529 \times 10^{-10} m \quad (2.3)$$

Bohr radius is the sum of electron Bohr radius (a_e) and hole Bohr radius (a_h)

$$a_r = a_e + a_h \quad (2.4)$$

$$a_e = \frac{\varepsilon \hbar^2}{m_e e^2}, a_h = \frac{\varepsilon \hbar^2}{m_h e^2} \quad (2.5)$$

R is the average radius of quantum dots, if $R \gg a_r$ we call it weak confinement, if $R \ll a_r$ we call it strong confinement. For CdTe a_r is about 7.5 nm. The most important part of the theory is the behaviour of the exciton. Exciton behaves like an atom, a good approximation is the three dimensional model of a particle in a spherical box [27]. To understand the three dimensional model of a particle in a box, first of all effective mass model, Bohr radius and one dimensional particle in a box must be studied.

2.2. EFFECTIVE MASS MODEL

The effective mass model is used to calculate the electronic structure of the quantum dots. The conduction and valence bands for bulk medium are approximated by simple isotropic bands. Using effective mass approximation and from Bloch's theorem the wavefunction can be written as,

$$\Psi_{nk} = U_{nk}(\vec{r})e^{(i\vec{k}\cdot\vec{r})} \quad (2.6)$$

where, U_{nk} is a function of the periodicity of the crystal lattice, the band index n and the wavevector is k . In the effective mass model the conduction band energy and the valence band energy are approximated as,

$$E_k^c = \frac{\hbar^2 k^2}{2m_{ef}^c} + E_g \quad (2.7)$$

$$E_k^v = -\frac{\hbar^2 k^2}{2m_{ef}^v} \quad (2.8)$$

The electrons and holes act like free particles which have an effective masses that incorporate the periodic potential felt by the carriers. Bloch's theorem states that the eigenfunctions for a system may be written as the product of a plane wave envelope function and a periodic function $U_{nk}(\vec{r})$ that has the same periodicity as the potential [28]. The electron effective mass depends on the wavevector \vec{k} and envelope wave function Ψ_n . Below in Figure 2.3, the difference between the nanomaterial and its bulk state of energy level and band gap is shown. Bohr radius of a particle is defined as [29]

$$a_b = \varepsilon \frac{m}{m^*} a_0 \quad (2.9)$$

where ε is the dielectric constant of the medium, m^* is the effective mass of the particle, m is the mass at rest of the free electron and Bohr radius of the hydrogen atom is a_0 . Excitonic transition energy and blue shift in the absorption are caused by the quantum confinement effect. This takes place when the particle size gets close to Bohr exciton radius. Quantum confinement effect also causes a change of continuous energy bands of a bulk medium to discrete energy levels. Discrete structure of energy levels gives discrete absorption spectrum.

Table 2.1. Quantum confined structure vs Bulk structure

Structure	Quantum Confinement	Number of free dimensions
Bulk	0	3
Quantum dot / Nanocrystals	3	0

As greater numbers of dimension are confined, the energy levels can be found more discrete. Strong confinement depends on the dimension, Figure 2.2 shows below the density of states in bulk, 2D, 1D and 0D semiconductor structure.

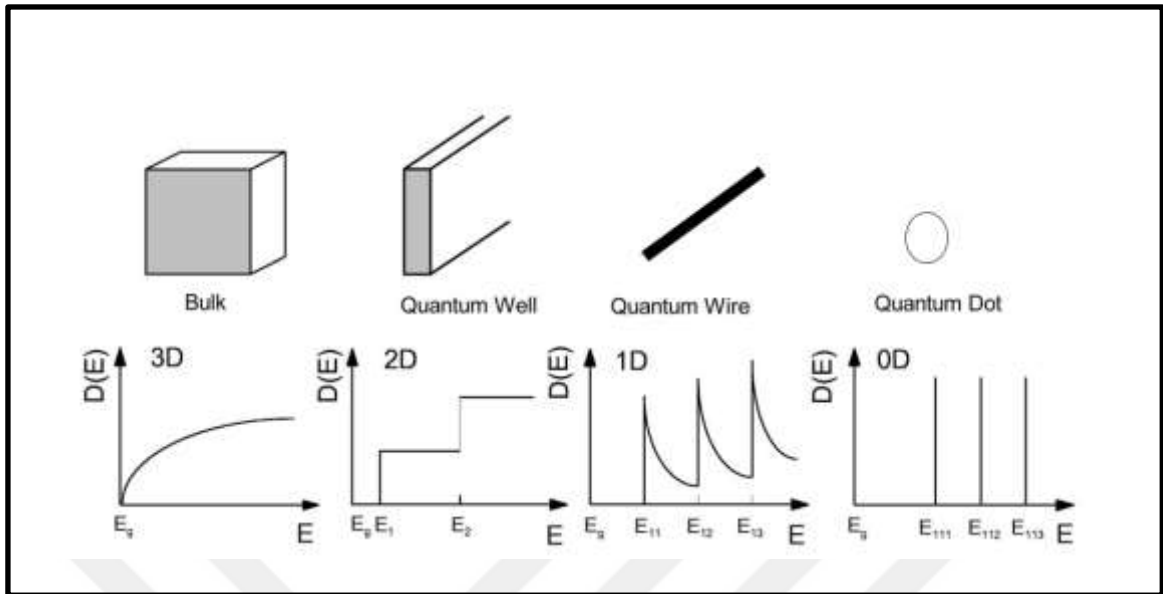


Figure 2.2. Density of electron states as a function of dimension.

The optical absorption spectrum is proportional to the density of states.

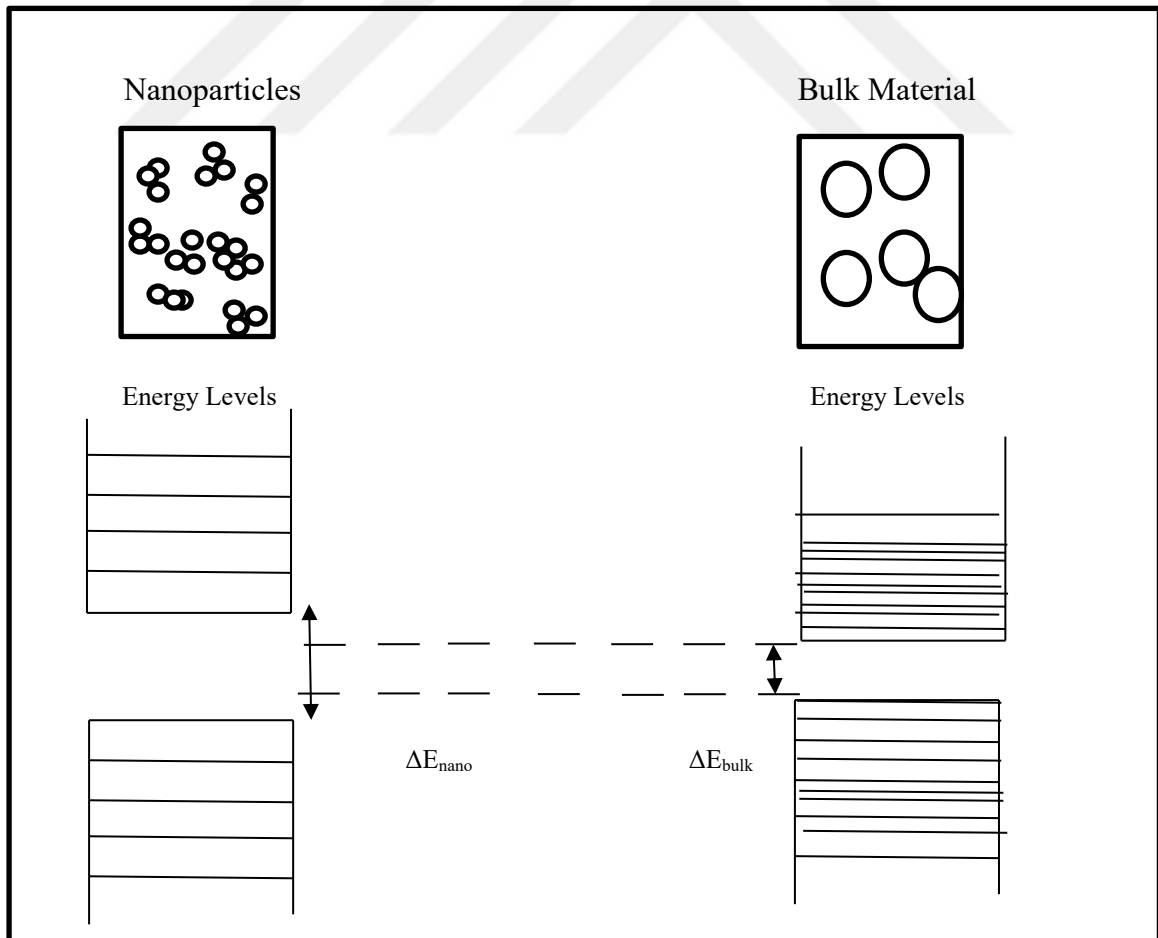


Figure 2.3. Bandgap difference between nanomaterial and bulk material.

CdTe quantum dots in glass are a kind of zero dimensional objects, various names are given for this type of systems such as quantum dots, nano crystals, quantum boxes etc. Assume a quantum box with infinite side lengths L_x, L_y, L_z . The wave function will be

$$\Phi_{lmn} = \phi_l(x)\phi_m(y)\phi_n(z) \quad (2.10)$$

Solution will be in the form of standing waves

$$\Phi_L(x) = \sqrt{\frac{2}{L_x}} \sin(k_x x) \quad (2.11)$$

The energy will be

$$E_T = E_g + E_{xl} + E_{ym} + E_{zn} \quad (2.12)$$

$$E_{xl} = \frac{\hbar^2 k_x^2}{2m} = \frac{\hbar^2}{2m} \left(\frac{\pi}{L_x}\right)^2 l^2 \quad (2.13)$$

A more realistic solution for our study Schrödinger Equation can be solved for a finite quantum well.

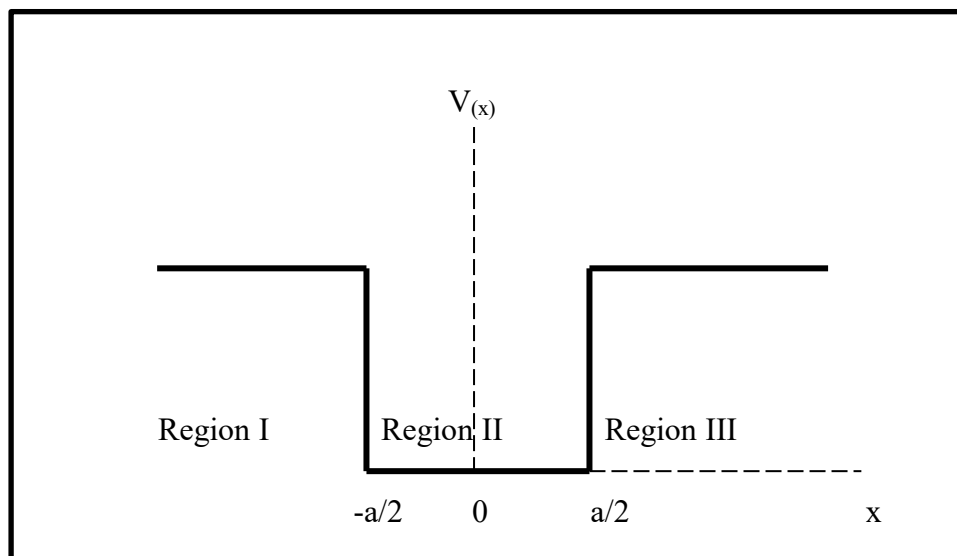


Figure 2.4. Finite square well, width a , depth V .

Region I

$$x \leq -a, V(x) = V_0 \quad (2.14)$$

Substituting this equation into time-independent Schrödinger equation, the equation below can be found, by solving Schrödinger Equation for infinite potential well, confined energy levels of nano structures can be predicted.

$$-\frac{\hbar^2}{2m} \frac{d^2\Psi}{dx^2} + V_0\Psi = E\Psi \quad (2.15)$$

$$\frac{d^2\Psi}{dx^2} = \frac{2m}{\hbar^2} (V_0 - E)\Psi \quad (2.16)$$

$$\frac{d^2\Psi}{dx^2} = \mathcal{K}^2\Psi \quad (2.17)$$

$$\mathcal{K}^2 = \frac{2m}{\hbar^2} (V_0 - E) > 0 \quad (2.18)$$

$$\mathcal{K} = \sqrt{\frac{2m}{\hbar^2} (V_0 - E)} , \quad (2.19)$$

This is real

Solution for this differential equation

$$\Psi = Be^{\mathcal{K}x} + De^{-\mathcal{K}x} , \text{ since } \Psi \rightarrow 0 \text{ and } x \rightarrow -\infty, \quad D = 0 \quad (2.20)$$

$\Psi = Be^{\mathcal{K}x}$ can be found for region I

A similar solution can be used for Region III

$$x \geq a, V(x) = V_0 \quad (2.21)$$

$$\Psi = Ae^{-\kappa x} + D'e^{\kappa x}, \text{ since } \psi \rightarrow 0 \text{ and } x \rightarrow +\infty, \quad D' = 0 \quad (2.22)$$

$$\Psi_{III} = Ae^{-\kappa x} \quad (2.23)$$

For region III

$$-a \leq x \leq a, \quad V = 0 \quad (2.24)$$

Substituting this equation into time-independent Schrödinger equation, the equation below can be found.

$$-\frac{\hbar^2}{2m} \frac{d^2\psi_{II}}{dx^2} + 0 = E \quad (2.25)$$

$$\frac{d^2\Psi_{II}}{dx^2} = -\frac{2m}{\hbar^2} E\Psi \quad (2.26)$$

$$\frac{d^2\psi}{dx^2} = -k^2\psi_{II} \quad k^2 = \frac{2mE}{\hbar^2} > 0, \quad \Rightarrow k = \sqrt{\frac{2m}{\hbar^2} E} \quad (2.27)$$

Since the potential well is symmetric, we have three solutions, one even, two other odd solutions.

$$\psi_{II} = C \cos(kx) \text{ for even parity}$$

$$\psi_{II} = D \sin(kx) \text{ for odd parity}$$

At $a/2$, for even parity

$$C \cos\left(k \frac{a}{2}\right) = Ae^{-\kappa \frac{a}{2}} \quad (2.28)$$

$$-Ck \sin\left(\kappa \frac{a}{2}\right) = -A\kappa e^{-\kappa \frac{a}{2}} \quad (2.29)$$

Dividing equation (2.25) by equation (2.26)

$$\frac{\kappa}{k} = \tan\left(\frac{ka}{2}\right) \quad (2.30)$$

For negative parity solutions

$$\frac{\kappa}{k} = -\cot\left(\frac{ka}{2}\right) \quad (2.31)$$

$$\frac{\kappa}{k} = \tan\left(\frac{ka}{2} + \frac{\pi}{2}\right) \quad (2.32)$$

$$\text{since } \kappa = \sqrt{\frac{2m}{\hbar^2}(V_0 - E)} \text{ and } k = \sqrt{\frac{2m}{\hbar^2}E} \quad (2.33)$$

In both equations above (2.27) and (2.28-2.29), the energy E , is the only unknown component. These two equations are transcendental equations, which means that they cannot be solved analytically then we have to solve them numerically. For numerical solutions these equations can be written as dimensionless form, Z and Z_0

$$Z = \frac{ka}{2} = \frac{a}{2} \sqrt{\frac{2m}{\hbar^2}E} \quad (2.34)$$

$$Z_0 = \frac{a}{2} \sqrt{\frac{2m}{\hbar^2} V_0} \quad (2.35)$$

Z_0 contains the depth of the potential well as V_0 and a as its width. Z contains energy E for solving.

$$\kappa = \sqrt{\frac{2m}{\hbar^2} (V_0 - E)} \text{ and } k = \sqrt{\frac{2m}{\hbar^2} E} \quad (2.36)$$

$$\kappa^2 = \frac{2m}{\hbar^2} (V_0 - E) = \frac{2m}{\hbar^2} V_0 - k^2 \quad (2.37)$$

$$\kappa^2 = k^2 \left\{ Z_0^2 \left(\frac{2}{a} \right)^2 \frac{1}{k^2} - 1 \right\} \quad (2.38)$$

$$\frac{\kappa^2}{k^2} \left\{ \frac{Z_0^2}{Z^2} - 1 \right\} \quad (2.39)$$

$$Z = \frac{ka}{2} = \frac{a}{2} \sqrt{\frac{2m}{\hbar^2} E} \quad (2.40)$$

Solving Z , we will find energy eigenvalues E_n for our finite well

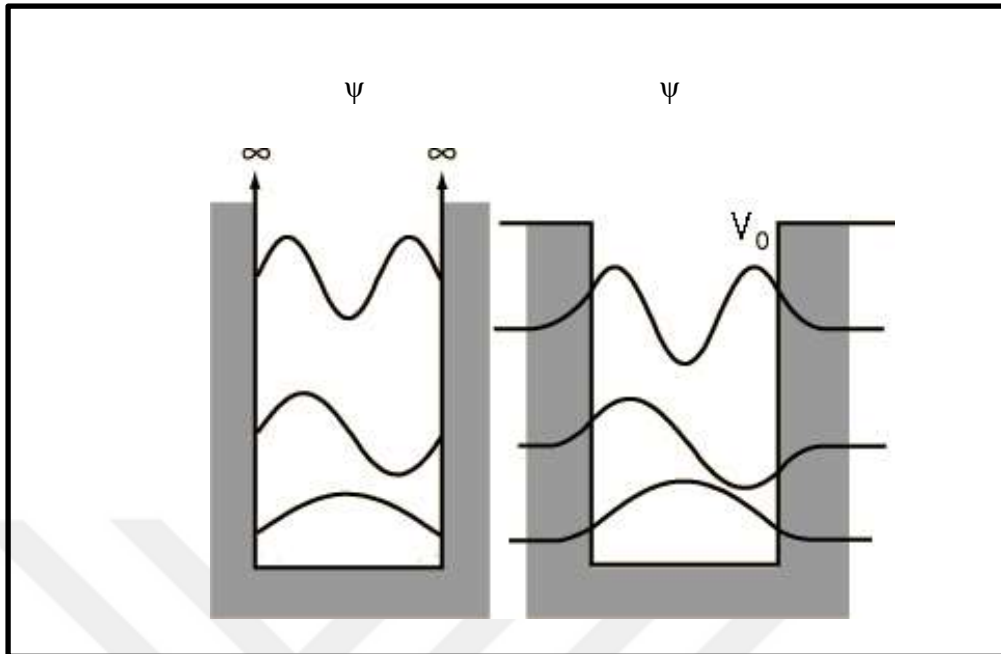


Figure 2.5. Wave functions for Infinite and Finite potential wells respectively.

2.3. QUANTUM DOT IN A SPHERICAL BOX

There are different descriptions of confinement regimes for quantum dots. Particle in a sphere model is a simple model to start understanding size-dependent properties of CdTe, quantum dots grown in borasilicate glass. The electron confined in a QD assumed spherical in shape with radius a , and the confining potential is infinitely deep potential [30].

$$\begin{aligned} V &= 0 & r &\leq a, \\ V &= \infty & r &> a. \end{aligned} \quad (2.42)$$

The Hamiltonian can be written below, for spherical coordinates

$$H = -\frac{\hbar^2}{2m^*} \left[\frac{1}{r^2} \frac{\partial}{\partial r} \left(r^2 \frac{\partial}{\partial r} \right) + \frac{1}{r^2 \sin \theta} \frac{\partial}{\partial \theta} \left(\sin \theta \frac{\partial}{\partial \theta} \right) + \frac{1}{r^2 \sin^2 \theta} \frac{\partial^2}{\partial \phi^2} \right], \quad (2.43)$$

By using the separation of variables method, one electron envelope wave function will be written by using

$$\psi(r, \theta, \phi) = R(r)Y(\theta, \phi) \quad (2.44)$$

Equation (2.39) can be rewritten by using time independent Schrödinger Equation

$$H\psi(r, \theta, \phi) = E\psi(r, \theta, \phi) \quad (2.45)$$

and we get

$$\frac{1}{R} \frac{d}{dr} \left(r^2 \frac{dR}{dr} \right) + \frac{2m^*}{\hbar^2} r^2 E = l(l+1) \quad (2.46)$$

$$\sin \theta \frac{\partial}{\partial \theta} \left(\sin \theta \frac{\partial Y}{\partial \theta} \right) + \frac{\partial^2 Y}{\partial \phi^2} = -l(l+1)Y \sin^2 \theta \quad (2.47)$$

$$Y(\theta, \phi) = \Theta(\theta)\Phi(\phi) \quad (2.48)$$

θ and ϕ dependent terms can be separated

$$\frac{1}{\Phi} \frac{d^2 \Phi}{d\phi^2} = -m^2 \quad (2.49)$$

The equation (2.49) is the harmonic oscillator equation [31].

$$\frac{1}{\sin\theta} \sin\theta \frac{d}{d\theta} \left(\sin\theta \frac{d\Theta}{d\theta} \right) + l(l+1) \sin^2\theta = m^2 \quad (2.50)$$

The solution to equation (2.51) is

$$\Phi_m(\phi) = C e^{im\phi} \quad (2.51)$$

where C is an arbitrary constant and $m = 0, \pm 1, \pm 2, \pm 3, \dots$. The condition is given in equation (2.52),

$$\Phi(\phi + 2\pi) = \Phi(\phi) \quad (2.52)$$

the solutions to the equations (2.47) and (2.50) [32-34] are

$$R(r) = A J_l(\lambda r) \quad (2.53)$$

$$\Theta(\theta) = B P_l^m(\cos\theta) \quad (2.54)$$

where $J_l(\lambda r)$ is the Spherical Bessel's Function in the order of l , $\lambda = \sqrt{\frac{2m^*}{\hbar^2} E}$ and $P_l^m(\cos\theta)$, is Legendre Function.

$$R_l(a) = A j_l(\lambda a) = 0 \quad (2.55)$$

$$\lambda = x_{n,l}/a \quad (2.56)$$

The wave function $R(r)$ can be written as

$$R_l(r) = A_l J_l \left(\frac{x_{n,l}}{a} r \right) \quad (2.57)$$

2.4. GROWTH OF QUANTUM DOTS

CdTe quantum dots in borosilicate glass were grown by heat treatment process. Size dispersion, average radius of quantum dots and the number of quantum dots per unit volume are major quantities to be controlled in the development of quantum dot based devices. Quantum dots in glass first nucleate during quenching the glass melt and then by diffusion of ions through the borosilicate glass they start to grow at heat treatment temperature. When the reactants (Cd, Te, Se, or Zn) have been consumed the small quantum dots disappear and redeposit on larger quantum dots, this situation is known as Oswald ripening. These are the three distinct precipitation stages: Nucleation, normal growth and oswald ripening [35]. At the first stage, the formation of the new phase depends on the thermal change of the medium, which brings the atoms to new positions compared to the untreated medium. This process is known as nucleation. The critical radius a^* of the nuclei is given by

$$a^* = \frac{2\sigma}{\Delta G_v} \quad (2.58)$$

The formation of nanocrystals, rate of nucleation R is given by

$$R = A \exp \left[- \left(\frac{\Delta G_c + \Delta G_a}{k_B T} \right) \right] \quad (2.59)$$

where $\Delta G_c = 16\pi\sigma^3/3\Delta G_v^2$ is the free energy to form a critical nucleus, ΔG_a is the activation energy for the atoms to jump across the nucleus matrix interface, ΔG_v is the free energy of bulk per unit volume, σ is the interface free energy per unit area. The distribution of the nuclei radius is given by $P(a)$.

$$P(a) = P_0 \exp\left(-\frac{4\pi\sigma(a - a^*)^2}{3K_B T}\right) \quad (2.60)$$

The supersaturation value controls the number of nuclei and the critical radius. The higher the supersaturation value, the smaller the critical radius and the smaller clusters can grow. From here, the standard deviation Δa of the nuclei radius of average size $a_{av} = a^*$ can be written as

$$\Delta a = \left(\frac{3K_B T}{8\pi\sigma}\right)^{1/2} \quad (2.61)$$

During nucleation process, the average radius size and size distribution depend only on σ and T .

2.5. ABSORPTION SPECTROSCOPY

Properties of borosilicate glass doped with CdTe nanoparticles properties are found to be strongly size dependent [27]. It is known that nanoscale systems have different properties than bulk systems. In this study the absorption spectroscopy is first used to find the bandgap of CdTe nanoparticles, then by using bandgap energy, the radii of the CdTe quantum dots doped in the borosilicate glass are estimated. Below Figure 2.6 sample of absorption spectroscopy graph comparing as received sample, melted sample and heat treated sample [36].

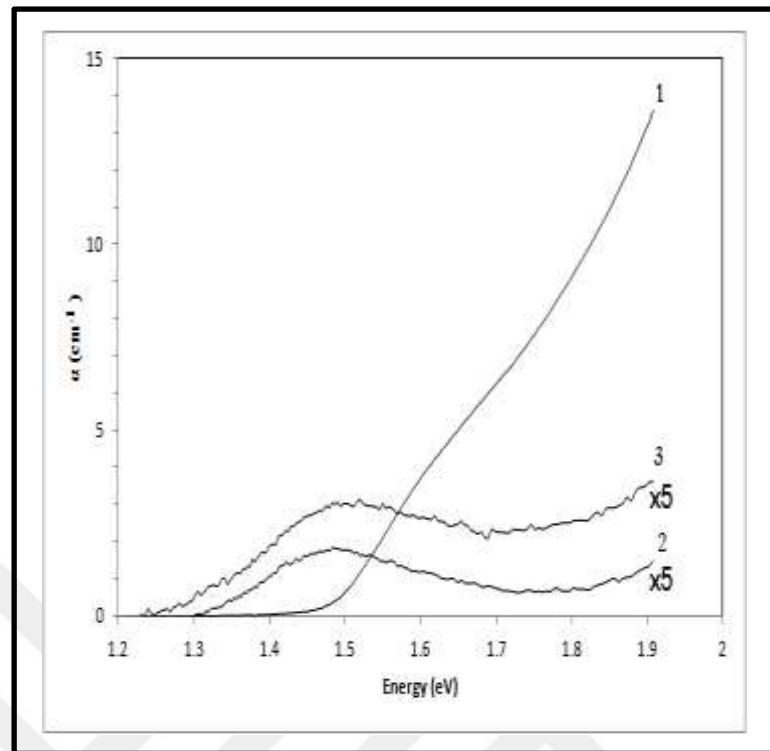


Figure 2.6. Optical absorption spectra for as received colour glass filter doped with CdTe (1), melted (2) and heat treated (3). Oriel Model 70310 serial no 176 monochromator is used to obtain absorption spectroscopy data.

Theoretical basis of estimating radii of the quantum dots depends on some mathematical and physical calculations and properties. Absorption spectroscopy is an analytical technique based on measuring the amount of light absorption of radiation passing through the sample. During this passage molecules can be excited by absorption of light. Molecular excitation energy is usually transferred to kinetic energy as heat by the collisions of the excited molecule with another molecule. The intensity of light transmitted is less than the intensity of the incident light. To calculate the absorbance and optical density the following equation named as Lambert-Beer is used below.

$$A = \log \left(\frac{I_0}{I} \right) \quad (2.62)$$

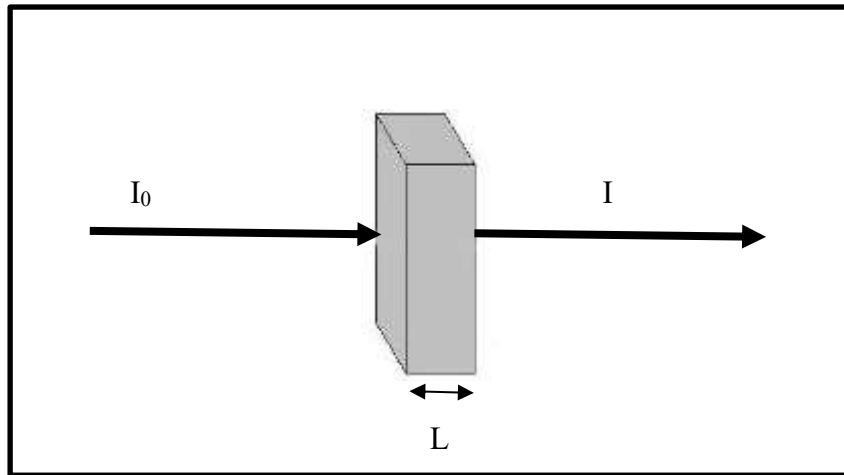


Figure 2.7. A denotes Absorbance, I_0 is the reference value of the media, I is the transmitted value after the sample in the equation above.

$$OD = \frac{A}{L} \quad (2.63)$$

where, OD means Optical Density, which describes the amount of attenuation, A absorbance, L thickness of the sample. In this equation L is measured by cm, A is measured by wavelength nm, OD is dimensionless. To find bandgap energies Tauc relation is used [37]. The absorption coefficient α for a medium can be written as equation (2.64)

$$\alpha = A(h\nu - E_g)^n \quad (2.64)$$

Where, E_g is the bandgap, A is constant and different for different transitions, $h\nu$ is the energy of the photon in (eV) and n is the nature of the sample transition. The “ n ” in the equation (2.64) has values 1/2, 2, 2/3, and 3 for allowed direct, allowed indirect, forbidden direct, forbidden indirect transitions respectively [38-40]. The E_g of the quantum dots can be calculated by extrapolating a straight line to the $(\alpha h\nu)^2$ versus $(h\nu)$ plot [41]. The intercept point on the energy axis optical band gaps can be determined. Equation (2.64) can be simplified as equation (2.65).

$$(\alpha h\nu)^2 = h\nu - E_g \quad (2.65)$$

$(\alpha \times hv)^2$ vs hv curves are plotted below, the straight lines on the graph show the bandgap energies.

$$hv = h \frac{c}{\lambda} = \frac{1240}{\lambda} \quad (2.66)$$

Equation (2.66) can be translated into

$$\left(\alpha \frac{1240}{\lambda} \right)^2 = \frac{1240}{\lambda} - E_g \quad (2.67)$$

A is the absorption value that could be detected by spectrometer, λ is the detected wavelength. In results section figure 4.16 extrapolating a straight line to $(\alpha hv)^2$ versus (hv) plot for given samples are shown. Each colour indicates a different sample with different sample thickness and annealing time. According to the results of bandgaps for the different samples, the particle sizes of quantum dots can be found by using effective mass approximation equation.

$$\Delta E_g = \frac{\hbar^2 \pi^2}{2R^2} \left(\frac{1}{m_e^*} + \frac{1}{m_h^*} \right) - \frac{1.786e^2}{4\pi\epsilon R} \quad (2.68)$$

2.6. URBACH DISORDER

The Urbach edge is measured by absorption spectroscopy and analysed for different types of media, mostly for crystallines and amorphous solids. The main purpose of the Urbach method is the temperature dependence, of the amorphous or crystalline solids which show disorder during the formation process. Urbach rule gives some important information about dynamic properties of first excitons [42]. The width of the optical absorption tail at long wavelengths depends on the spread of electron energy levels within the structure, called the Urbach energy [43]. The Urbach energy (E_u) is proportional to the reciprocal of the slope of the straight portion of $\ln\alpha$ against energy (E) curve according to the equation below where E_g is the bulk bandgap energy of CdTe

$$\alpha = \alpha_0 e^{\left(\frac{h\nu}{E_u}\right)} \quad (2.69)$$

$$\ln\alpha = \ln\alpha_0 + \frac{h\nu}{E_u} \quad (2.70)$$

Urbach Energy depends on the disorder [44].

$$E_u = \frac{E_p}{2\sigma_0} \left[X + \coth\left(\frac{E_p}{2k_B T}\right) \right] \quad (2.71)$$

$$X = \frac{\langle U_x^2 \rangle}{\langle U^2 \rangle_0} \quad (2.72)$$

where X is a measure of disorder and temperature. $\langle U_x^2 \rangle$, is the mean square deviation of atomic positions caused by actual structural disorder, and $\langle U^2 \rangle_0$, is the zero-point uncertainty in the atomic positions.

2.7. RAMAN SPECTROSCOPY

Raman Spectroscopy [45-46] is based on the Raman Effect, which is the inelastic scattering of photons by molecules. In a typical Laser Raman Spectroscopy, light from a laser in the UV-Vis-IR [47] range of a known wavelength and polarization is allowed to be scattered from a Raman active sample. The scattered light is then analyzed for frequency and polarization. If the emitted photon has the same wavelength as the scattered photon; the phenomenon is known as ‘‘Rayleigh scattering’’. A small fraction of the incident photons undergoes an interaction with the target sample and thereby experiences inelastic scattering. In such a case, the incident laser light interacts with molecular vibrations, that is, phonons, or other possible excitation sources present in the system and thereby resulting in a shift in the energy of the scattered laser photons either up or down. If the frequency of the scattered photon is lowered, then the phenomenon is called ‘‘Stokes scattering’’. If the energy of the photon is shifted upward it is called ‘‘anti-Stokes scattering’’.

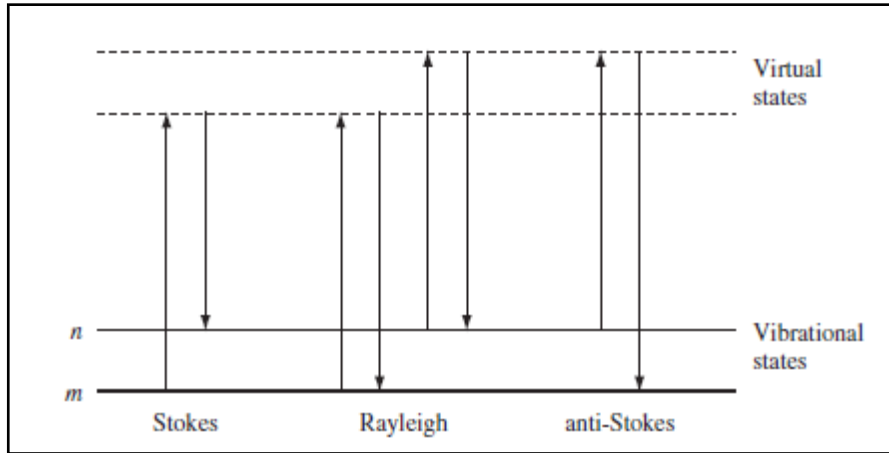


Figure 3.12. Raman Scattering Process. Scattered energy shown as downward arrows, diagram. The lowest vibrational energy state, m is shown at the bottom of the diagram and the increasing energy state is above m . Both the low energy and the scattered energy have much larger energies than the vibrational energy [46].

The shift in energy provides information about the vibrational modes of the molecule. Although Raman scattered light is frequency-shifted with respect to the excitation frequency, the magnitude of the shift in energy is independent of the excitation wavelength. The resulting “Raman shift” is therefore an intrinsic property of a molecule which makes the Raman Spectroscopy a powerful experimental tool for analytical studies. The vibrational modes (or frequencies) for a sample under consideration can be determined by Raman spectroscopy. The Raman shift or the difference in wavelength between the incident Laser light and scattered light is called Raman shift which equals the vibrational mode Renshaw in Via Raman Microscope is with 514.5 nm green Argon laser used in this thesis. The Raman shift (RS) which is related to the vibrational frequency of the crystal under consideration is given by equation (3.1).

$$RS(cm^{-1}) = \left(\frac{10^7}{\lambda_i(nm)} - \frac{10^7}{\lambda_s(nm)} \right) \quad (3.1)$$

where λ_i is the wavelength of incident laser light and λ_s is the wavelength of scattered laser light.

The vibrational frequencies (or modes) are the finger prints for crystal structures. Different crystals have different frequencies. Some of fundamental vibrational frequencies are listed in the table 2.3. below [48,50]

Table 2.2. Fundamental vibrational frequencies

Crystals	Vibrational Frequencies (cm⁻¹)
CdTe	170.8
CdS	301.0
CdSe	210.3
ZnTe	217
ZnS	320

The crystal under investigation is excited by strong laser light at frequency ω_1 and the frequency scattered light is measured. The difference between the two gives the vibrational frequency of the crystal. However the vibrational frequencies we observe in Raman measurements might be shifted due to nanometer size of the crystal (phonon confinement) and the strain between the nanocrystal and host matrix. That is why it is an important task to distinguish the shift due to phonon confinement and strain. An order of magnitude estimate can be performed by using Grüneisen method [51].

Grüneisen proposed that the ratio of percentage decrease in vibrational frequencies (ω) of the individual atoms to percentage increase in volume (V) is a constant which depends on the properties of the solid, that is,

$$\gamma = -\frac{\partial \ln \omega}{\partial \ln V} = -\frac{d\omega/\omega}{dV/V} \quad (2.73)$$

where γ is the Grünesian parameter.

Integrating Equation (2.45) over ω from frequency ω_1 at a volume of V_1 to ω_2 at V_2

$$\int_{\omega_1}^{\omega_2} \frac{d\omega}{\omega} = -\gamma \int_{V_1}^{V_2} \frac{dV}{V} \quad (2.74)$$

$$\ln \frac{\omega_2}{\omega_1} = -\gamma \ln \frac{V_2}{V_1} \quad (2.75)$$

Considering a unit cell volume for cubic crystal of lattice constant a ,

$$V = a^3 \quad (2.76)$$

$$\ln \frac{\omega_2}{\omega_1} = \ln \left(\frac{a_2}{a_1} \right)^{-3\gamma} \quad (2.77)$$

$$\frac{\omega_2}{\omega_1} = \left(\frac{a_2}{a_1} \right)^{-3\gamma} \quad (2.78)$$

$$\omega_2 = \omega_1 \pm \Delta\omega \quad (2.79)$$

$$a_2 = a_1 \pm \Delta a \quad (2.80)$$

$$\frac{\omega_1 \pm \Delta\omega}{\omega_1} = \left(\frac{a_1 \pm \Delta a}{a_1} \right)^{-3\gamma} \quad (2.81)$$

$$1 \pm \frac{\Delta\omega}{\omega_1} = \left(1 \pm \frac{\Delta a}{a_1} \right)^{-3\gamma} \quad (2.82)$$

Using Taylor's approximation

$$\frac{\Delta\omega}{\omega_1} = 3\gamma \frac{\Delta a}{a} \quad (2.83)$$

There are three contributions to the shift in Raman modes (P_i) with respect to bulk phonon frequency $\langle LO_i^B \rangle$.

- i- Phonon confinement which produces a red shift ($\Delta \omega^c$),

- ii- compressive strain on the nonacrystals exerted by the glass host ($\Delta\omega$) which produces blue shift. Since the thermal expansion coefficient for glass is greather than that of the crystal
- iii- iii-Change in composition. Assuming no change in composition. The overall Raman shift. Following the work by Spangola et al. the blue shift in Raman spectra due to the of the crystal might be determined.

$$P_i = LO_i^B + \Delta\omega^S + \Delta\omega^C \quad (2.84)$$

$$\Delta\omega^S = P_i - LO_i^B - \Delta\omega^C \quad (2.85)$$

$$\frac{\Delta\omega^S}{LO_i^B} = \frac{P_i - \Delta\omega^C}{LO_B} - 1 \quad (2.86)$$

$$1 + \frac{\Delta\omega^S}{LO_B} = \frac{P_i - \Delta\omega^C}{LO_B} \quad (2.87)$$

$$\left(1 - \frac{\Delta a}{a}\right)^{-3\gamma} = \frac{P_i - \Delta\omega^C}{LO_b} \quad (2.88)$$

$$1 + \frac{3\Delta a}{a} = \left(\frac{P_i - \Delta\omega^C}{LO_B}\right)^{-1/\gamma} \quad (2.89)$$

$$\frac{\Delta a}{a} = 1 - \left(\frac{P_i - \Delta\omega^C}{LO_B}\right)^{-\frac{1}{\gamma}} \quad (2.90)$$

In the paper by Spagnolo et al [52] the strain versus average radius is given in results section using Figure 4.22.

3. MATERIALS AND METHODS

How to grow Group II-VI Quantum Dots in glass will be explained in detail in this section.

3.1. PREPARING SAMPLES

In this study, Schott RG 830 optical filters are used. RG 830 optical filter glasses have a composition of Cadmium, Cadmium Oxide, Tellurium, Selenium, Zinc Oxide, the detailed chemical composition is given in the Appendix C from the manufacturer's technical safety information sheet. The size of the untreated plate sample was 165 mm x 165 mm x 4 mm. At the beginning the main problem is to prepare glass samples from this plate to the size of 10 mm x 10 mm x 2 mm.



Figure 3.1. RG 830 Plate.

A grid template with a size of 10 mm x 165 mm is prepared, using this template RG 830 plate cut into 10 mm (width) x 165 (height) mm x 4 mm (thickness) by a standard diamond glass knife. Then these 15 pieces are cut into two to reduce the thickness to 2 mm, homemade wooden rail with a thickness of 4mm is prepared and Buehler diamond disc (15 HC Serial Number 11-4344) attached to electrical motor with a water cooling system, is used for cutting 4mm thickness of glass to 2 mm. below pictures of the system and its components can be seen.



Figure 3.2. Wooden rail for cutting the width of the sample glass.



Figure 3.3. Close view of wooden rail and the glass sample fitted inside.



Figure 3.4. Buehler wafering blade used to cut the sample.

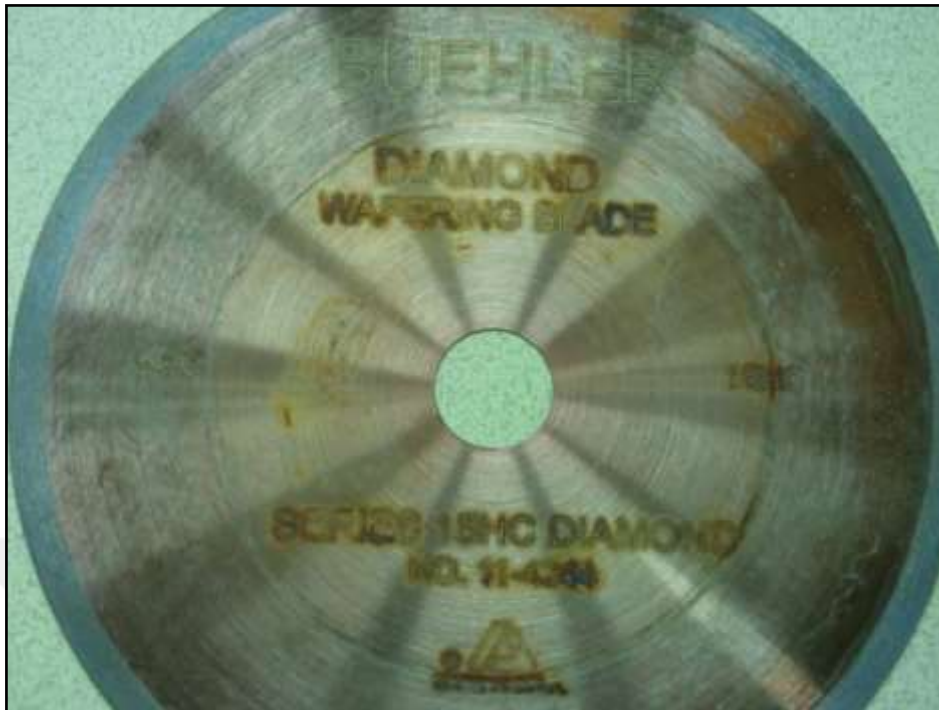


Figure 3.5. Buehler Diamond Disc.

Complete system and the act of cutting 4mm thickness of glass into 2mm thickness shown below.

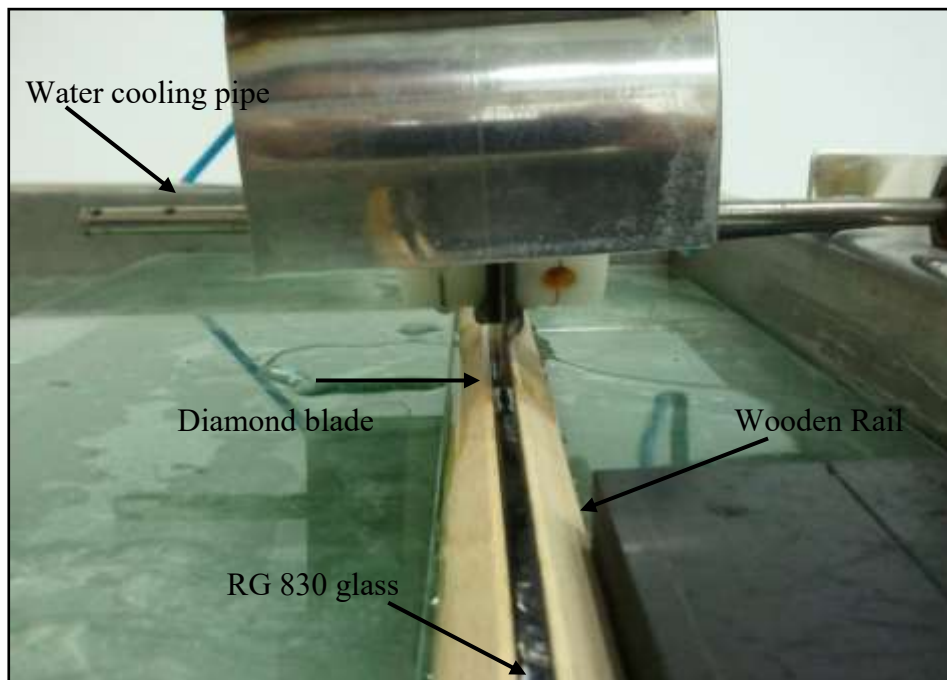


Figure 3.6. Glass cutting system.



Figure 3.7. Close view of glass cutting system

Now the sizes become 10 mm x 16 mm x 2 mm, after this process, a new grid template prepared and using standard glass knife slices reduced to 10 mm x 10 mm x 2 mm, as is seen below. Now RG 830 plate sliced into pieces and ready for heat treatment.

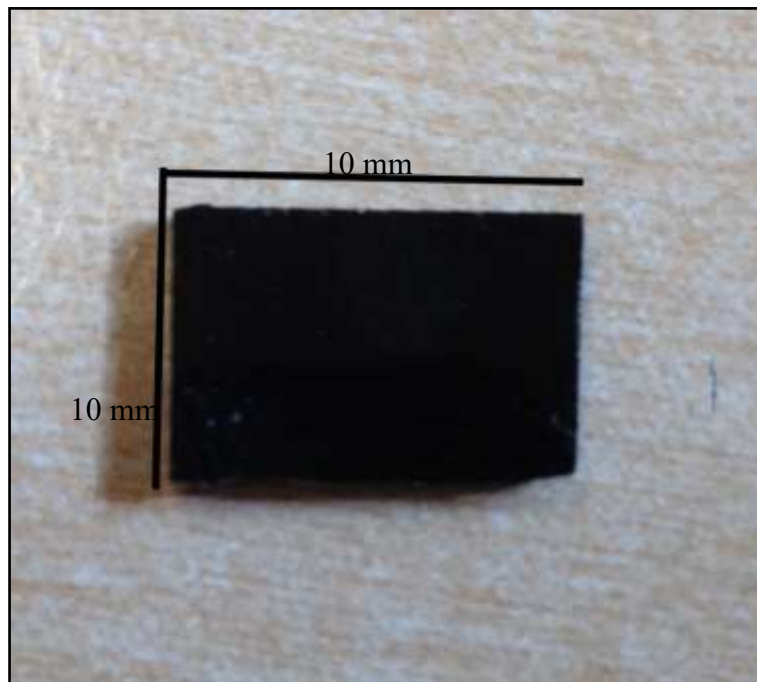


Figure 3.8. After slicing the plate glass RG830

3.1.1. Heat Treatment Procedure, Quenching

Heat treatment procedure consists of three sections. First of these three sections is tempering the sample on a 20 mm x 20 mm platinum plate at 1050 °C for 15 minutes. Hart Scientific Block Calibrator is used as a heat source, with a stability of 0.5 °C. Tempering procedure starts with heating the calibrator to 1050 °C, at which it waits for at least 30 minutes for stability. Calibration methods are used to define the temperature change in the calibrator. A newly calibrated S type thermocouple is used for measuring the temperature more precisely. When the calibrator stabilized at 1050 °C the sample is placed on a platinum plate dimensions of 20 mm x 20 mm the plate attached on a L-shaped iron clamp which is also at 1050 °C. The sample placed on the platinum plate is located at the bottom of the furnace by the help of the iron clamp for 15 minutes. After 15 minutes the sample is taken out from the furnace suddenly and quickly cooled with an air blower. At this moment, it is seen that dark coloured samples become transparent. Basically, transparency can be explained as, the case where if a material appears transparent then it does not strongly absorb or diffract light. Transparent formation occurs because of amorphous structure of the glass, at this time there are no quantum dots or crystal structure in the glass. Due to the quick cooling, stress occurs on the glass sample. To avoid this, the sample will be annealed with a temperature of 400 °C for two hours. After the annealing prepared samples are now ready for growing CdTe quantum dots. To grow CdTe quantum dots in glass matrix samples are heat treated at 600 °C for 1, 6, 8, 10, 12 and 24 hours. In this process samples begin to change their colours from transparent to dark brown, depending on the time elapsed in the furnace at 600 °C. To analyze these samples with Raman spectroscopy and UV-Vis spectroscopy, the thickness of each sample must be below 0.8 mm. Thinning is a difficult process, many of the prepared samples were broken during thinning. For thinning, 300 mm x 400 mm x 10 mm glass plate is used as a base, each sample attached to another glass plate 40 mm x 40 mm x 5 mm with Pattex Super Glue, for holding the sample standard glass vacuum attachments are used. Thinning procedure is made under flowing water, using sand paper on the base plate starting from grade number 80 to 2000 by rubbing the sample. When the samples' thickness becomes less than <0.8 mm, polishing is made with diamond paste. Polishing is done for removing little scars on the surface of the sample.

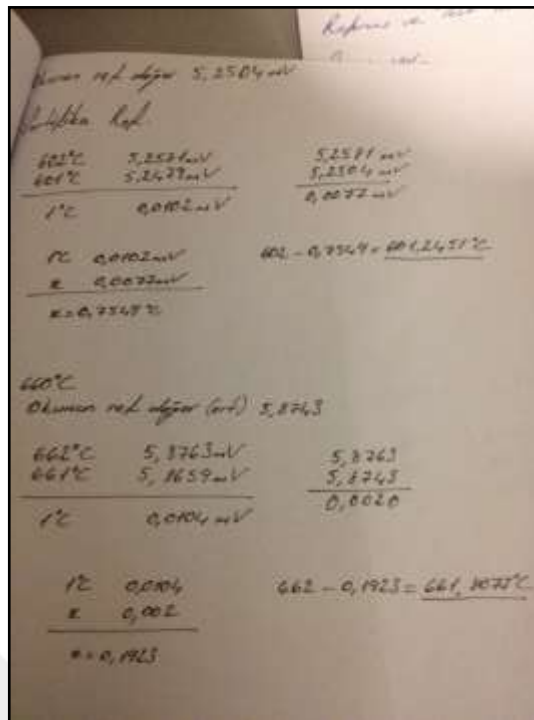


Figure 3.11. Calibration notes

Due to the importance of heat treatment, the temperature inside the furnace must be well known. As mentioned above not only the thermometer of the furnace, but also an externally already calibrated S type thermocouple is used to read the temperature inside the furnace. In figures 3.10-3.11 pictures of handwritten calculations during the temperature reading is shown. Fluke 5.5 digit multimeter is used to obtain thermocouple readouts as mV and then converted into Celcius scale.

3.2. ANALYSING SAMPLES

3.2.1. Raman Spectroscopy

Raman measurements are taken by using Renishaw InVia Raman Spectrometer.



Figure 3.13. Raman spectrometer.

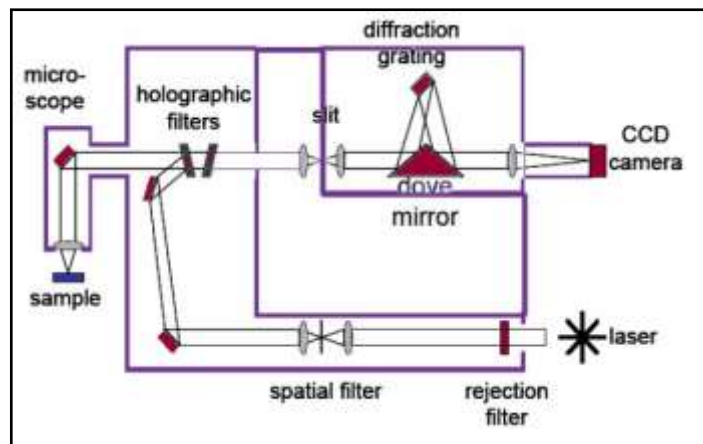


Figure 3.14. Schematic diagram for Raman Spectroscopy [53].

3.2.2. Absorption Spectroscopy

Optical absorption coefficient as a function of energy was determined by optical transmission measurements. As shown in figure 3.14 the samples were excited by tungsten light source which was focused on the sample and collected by a pair of plans-convex lens. The intensity as a function of wavelength was measured by a monochromator of focal length of 1/8 m. and a silicon photodiode connected at the output of the monochromator seen in figure 3.15.

Oriel Model 70310 serial no 176 monochromator and Oriel Model 71580 with serial no 367 sensor is used to obtain absorption spectroscopy data. The whole device is custom-made for this research. Specifications of the monochromator can be found in Appendix C. To obtain better experimental results before each sample the reference value of the incident light from source is recorded, in addition to recording the reference value, before each set of samples, calibration procedure for the monochromator is applied. The calibration procedure of the monochromator is shown in the manufacturer's manual. The procedure is added in Appendix D. In figure 3.15 custom-made Absorption Spectrometer Set-up can be seen.

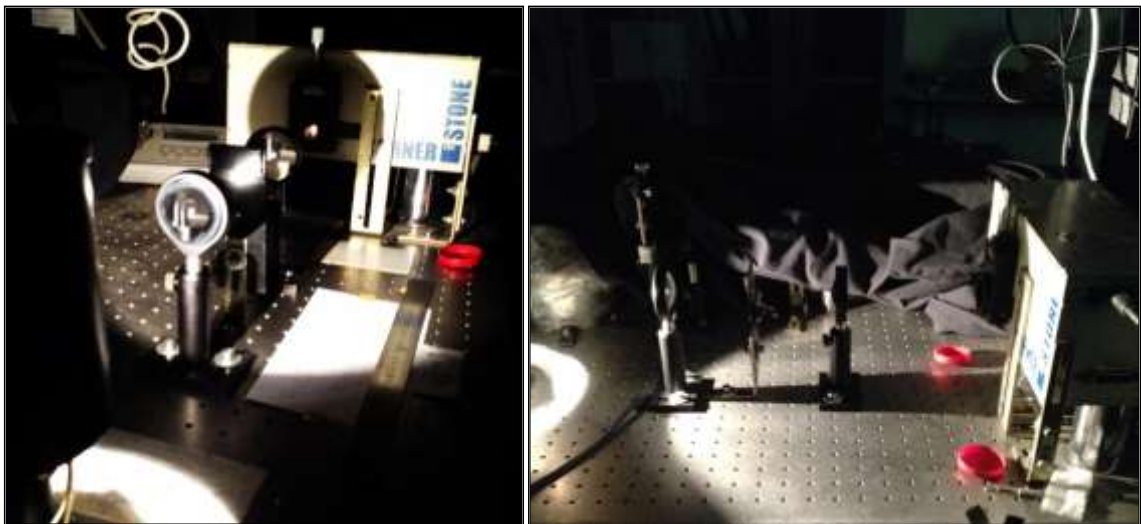


Figure 3.15. Absorption Spectrometer Set-up



Figure 3.16. Monochromator.

4. RESULTS AND DISCUSSION

4.1. RESULTS

Different size CdTe nanocrystals were grown in borosilicate glass by heat-treatment above glass transition temperature through diffusion limited growth by solid phase precipitation. The samples under investigation are listed below. Their size were determined with the help of quantized state effective mass theory under strong confinement regime and numerical solution. The samples were characterized by optical absorption and Raman spectroscopies. The vibrational phonon modes between $140\text{-}160\text{ cm}^{-1}$ in Raman spectra show that Zn precipitates into CdTe nanoparticles during growth. The blue shift in Raman lines relative to the bulk phonon mode is observed. The defect levels below band gap are discussed by Urbach method. The reciprocal of the slope of the straight line fit to the linear portion of the natural logarithm versus photon energy is related to the Urbach energy which is a measure of structural disorder.

4.1.1. Numerical Solutions for Finite Well Using Matlab Programme

Using the equations (2.27, 2.28 and 2.29) in section 2.2, the energy E is the only unknown component. These two equations are transcendental equations, which means that they cannot be solved analytically we have to solve them numerically. Using matlab program, these numerical solutions are obtained for finite well [54-56]. Figure 4.1 shows the numerical solutions for finite well, energy plotted against radius of quantum dot in nm scale.

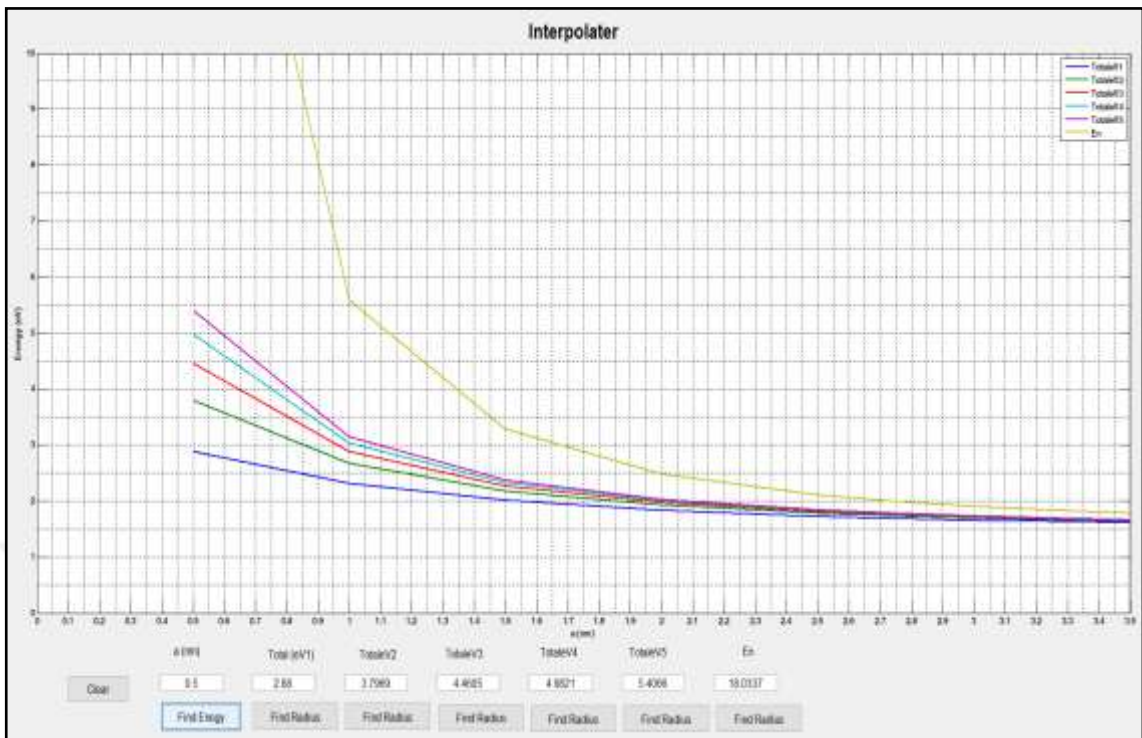


Figure 4.1. Energy levels for a particle in a potential well. Energy plotted against a (nm) for $V = 0.5$ (eV)

Table 4.1. Calculations of energy levels for a particle in a potential well. Energy listed against a (nm)

a (nm)	Total (eV ₁)	Total (eV ₂)	Total (eV ₃)	Total (eV ₄)	Total (eV ₅)	E_n (eV)
0.50	2.88	3.80	4.46	4.98	5.41	18.03
1.00	2.31	2.67	2.88	3.03	3.14	5.59
1.50	2.01	2.17	2.26	2.32	2.37	3.28
2.00	1.83	1.92	1.97	2.00	2.02	2.48
2.50	1.72	1.78	1.81	1.83	1.84	2.10
2.75	1.69	1.73	1.75	1.77	1.78	1.99
3.00	1.65	1.69	1.71	1.72	1.73	1.90
3.25	1.64	1.66	1.68	1.69	1.69	1.83
3.50	1.61	1.64	1.65	1.66	1.66	1.78
3.75	1.60	1.61	1.62	1.63	1.63	1.73
4.00	1.58	1.60	1.60	1.61	1.61	1.70
4.35	1.56	1.58	1.58	1.59	1.59	1.66
4.50	1.56	1.57	1.57	1.58	1.58	1.64
4.75	1.55	1.56	1.56	1.56	1.57	1.62
5.00	1.54	1.55	1.55	1.55	1.55	1.61

When figure 4.1 is interpolated with the help of Table 4.1 it can be noted that

- i) Kinetic energy of particles increases as the potential well height increases for a given quantum dot's radius. This can be explained as follows: As the potential well height increases the particle becomes more localized meaning uncertainty equation

$$\Delta x \Delta p \geq \frac{\hbar}{2} \quad (2.41)$$

- ii) As the size decreases the energy of the particles increases for a given potential well height.

4.1.2. Raman Spectroscopy Results

The results of Raman measurements are given in this section along with a curve fit which explores fine structure. Below the figures from 4.1 to 4.20 Raman spectroscopy plots are given, the green lines in the plots show the peaks and the hidden peaks found by using Lorentz function, also in the figures from from 4.1 to 4.20 each sample investigated by two different intensity parameter as 30 mW and 150 mW and on the average measurement with 10 measurements and 20 measurements. Raman intensity is an important tool to get better results depending on the optical properties such as cleanness and colour of an analyzed glass [57,58]. The figures from 4.1 to 4.4 are the Raman measurements for as received sample. The figures from 4.5 to 4.8 are for melted sample. The figures from 4.9 to 4.12 are for heat treated sample and the figures from 4.13 to 4.20 are for the samples that are heat treated at 600°C for 2, 6, 8, 12 and 24 hours.

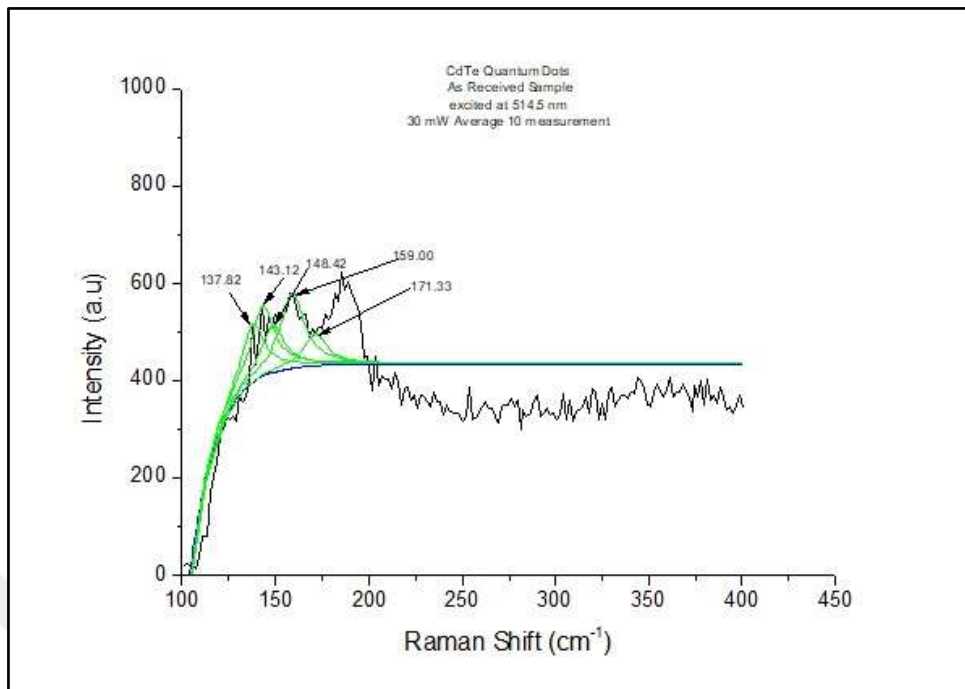


Figure 4.2. CdTe QD's as received sample excited at 30 mW with an average 10 measurements.

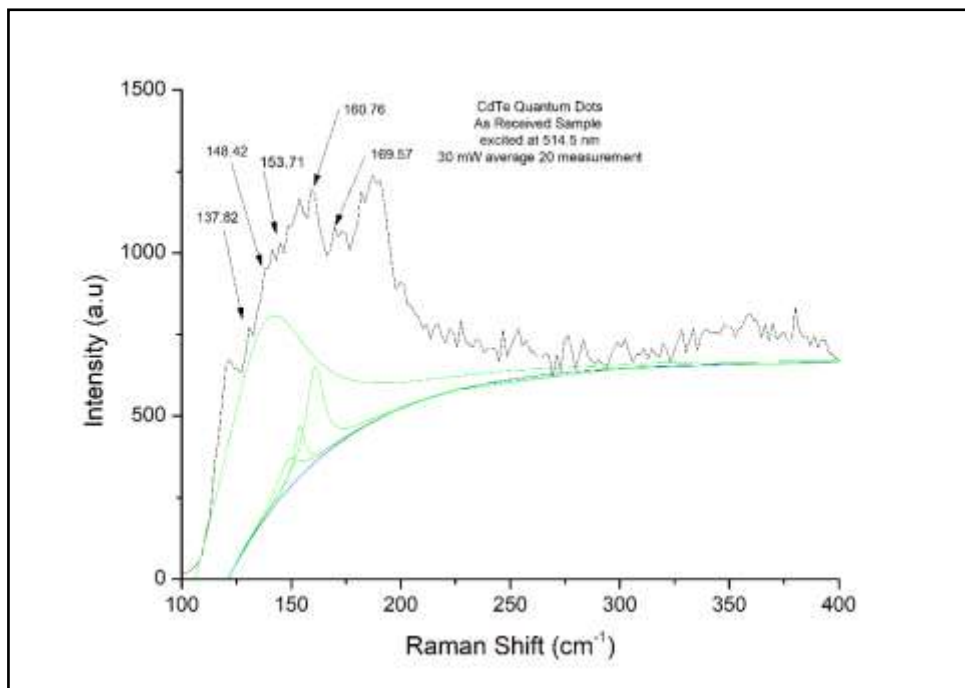


Figure 4.3. CdTe QD's as received sample excited at 30 mW with an average 20 measurements.

The difference in figures 4.2 and 4.3 above, is the change in the average measurements. The Raman shifts for both measurements at 137.82 cm^{-1} and 148.42 cm^{-1} nodes did not change by the average measurement but some new hidden nodes appeared. Below in Figures 4.4 and 4.5 Raman intensity is increased from 30 mW to 150 mW for the as received sample. The results are investigated for an average of 10 and 20 measurements.

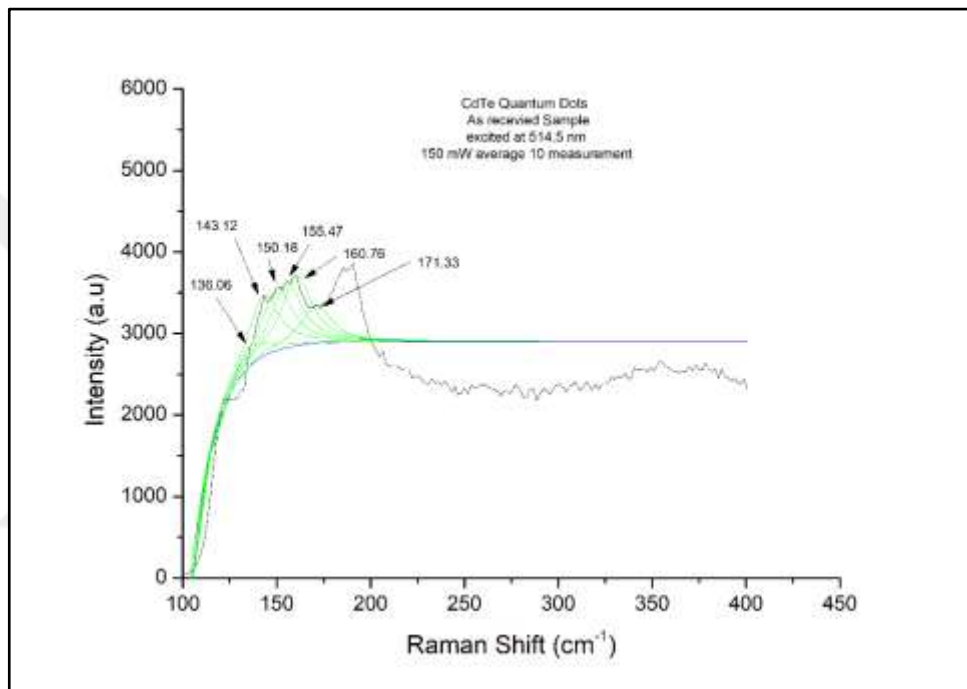


Figure 4.4. CdTe QD's as received sample excited at 150 mW with an average 10 measurements.

Changing the average measurements from 10 to 20, some peaks of the Raman shift slightly changed first, second, third and the fifth peaks changed within $\pm 1\text{ cm}^{-1}$, while the two peaks 155.47 cm^{-1} and 171.33 cm^{-1} did not show any change. The reference value of CdTe vibrational frequency is 170.80 cm^{-1} [48].

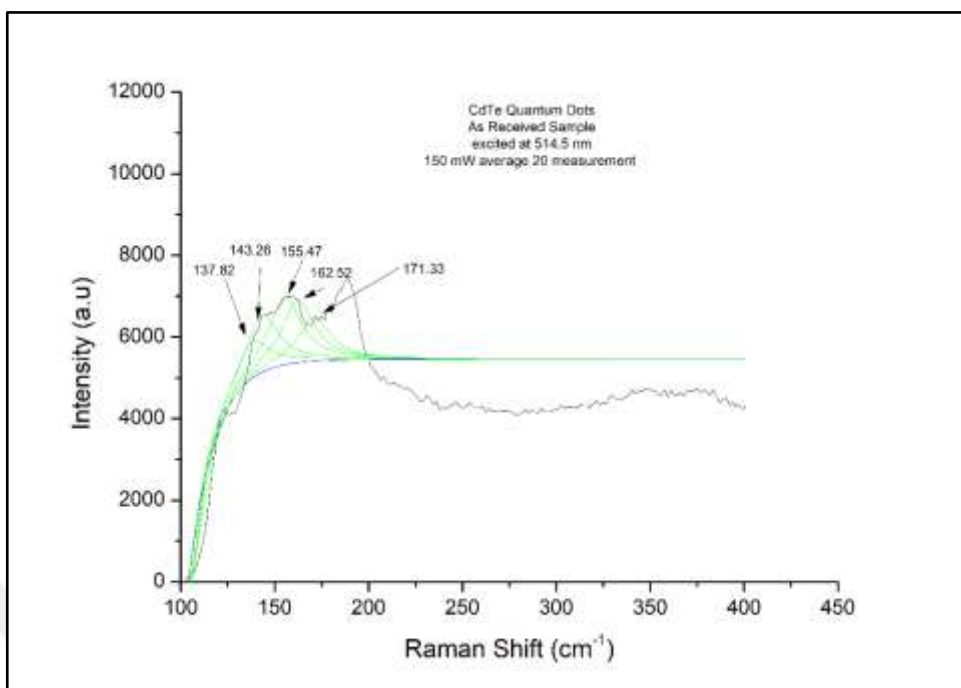


Figure 4.5. CdTe QD's as received sample excited at 150 mW with an average 20 measurements.

The figures below from 4.6 to 4.9 are the melted samples.

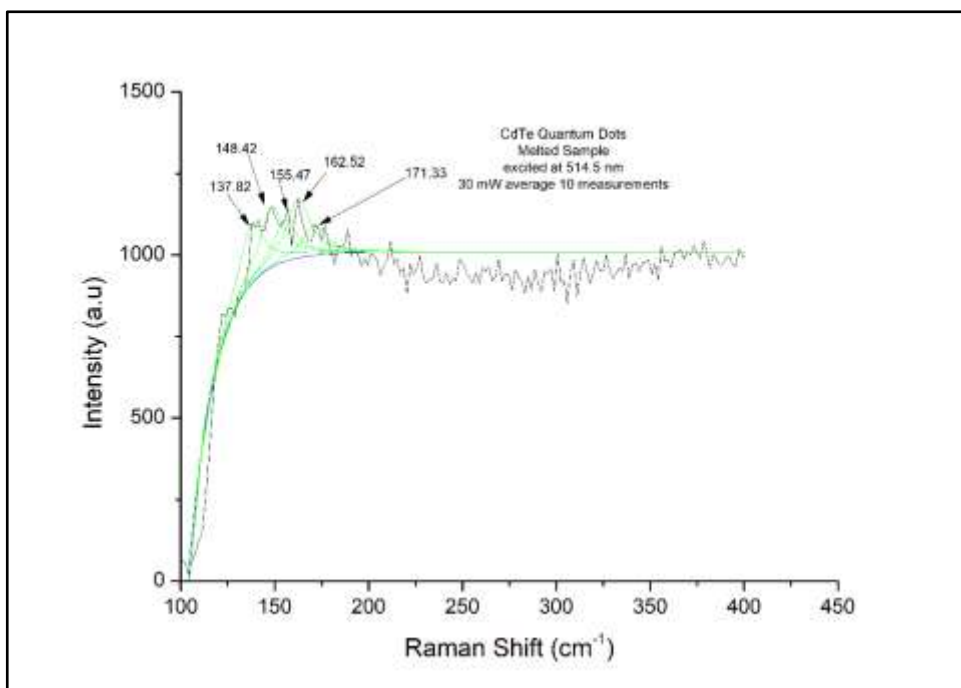


Figure 4.6. CdTe QD's melted sample excited at 30 mW with an average 10 measurements.

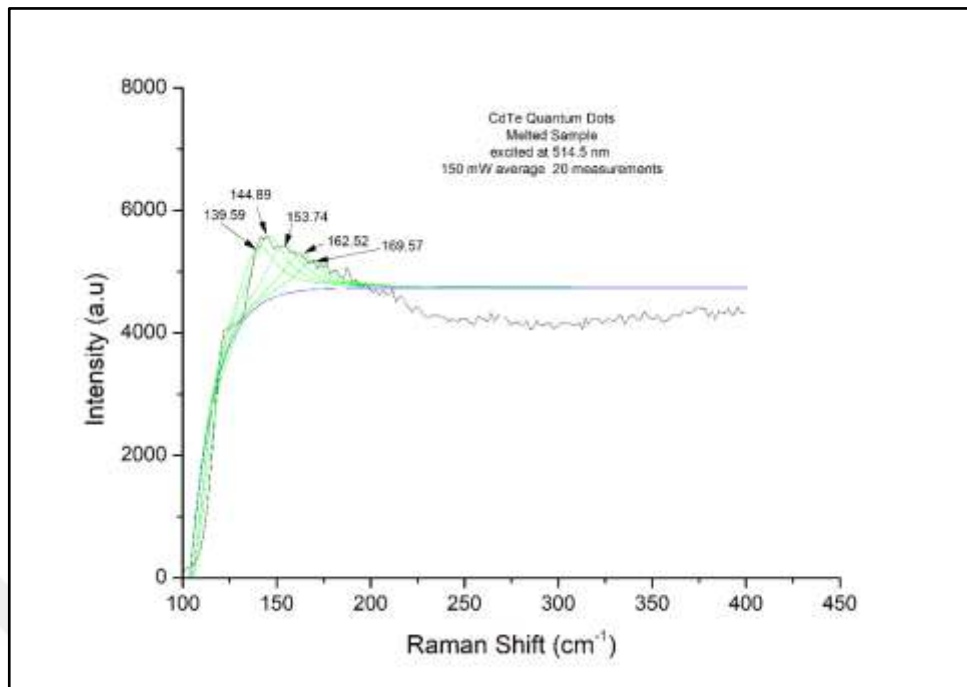


Figure 4.7. CdTe QD's melted sample excited at 30 mW with an average 20 measurements.

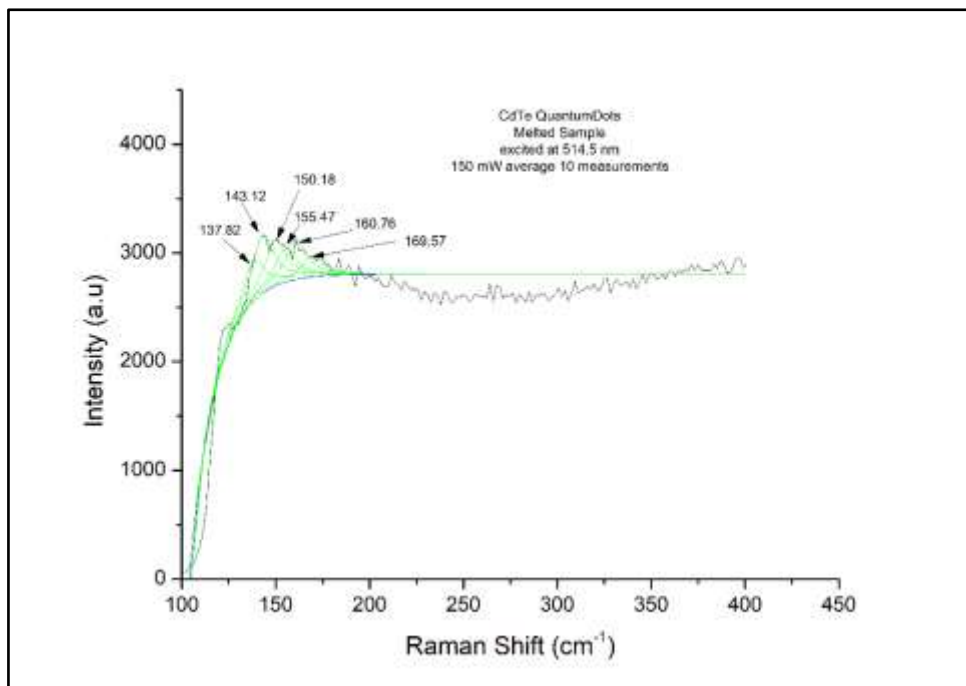


Figure 4.8. CdTe QD's melted sample excited at 150 mW with an average 10 measurements.

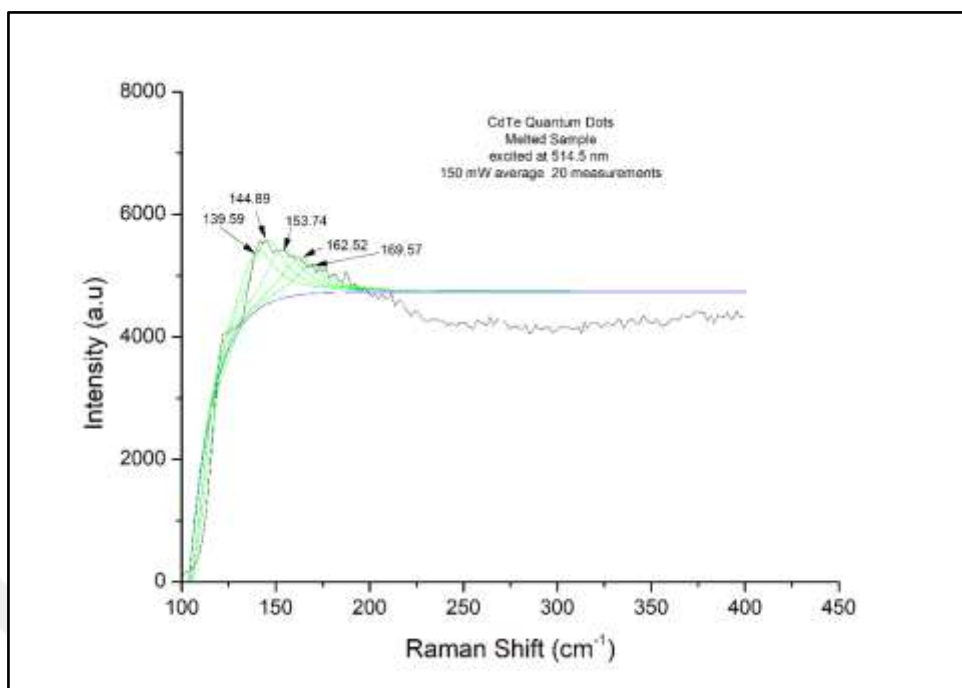


Figure 4.9. CdTe QD's melted sample excited at 150 mW with an average of 20 measurements.

Melted sample is investigated like the as received sample again. First the average measurement is changed from 10 measurements to 20 measurements excited at 30 mW than the intensity changed from 30 mW to 150 mW and again number of measurements changed from 10 to 20 measurements. For the Figures from 4.7 to 4.9 the Raman shift at 169.57cm^{-1} did not change, but in Figure 4.6 the peak appears at 171.33cm^{-1} . The figures below from 4.10 to 4.13 are for the heat treated sample. Raman shifts are again investigated with the same method. In Figures 4.10 and 4.11 the heat treated sample excited at 30 mW and the different average measurements from 10 to 20 is recorded, in Figures 4.12 and 4.13 the heat treated sample is excited at 150 mW with the same average measurement method.

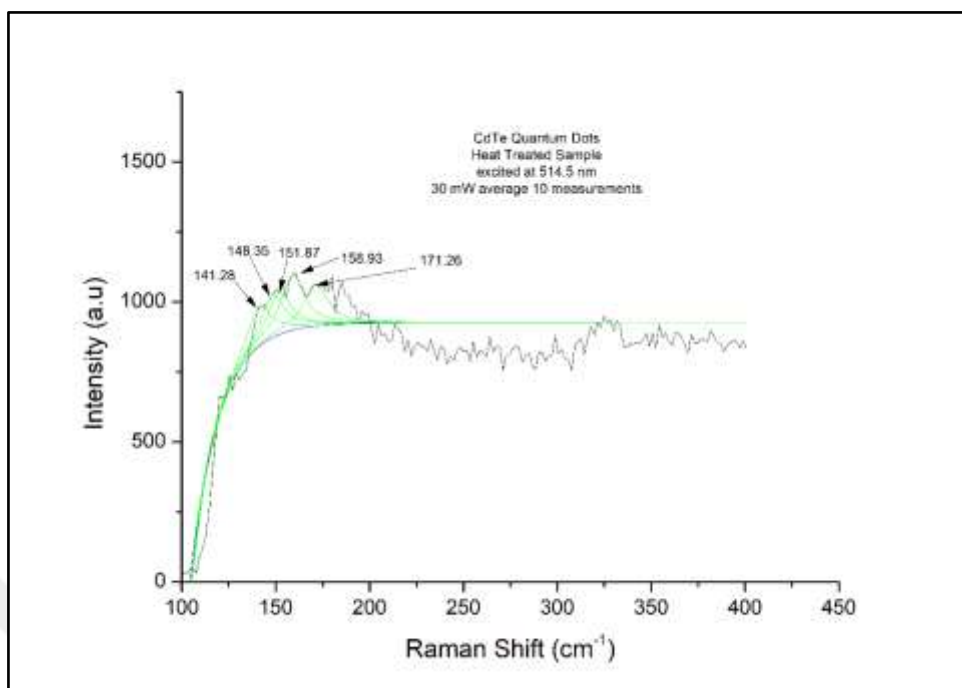


Figure 4.10. CdTe QD's heat treated sample excited at 30 mW with an average of 10 measurements.

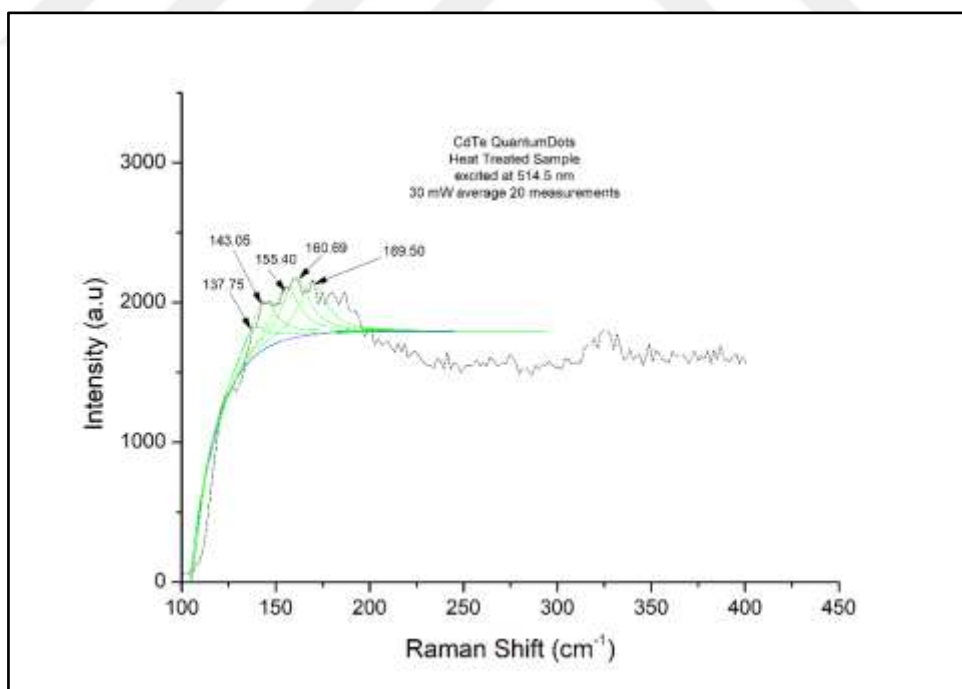


Figure 4.11. CdTe QD's heat treated sample excited at 30 mW with an average of 20 measurements.

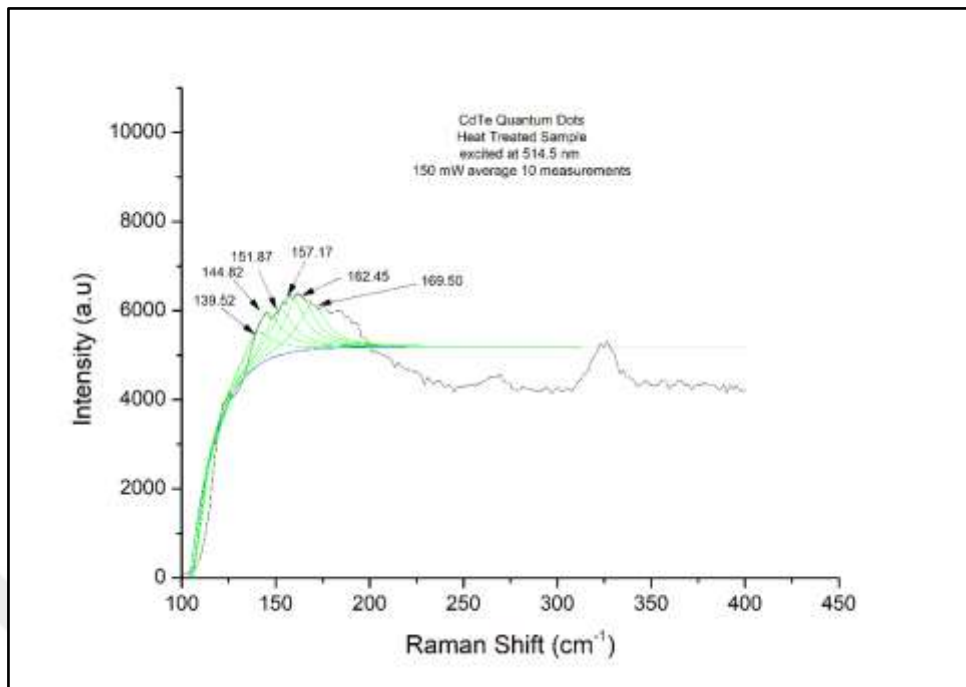


Figure 4.12. CdTe QD's heat treated sample excited at 150 mW with an average of 10 measurements.

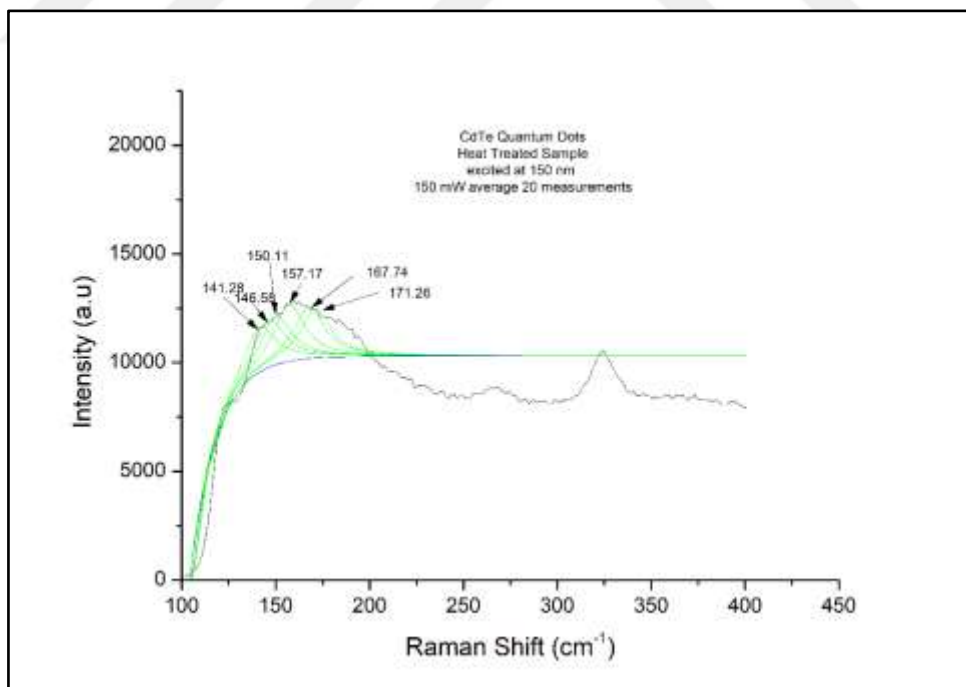


Figure 4.13. CdTe QD's heat treated sample excited at 150 mW with an average 20 of measurements.

Heat treated sample measurement results are between the range of 169.50 cm^{-1} to 171.26 cm^{-1} which is also correlated with the reference value of CdTe. All the measurements are made for to understand the difference or the relation between the intensity parameter and the number of measurements for as received, melted and heat treated sample.

Below from the figures 4.15 to 4.21 the heat treatment for all the samples are at 600°C , all the samples are excited at 150 mW with an average of 20 measurements but the heat treatment periods are changed from two hours to 24 hours. The change in the duration time is related with the quantum dots sizes inside the glass.

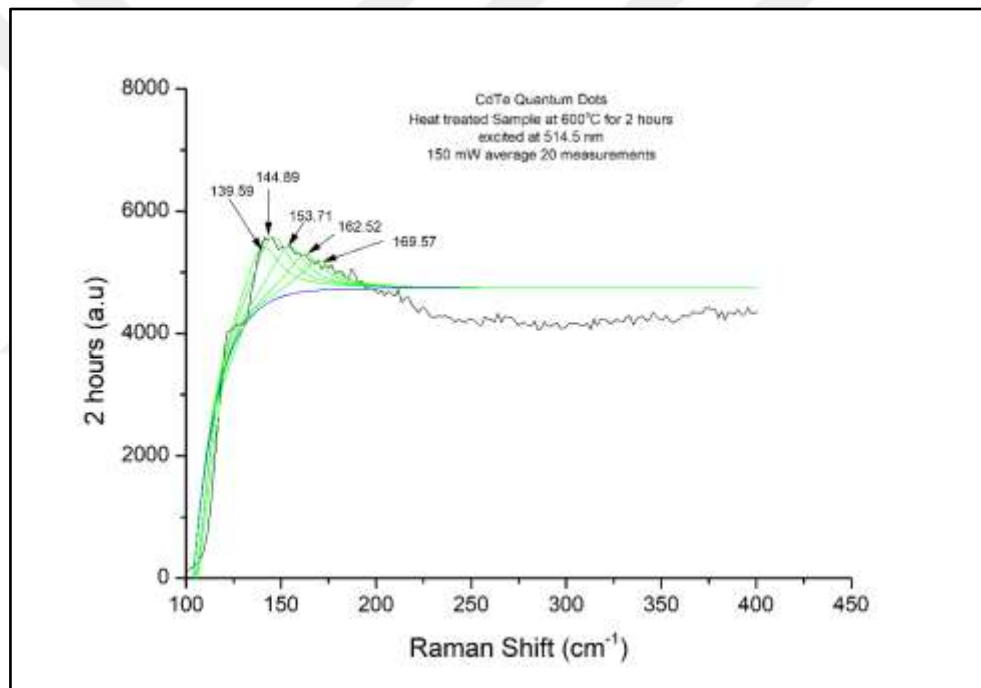


Figure 4.14. CdTe QD's heat treated sample at 600°C for two hours, excited at 150 mW with an average of 20 measurements.

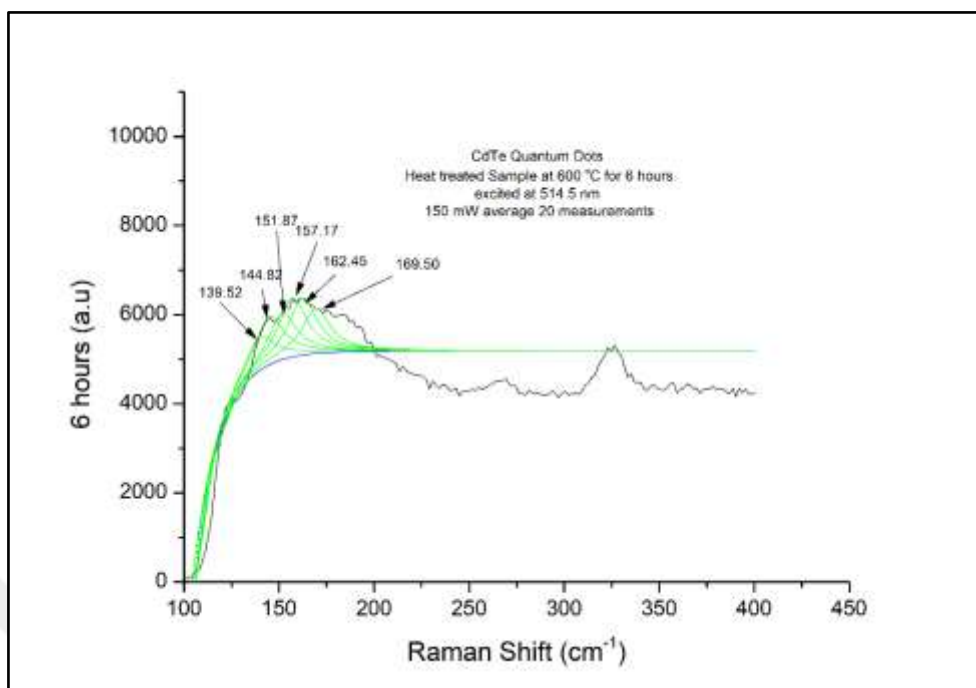


Figure 4.16. CdTe QD's heat treated sample at 600 °C for 6 hours, excited at 150 mW with an average of 20 measurements.

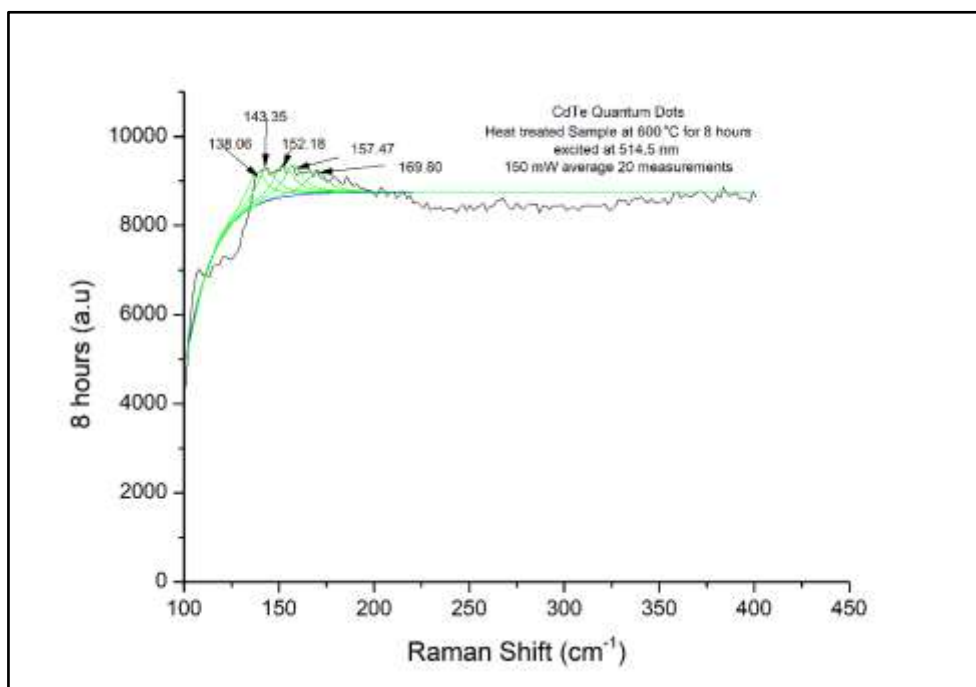


Figure 4.17. CdTe QD's heat treated sample at 600 °C for 8 hours, excited at 150 mW with an average of 20 measurements.

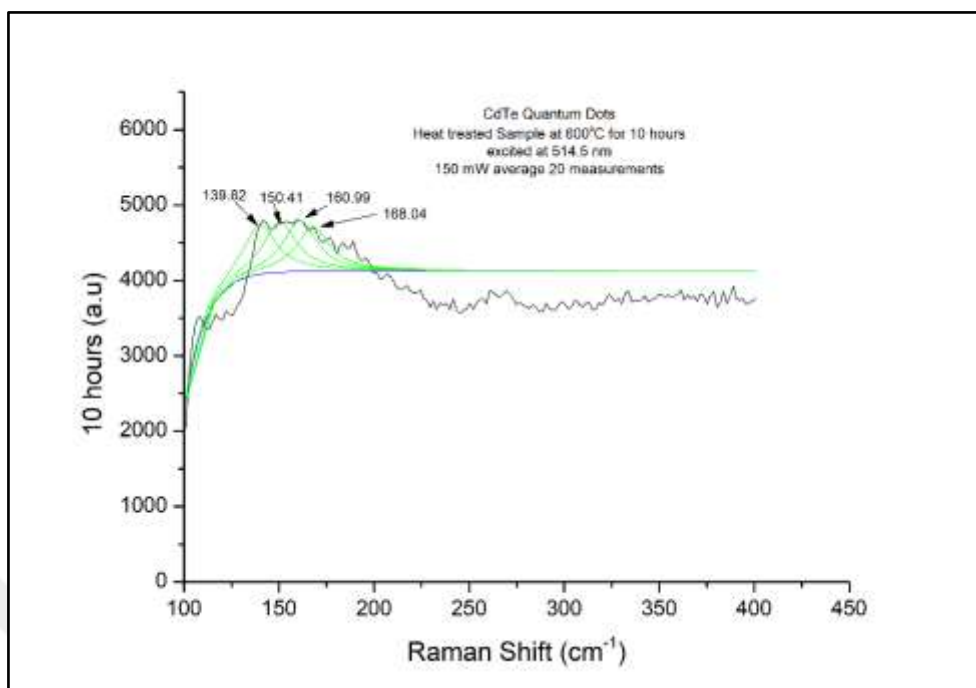


Figure 4.15. CdTe QD's heat treated sample at 600°C for 10 hours, excited at 150 mW with an average of 20 measurements.

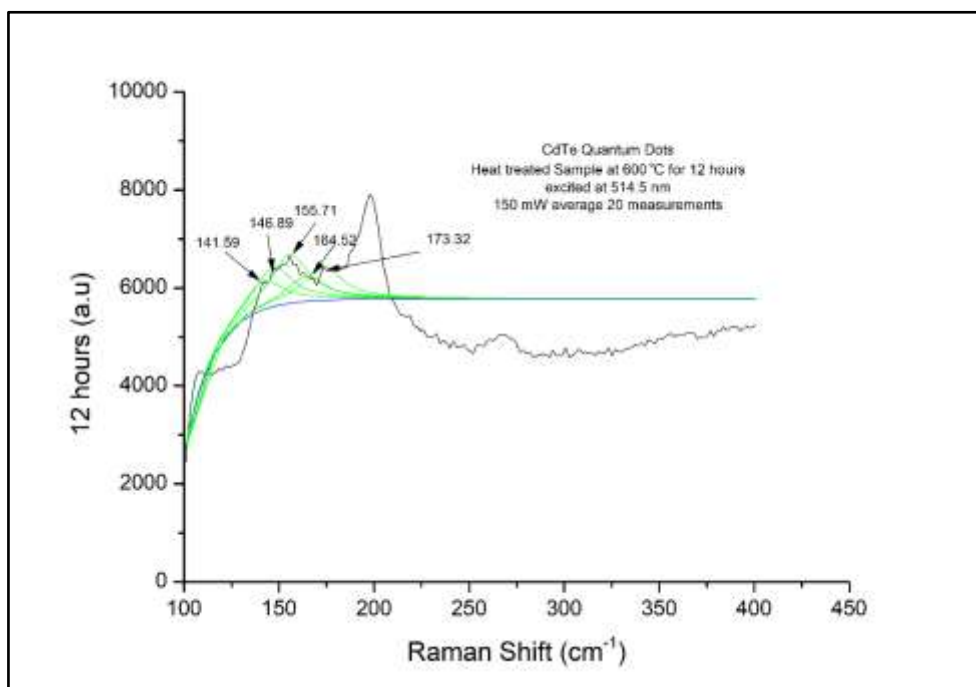


Figure 4.19. CdTe QD's heat treated sample at 600°C for 12 hours, excited at 150 mW with an average of 20 measurements.

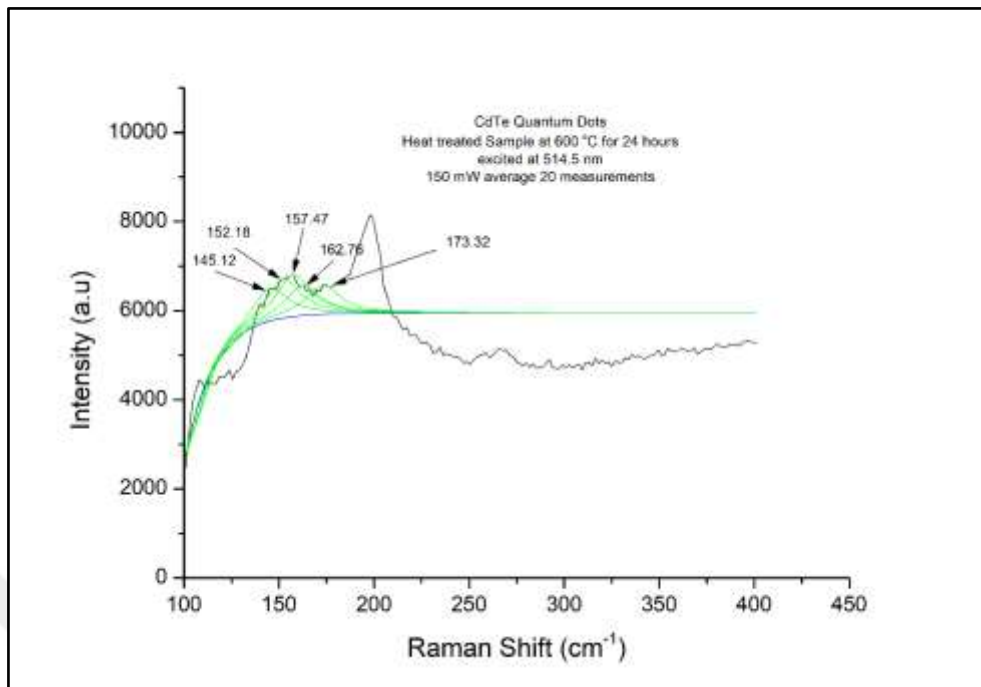


Figure 4.20. CdTe QD's heat treated sample at 600°C for 24 hours, excited at 150 mW with an average 20 of measurements.

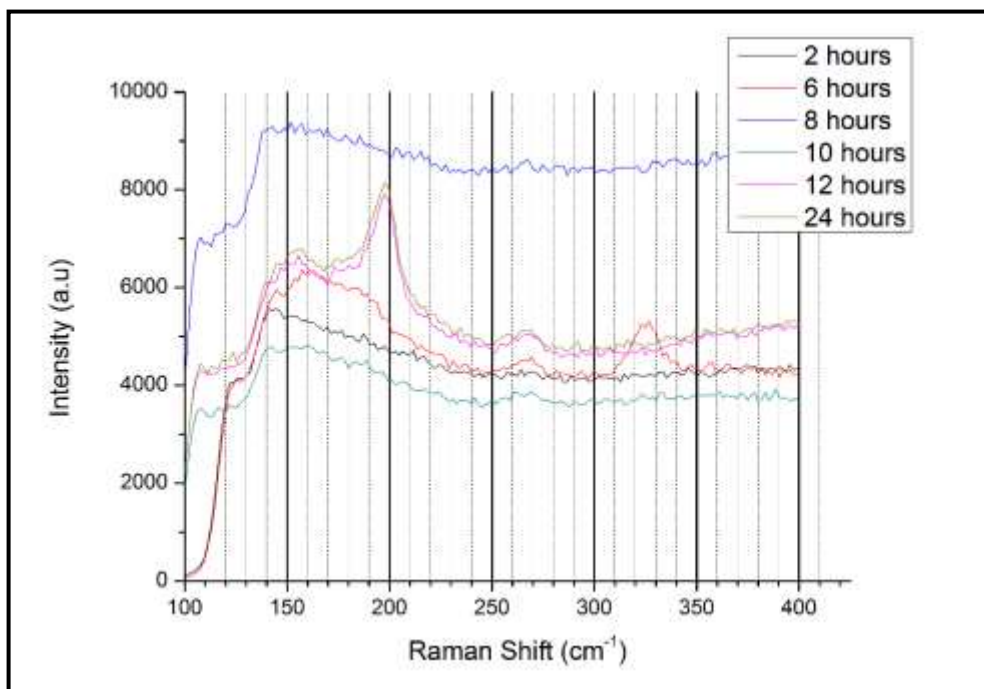


Figure 4.21. Raman peaks for heat treated samples at 600°C for 2, 6, 8, 10, 12 and 24 hours, excited at 150 mW with an average of 20 measurements.

Raman Peaks are listed below from Table 4.2 to Table 4.6 for all the samples that are investigated. In Table 4.2 and table 4.4 same samples investigated with different intensities as 30 mW and 150 mW with an average measurement of 10 times. In Table 4.2 and Table 4.4 the samples are again investigated in different intensities as 30 mW and 150 mW with an average measurement of 20 times.

Table 4.2. CdTe Quantum Dots excited by Argon laser at 514.5 nm with a power of 30 mW average of 10 measurements.

CdTe Quantum Dots excited at 514.5 nm 30 mW average 10 measurement					
	Peak 1 Raman Shift (cm⁻¹)	Peak 2 Raman Shift (cm⁻¹)	Peak 3 Raman Shift (cm⁻¹)	Peak 4 Raman Shift (cm⁻¹)	Peak 5 Raman Shift (cm⁻¹)
As Received	137.82	143.12	148.42	159.00	171.33
Melted	137.82	148.42	155.47	162.52	171.33
Heat Treated	141.26	148.35	151.87	158.93	171.26

Table 4.3. CdTe Quantum Dots excited by Argon laser at 514.5 nm with a power of 30 mW average of 20 measurements.

CdTe Quantum Dots excited at 514.5 nm 30 mW average 20 measurement					
	Peak1 Raman Shift (cm⁻¹)	Peak 2 Raman Shift (cm⁻¹)	Peak 3 Raman Shift (cm⁻¹)	Peak 4 Raman Shift (cm⁻¹)	Peak 5 Raman Shift (cm⁻¹)
As Received	137.82	148.42	153.71	160.76	169.57
Melted	139.59	144.89	153.74	162.52	169.57
Heat Treated	137.75	143.05	155.4	160.69	169.50

Table 4.4. CdTe Quantum Dots excited by Argon laser at 514.5 nm with a power of 150 mW average of 10 measurements.

CdTe Quantum Dots excited at 514.5 nm 150 mW average 10 measurement					
	Peak 1 Raman Shift (cm⁻¹)	Peak 2 Raman Shift (cm⁻¹)	Peak 3 Raman Shift (cm⁻¹)	Peak 4 Raman Shift (cm⁻¹)	Peak 5 Raman Shift (cm⁻¹)
As Received	136.06	143.12	150.18	155.47	171.33
Melted	137.82	143.12	150.18	155.47	169.57
Heat Treated	139.52	144.82	151.87	157.17	169.50

Table 4.5. CdTe Quantum Dots excited by Argon laser at 514.5 nm with a power of 150 mW average 20 measurement

CdTe Quantum Dots excited at 514.5 nm 150 mW average 20 measurement					
	Peak 1 Raman Shift (cm⁻¹)	Peak 2 Raman Shift (cm⁻¹)	Peak 3 Raman Shift (cm⁻¹)	Peak 4 Raman Shift (cm⁻¹)	Peak 5 Raman Shift (cm⁻¹)
As Received	137.82	143.26	155.47	162.52	171.33
Melted	139.59	144.89	153.74	162.52	169.57
Heat Treated	141.28	146.58	150.11	157.17	167.74

Table 4.6. CdTe Quantum Dots excited by Argon laser at 514.5 nm with a power of 150 mW average of 20 measurements.

CdTe Quantum Dots excited at 514.5 nm 150 mW average 20 measurement					
Heat Treated at 600°C for	Peak 1 Raman Shift (cm⁻¹)	Peak 2 Raman Shift (cm⁻¹)	Peak 3 Raman Shift (cm⁻¹)	Peak 4 Raman Shift (cm⁻¹)	Peak 5 Raman Shift (cm⁻¹)
2 hours	139.59	144.89	153.71	162.52	169.57
6 hours	139.52	144.82	151.87	162.45	169.50
8 hours	138.06	143.35	152.16	157.47	169.80
10 hours	139.82	(-)	150.41	160.99	168.04
12 hours	141.59	146.89	155.71	164.52	173.32
24 hours	145.12	152.18	157.47	162.76	173.32

Finally using the tables from 4.2 to 4.6 we can see the correlation between the reference peak value of CdTe to our samples in the peak 5 this will be investigated in the discussion section.

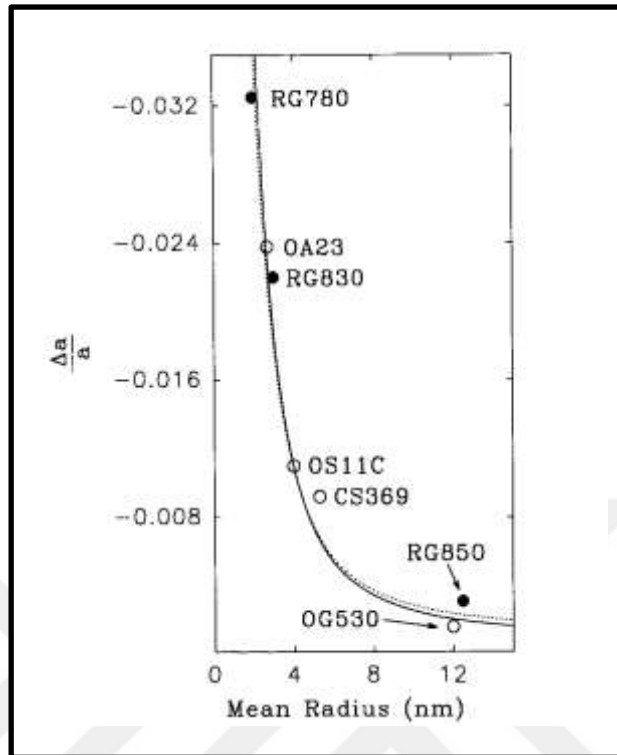


Figure 4.42. Strain as a function of nanocrystal radius

Digitizing the plot we find

$$\frac{\Delta a}{a} = -0.004352 + \frac{0.067852}{R \text{ (nm)}} \quad (2.91)$$

which equals, by using Eq 2.90

$$-0.004352 + \frac{0.067852}{R_{(nm)}} = \frac{\left(\frac{P_i - \Delta\omega^c}{LO_B}\right)^{-1/\gamma} - 1}{3} \quad (2.92)$$

The raman shift due to size is calculated.

$$\Delta\omega^c = P_i - \left[\left(1 + 0.004352 - \frac{0.067852}{R_{(nm)}} \right)^{-\gamma} \right] LO_B \quad (2.93)$$

Table 4.7. Three samples for size confinement versus radius graphic

	Radius (nm)	P_i	LO_B	Grünesian Parameter
As Received	2.14	159.926	166.73	0.91
12 Hours	2.35	153.638	166.73	0.91
24 Hours	2.86	153.698	166.73	0.91

where P_i is Raman node, γ is Grüneisen parameter and LO_B , is bulk structure as 166.73 in Eq 2.64. Solving the equation Eq 2.64 for three different samples, as received, 12 hrs and 24hrs. $\Delta\omega^c$. Corolation between $R_{(nm)}$ size confinement shift and radius can be seen in the Table 2.4 below.

Table 4.8. Size Confinement and Radius

	Radius (nm)	Size Confinement Shift
As Received	2.14	7.03
12 Hours	2.35	0.58
24 Hours	2.86	2.99

4.1.3. Absorption Spectroscopy Results

Samples are investigated by using UV-VIS Spectrometer, three different types of data plotted. Figure 4.23 is the general outlook for the samples prepared with thickness 0.67 mm and heat treated for 12 hours, 0.79 mm and heat treated for 12 hours and 0.77 mm and heat treated for 24 hours. The figures from 4.24 to 4.26 optical absorption spectra for three samples are presented, these samples are; as received, heat treated and melted. Optical transmission measurements were conducted and optical absorption coefficient was calculated by using Lambert-Bear law

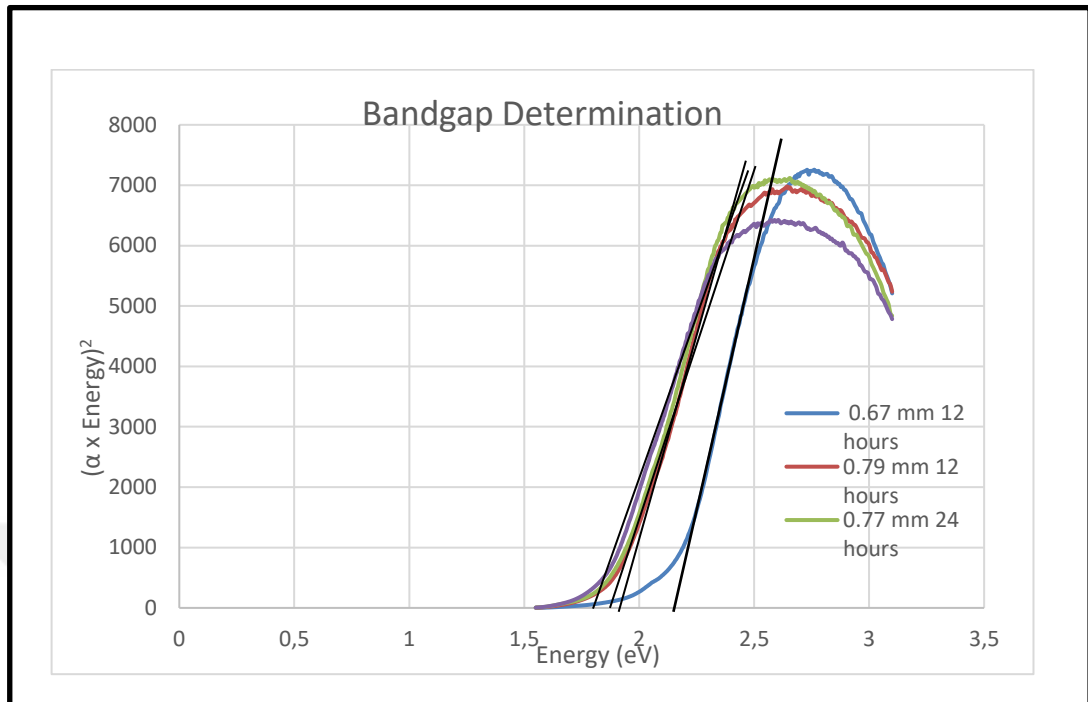


Figure 4.16. $(OD \times hv)^2$ plotted versus photon energy hv to find bandgap energy.

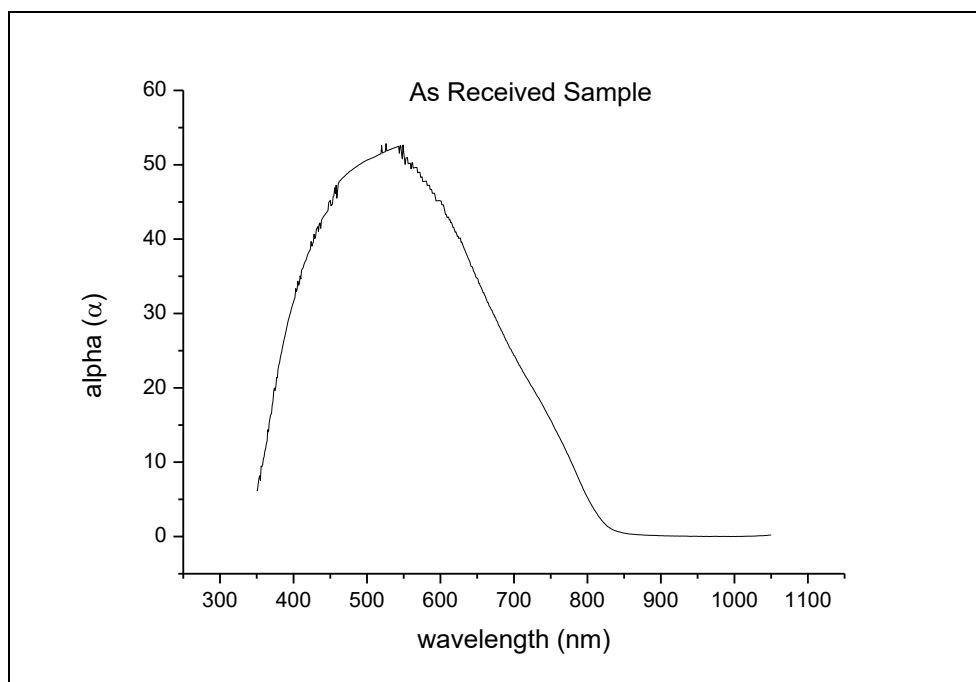


Figure 4.22. Absorption spectroscopy for as received sample

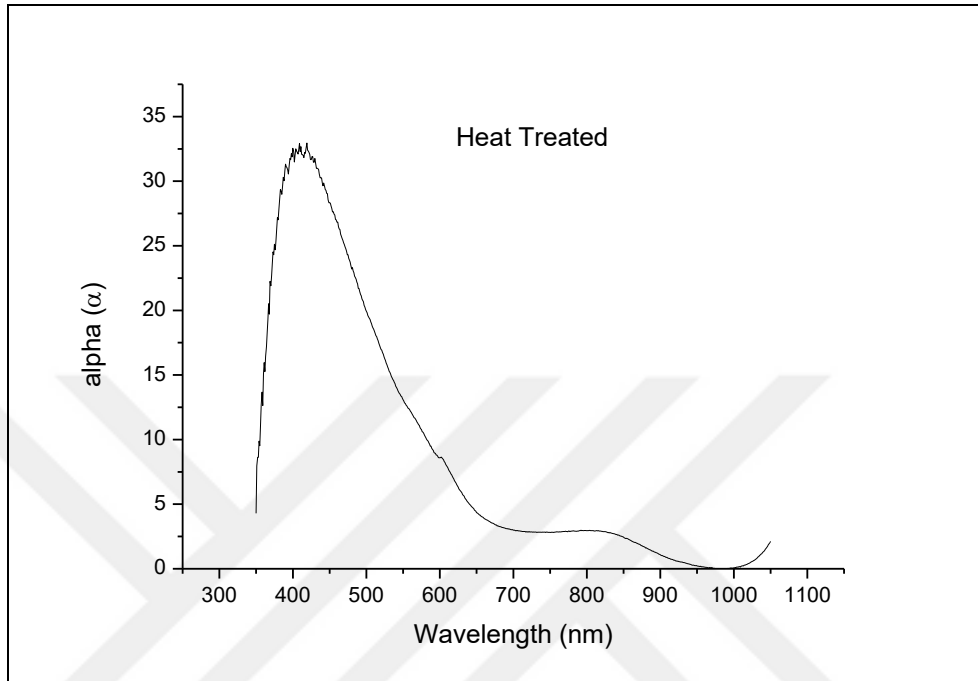


Figure 4.23. Absorption spectroscopy for heat treated sample.

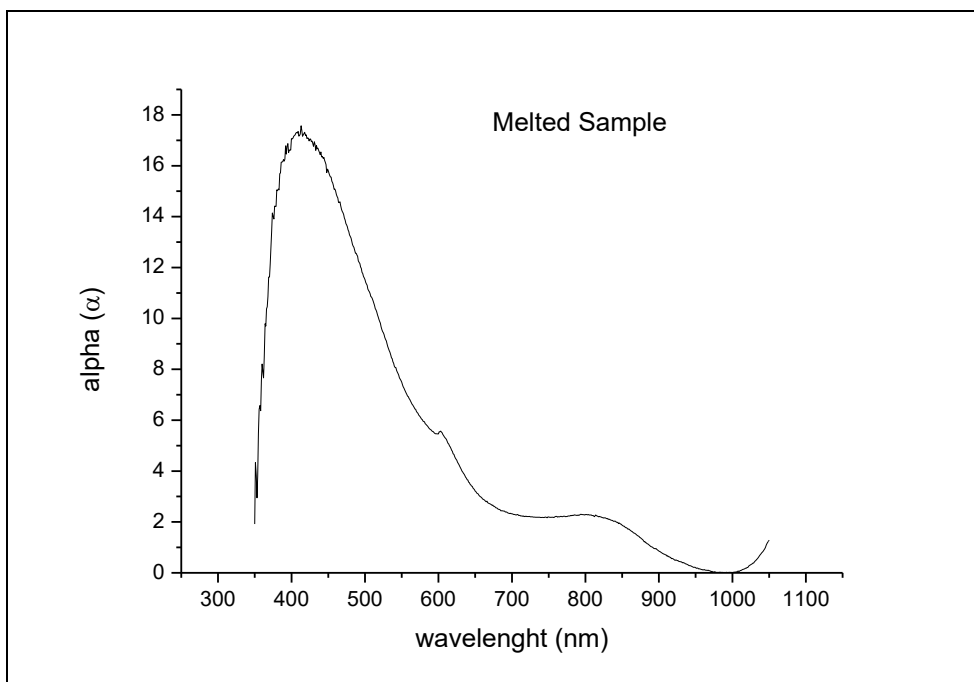


Figure 4.24. Absorption Spectroscopy for melted sample.

In Figure 4.27, 4.29, 4.31 $(\alpha h\nu)^2$ is plotted against photon energy to calculate the asymptotic optical absorption edge (Tauc plot) intercept points shown in the each plot is the optical gap and in figures 4.28, 4.30 and 4.32 $\ln\alpha(\alpha)$ plotted against photon energy to calculate Urbach energy for as received, heat treated and melted sample in order.

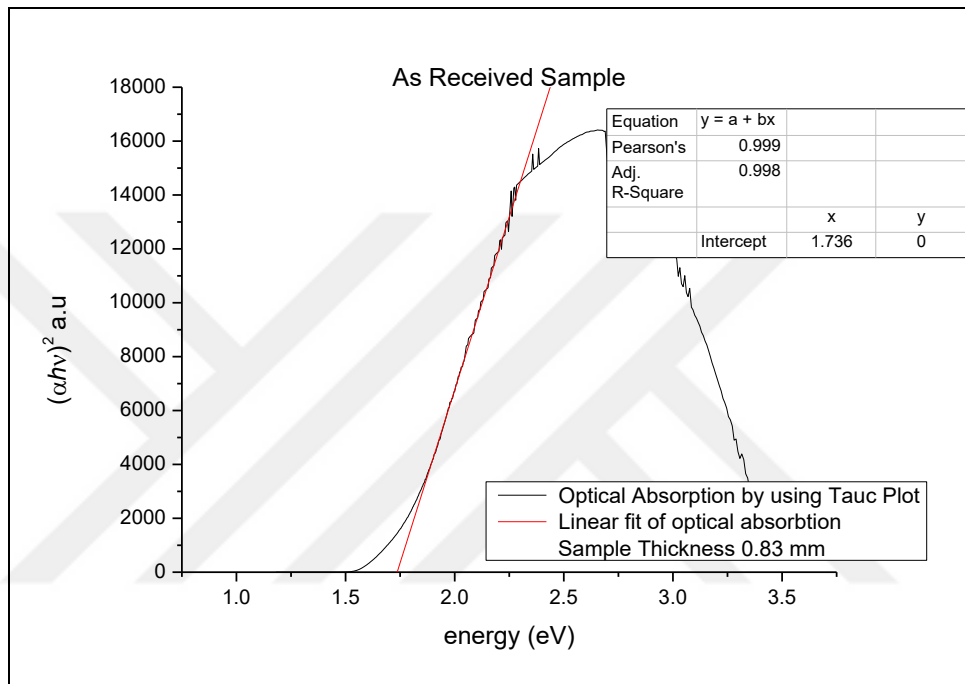


Figure 4.25. Optical Absorption by using Tauc plot for as received sample

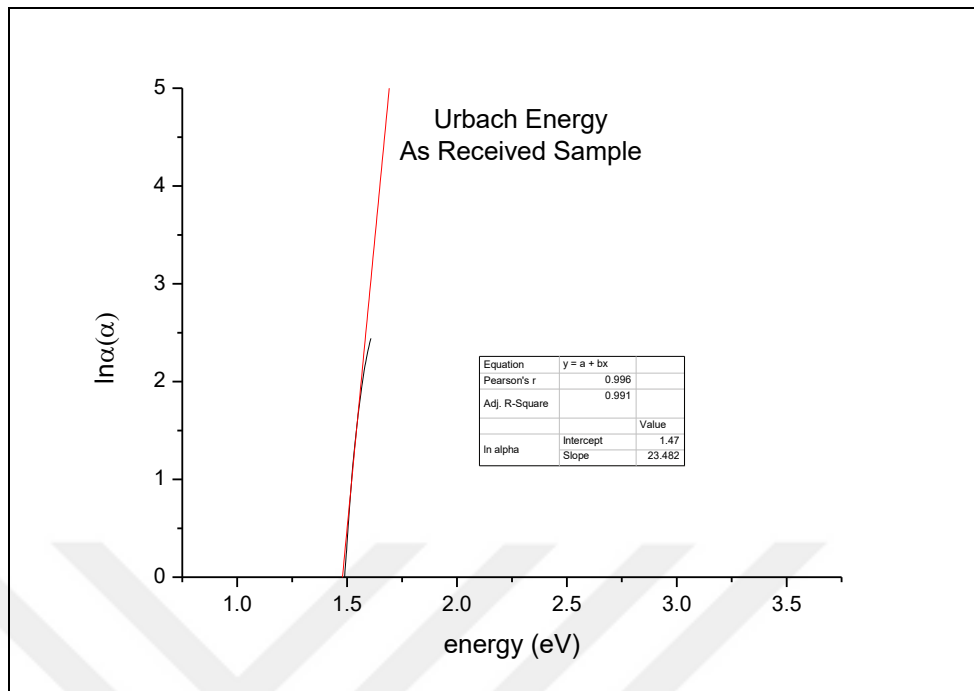


Figure 4.26. Urbach Energy for as received sample.

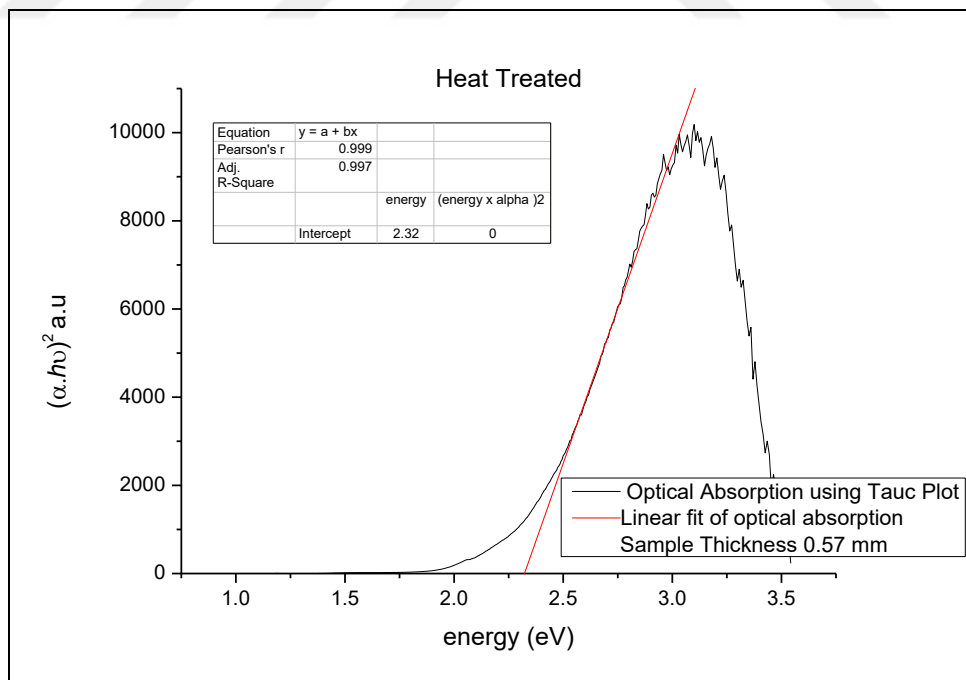


Figure 4.17. Optical absorption using Tauc plot for heat treated sample.

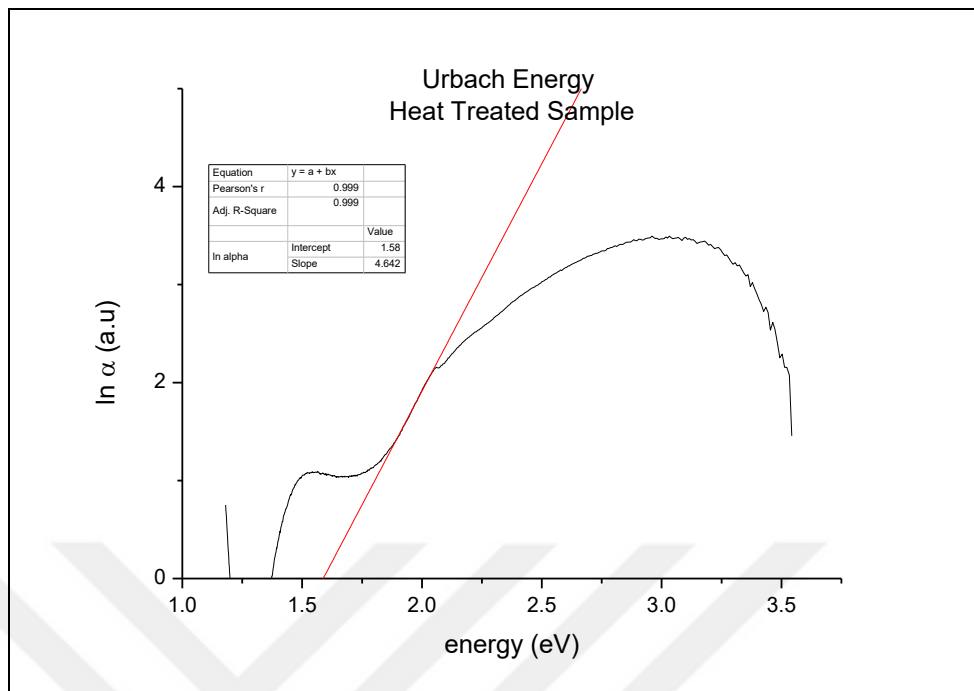


Figure 4.18. Urbach energy for heat treated sample.

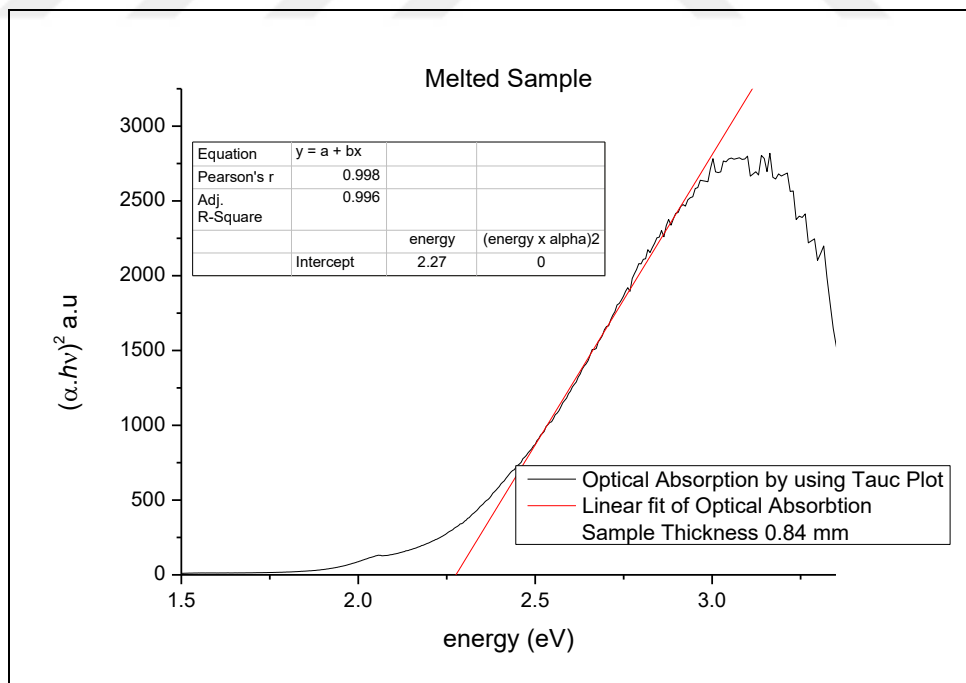


Figure 4.19. Optical absorption by using Tauc plot for melted sample.

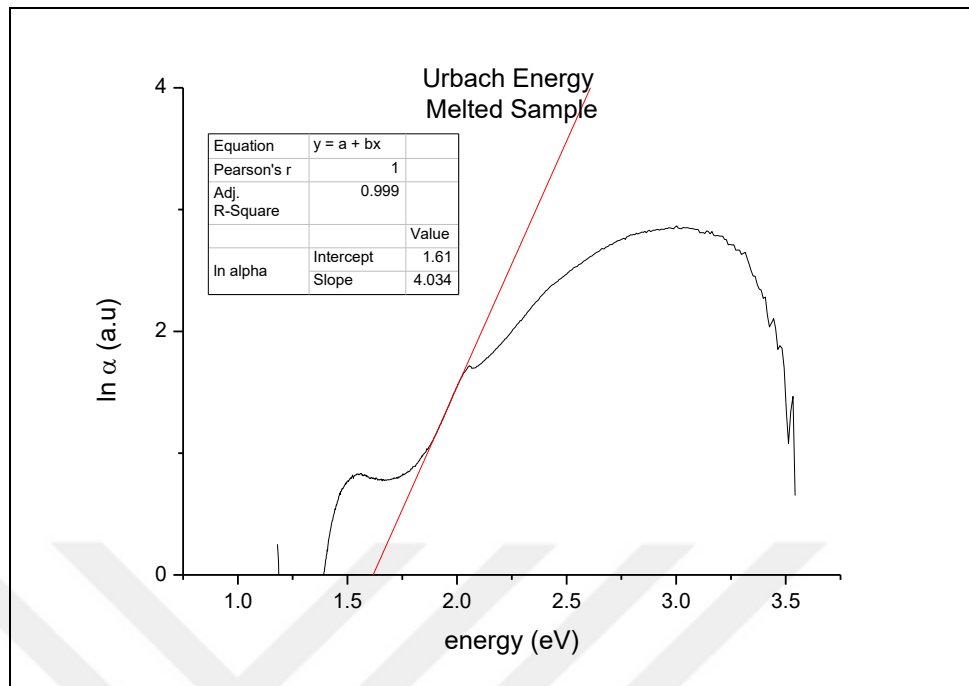


Figure 4.20. Urbach energy for melted sample

Above the Figures from 4.20 to 4.25, bandgap energies, Urbach disorder and absorption spectroscopies of as received, heat treated and melted samples are plotted. From the figures 4.20, 4.22 and 4.24 bandgap energies of each sample are 1.73 eV, 2.32 eV and 2.27 eV respectively. These results are correlated with the bandgap theory, when the sizes of the nano particles in the samples are decreasing, band gaps of the samples are increasing. According to these results, change in the Urbach energies are expected, in figures 4.21, 4.23 and 4.25 Urbach energies of the samples are examined and the results are 0.04 eV, 0.21 eV and 0.24 eV, according to results for the as received, heat treated and melted sample the change in the amorphous structure of the glass can be observed. Below the Figures starting from 4.26 to 4.40 heat treatment processed samples results will be given.

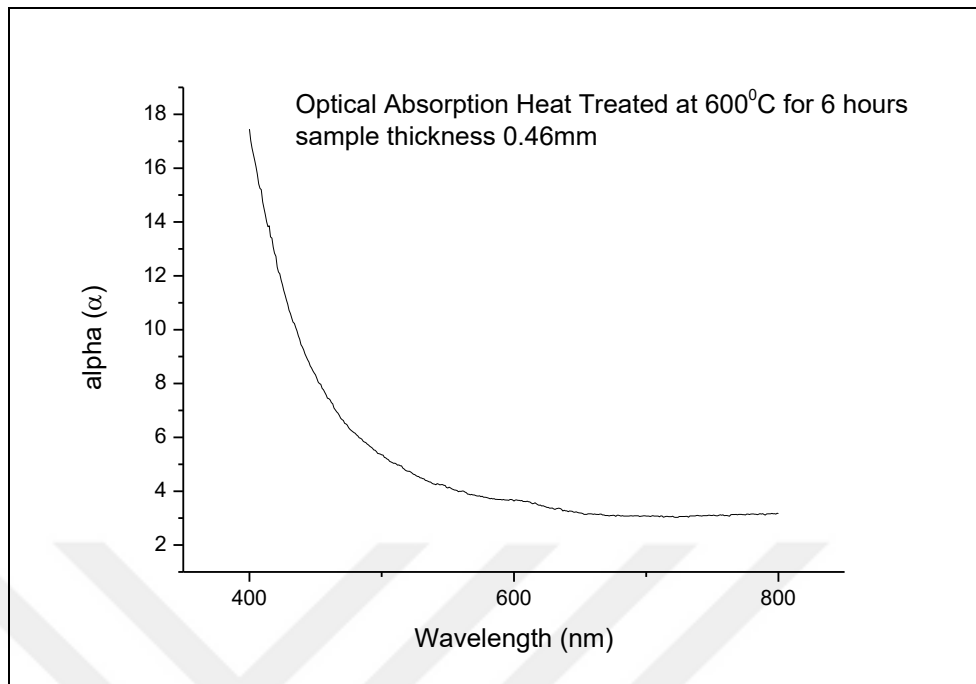


Figure 4.21. Optical Absorption heat treated at 600 °C for 6 hours, thickness of 0.46 mm.

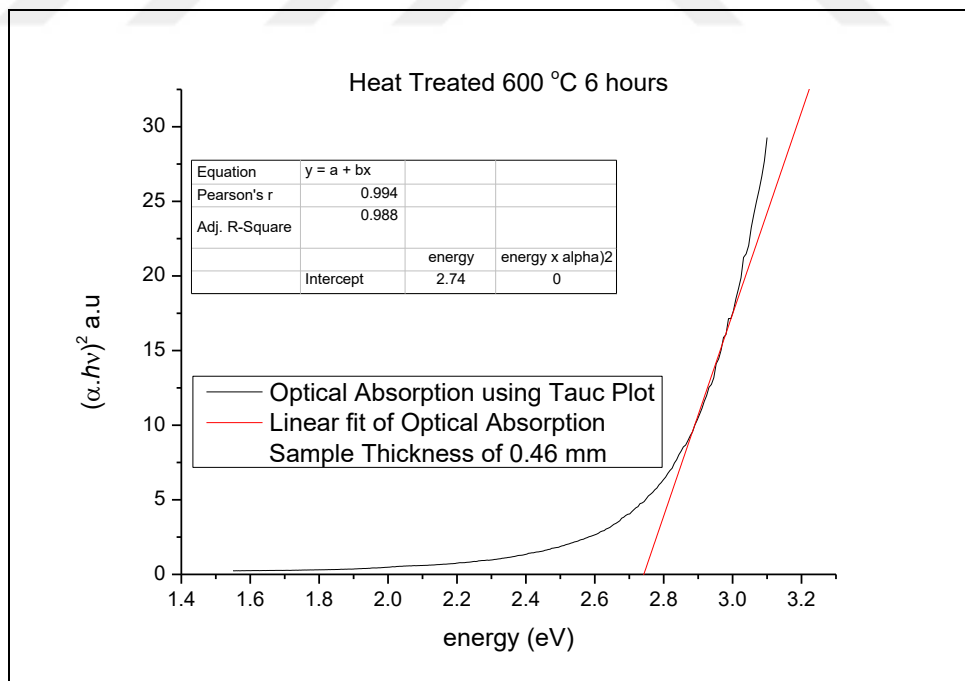


Figure 4.22. Optical absorption using Tauc plot heat treated for 6 hours at 600°C.

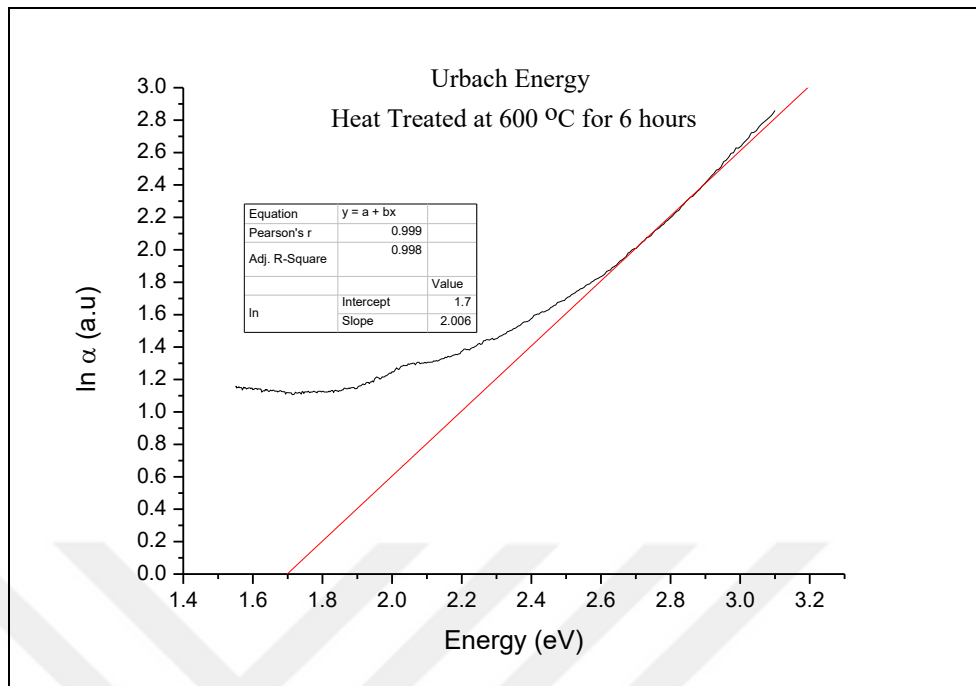


Figure 4.23. Urbach energy heat treated at 600 °C for 6 hours

From the figure 4.26 to 4.28 heat treated sample for 6 hours with a thickness of 0.46 mm is examined in the Figure 4.27 band gap of the sample is 2.74 eV and Urbach energy for the sample is 0.5 eV noted.

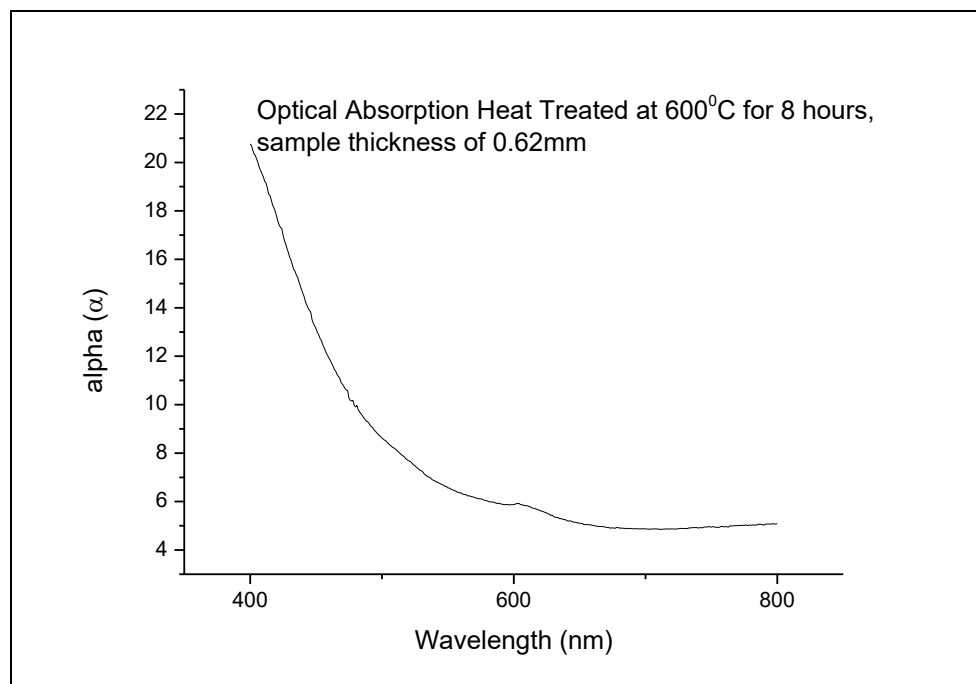


Figure 4.24. Optical absorption heat treated at 600 °C for 8 hours, thickness of 0.62mm.

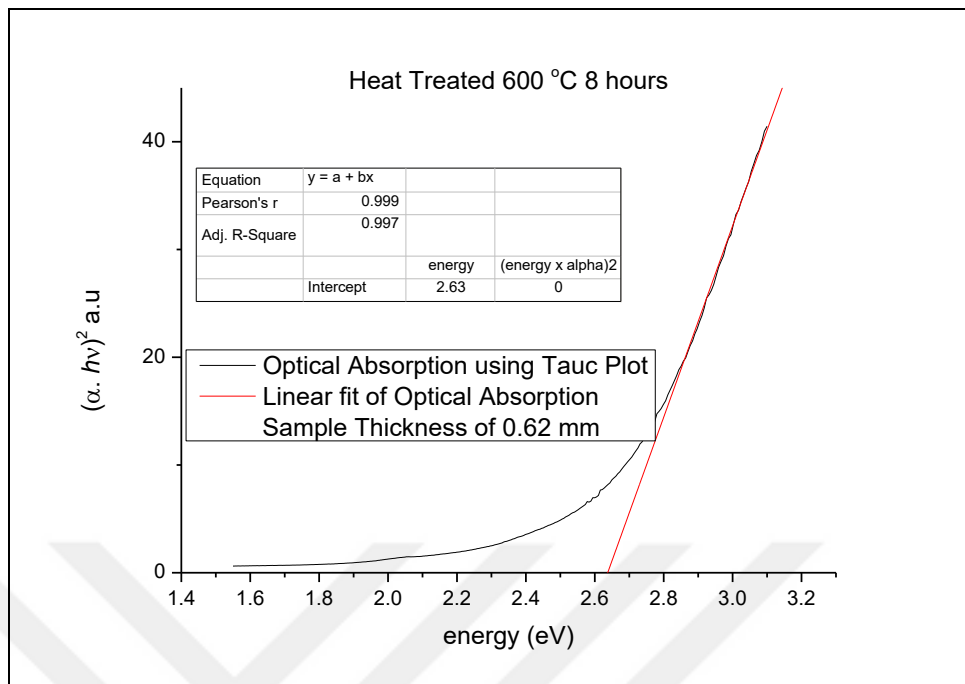


Figure 4.25. Optical absorption using Tauc plot heat treated at 600 °C for 8 hours, thickness of 0.62mm.

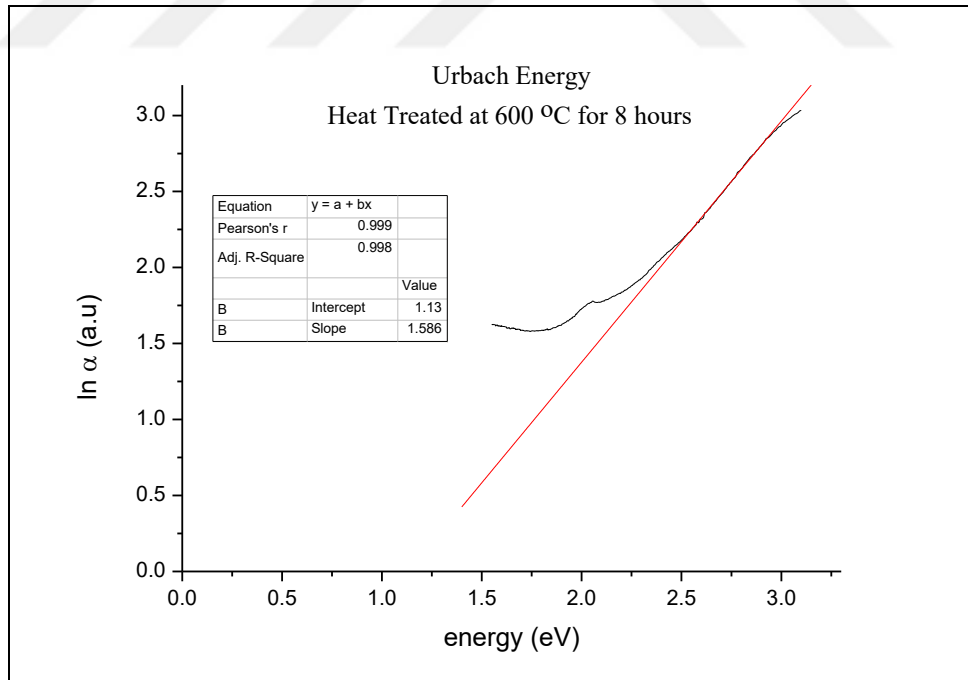


Figure 4.26. Urbach energy heat treated at 600 °C for 8 hours

From the figures 4.29 to 4.31 heat treated sample for 8 hours with a 0.62 mm thickness is examined in figure 4.30 band gap of the sample is 2.63 eV and Urbach energy for the sample is 0.63 eV noted.

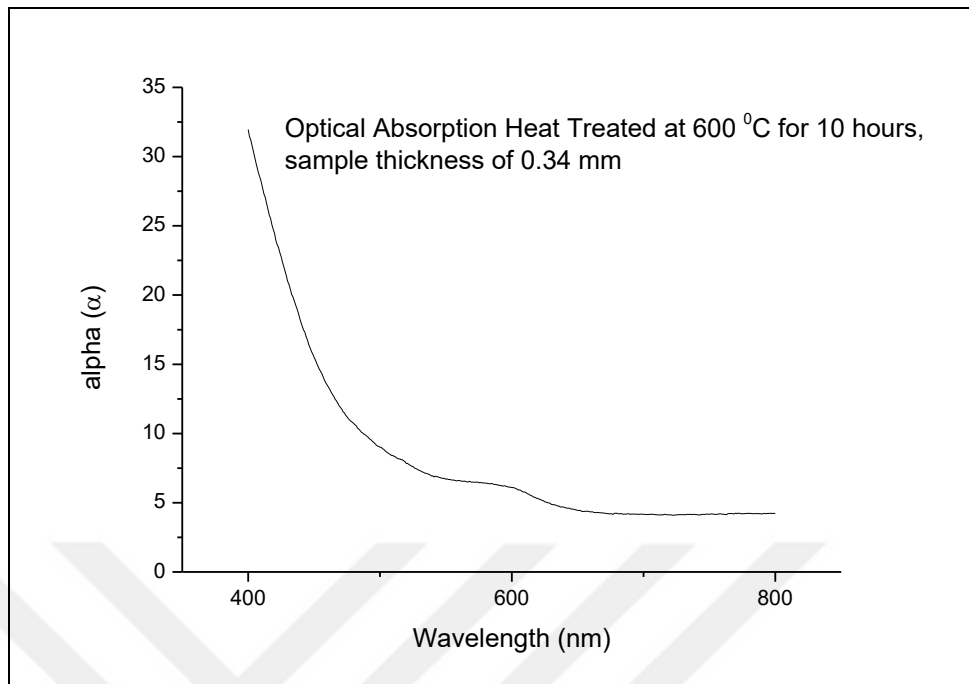


Figure 4.27. Optical absorption heat treated at 600 °C for 10 hours, thickness of 0.34 mm.

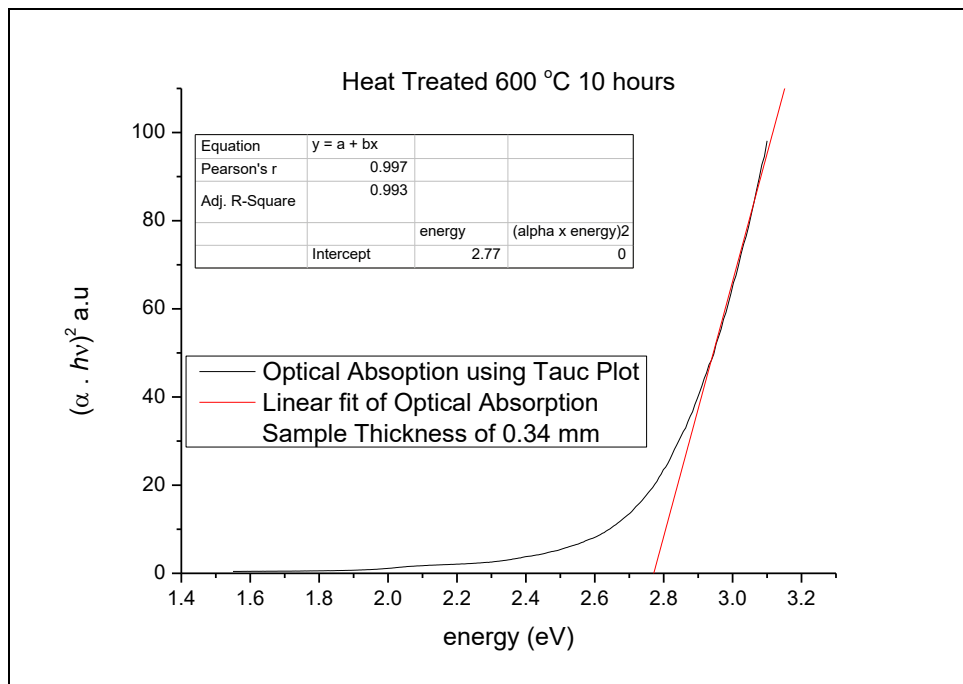


Figure 4.28. Optical absorption using Tauc plot for heat treated at 600 °C for 10 hours.

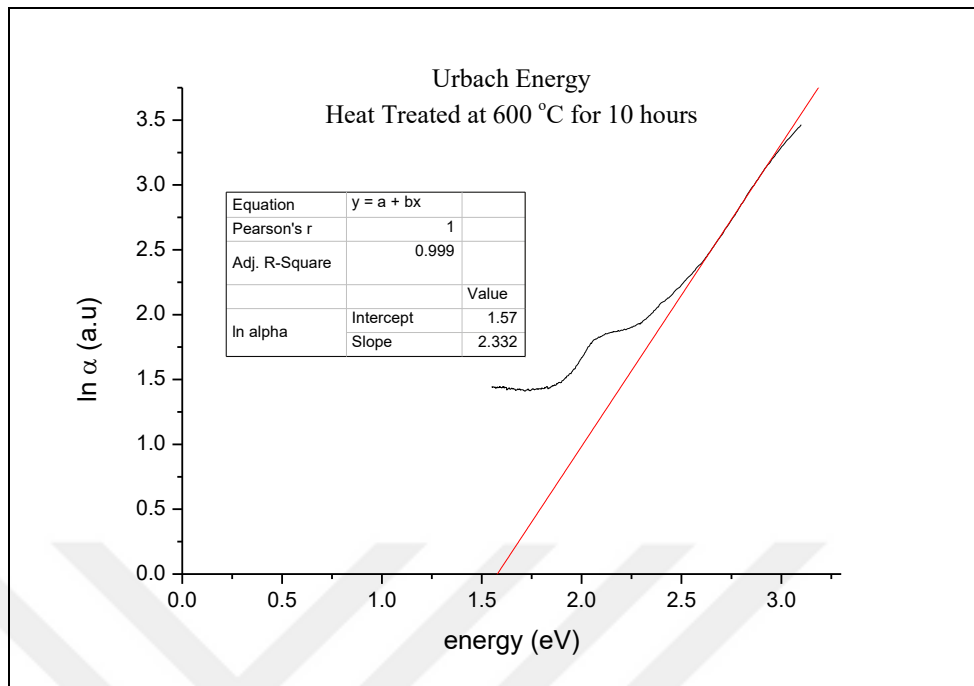


Figure 4.29. Urbach energy heat treated at 600 °C for 10 hours.

From the figures 4.32 to 4.34 heat treated sample for 10 hours with a 0.34 mm thickness is examined in the Figure 4.33 band gap of the sample is 2.77 eV and Urbach energy for the sample is 0.43 eV noted.

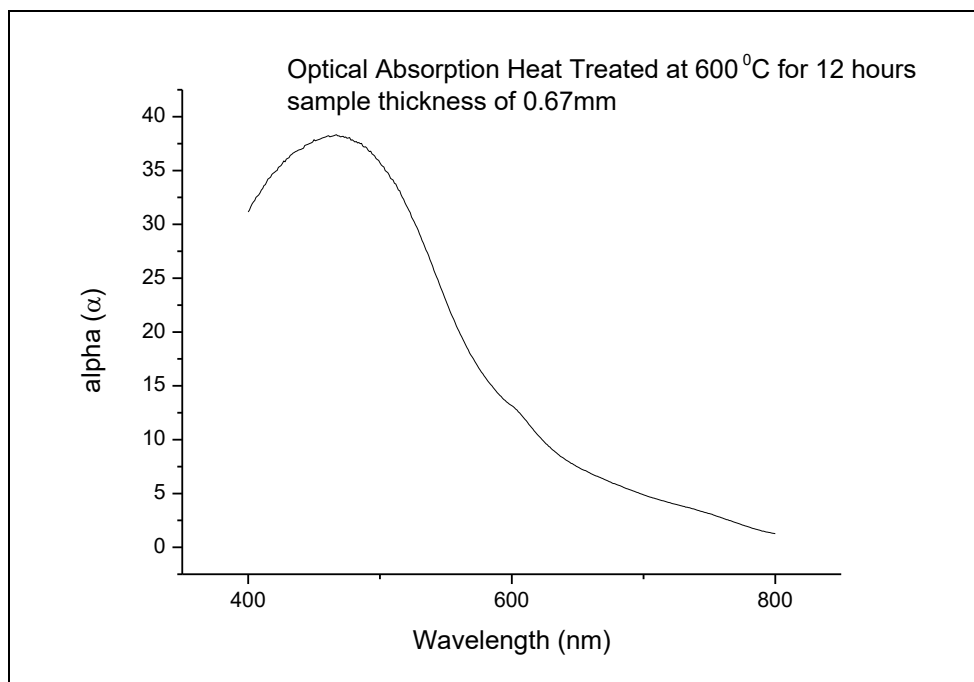


Figure 4.30. Optical absorption heat treated at 600 °C for 12 hours thickness of 0.67mm.

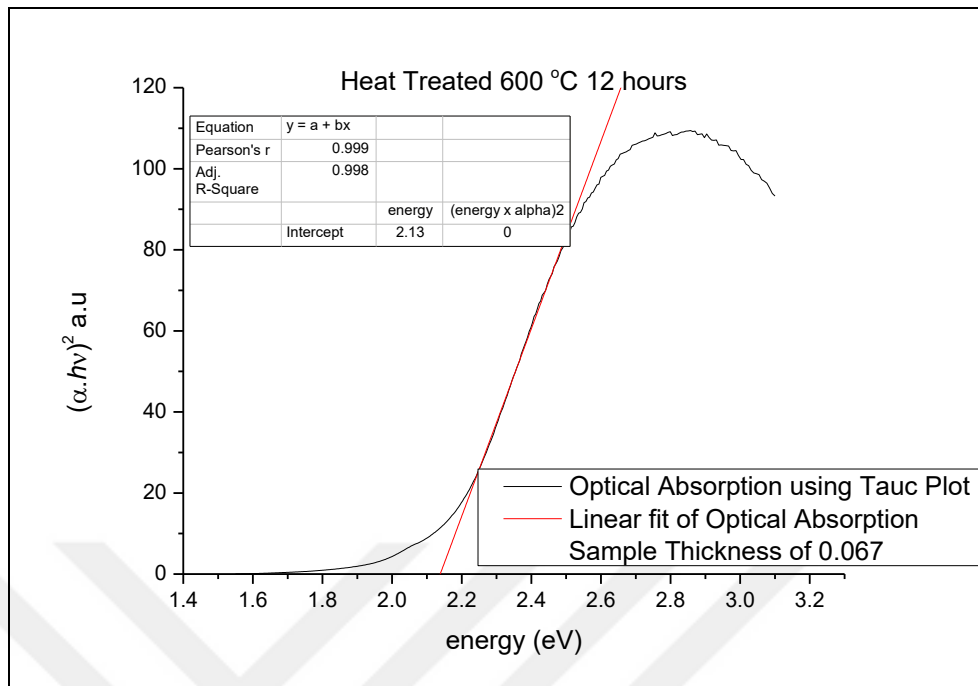


Figure 4.31. Optical absorption using Tauc plot heat treated at 600 °C for 12 hours.

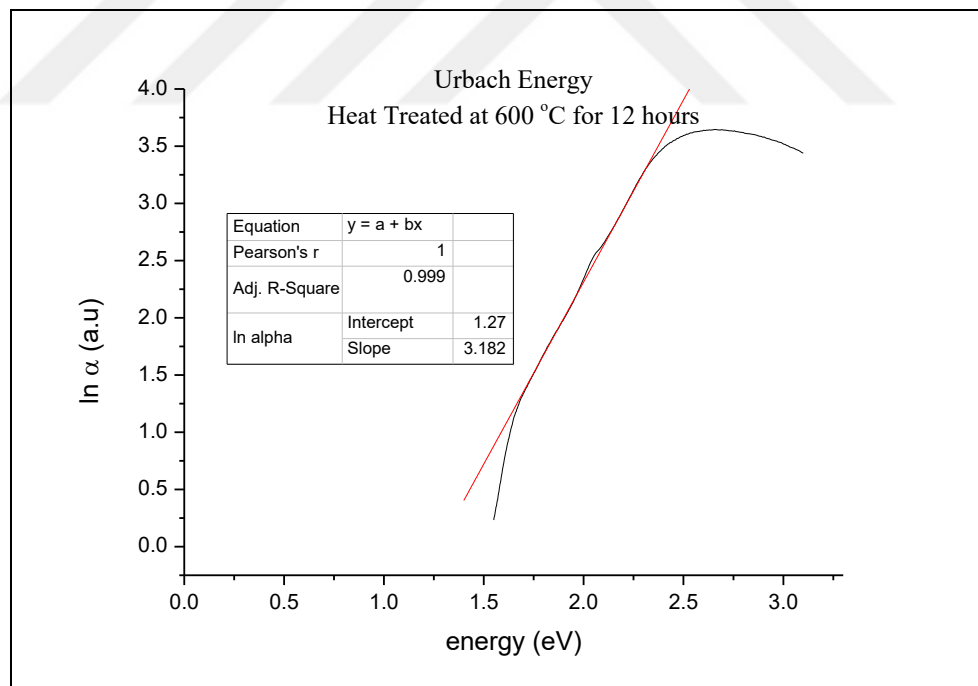


Figure 4.37. Urbach energy heat treated at 600 °C for 12 hours.

From the figure 4.35 to 4.37 heat treated sample for 12 hours with a 0.67 mm thickness is examined in the Figure 4.36 band gap of the sample is 2.13 eV and Urbach energy for the sample is 0.31 eV noted.

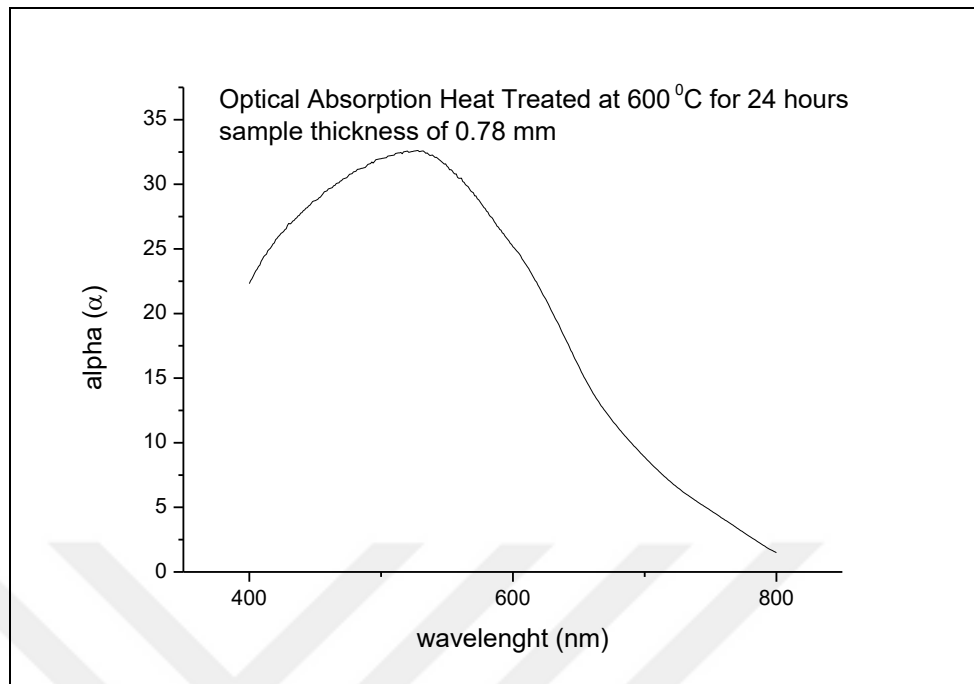


Figure 4.38. Optical absorption heat treated at 600 °C for 24 hours, thickness of 0.78 mm.

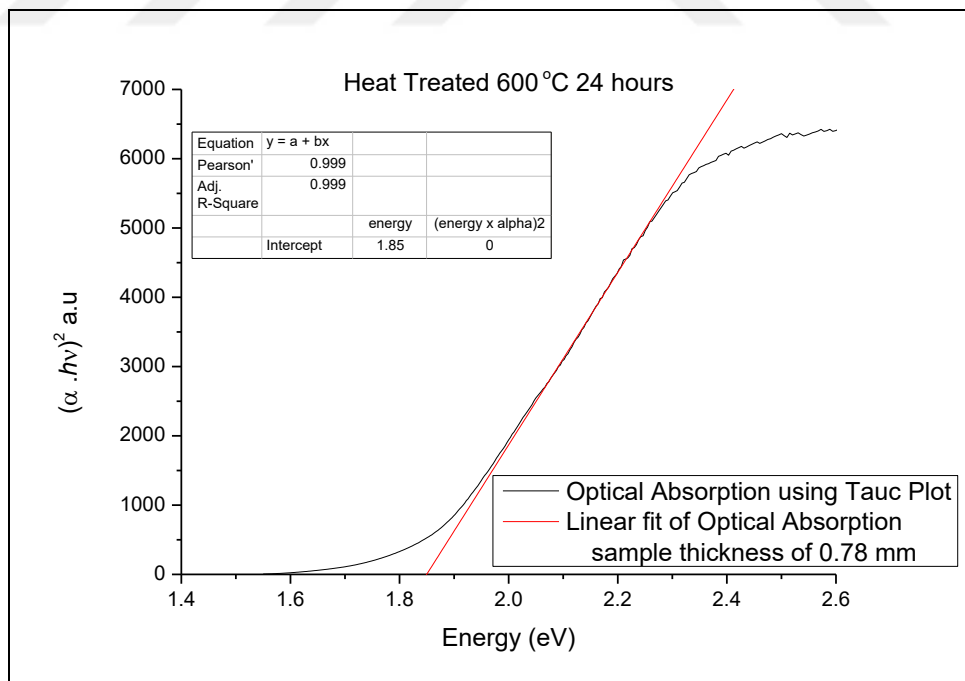


Figure 4.39. Optical absorption using Tauc plot heat treated at 600 °C for 24 hours.

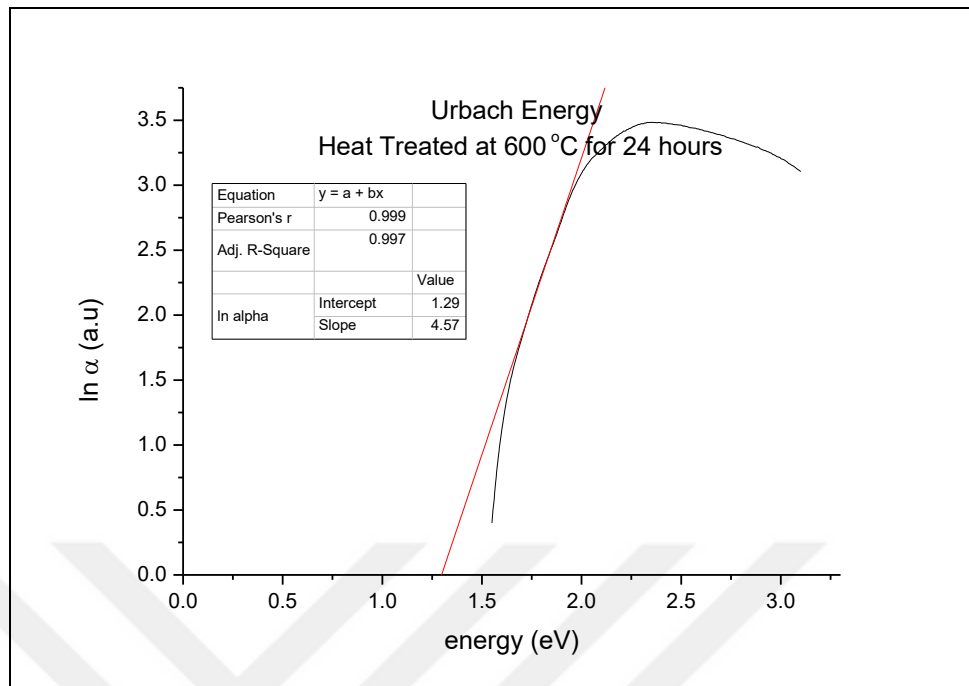


Figure 4.40. Urbach energy heat treated at 600 °C for 24 hours.

From the figures 4.38 to 4.40 heat treated sample for 24 hours with a 0.78 mm thickness is examined in the Figure 4.36 band gap of the sample is 1.85 eV and Urbach energy for the sample is 0.21 eV noted. Using the results above for the heat treated samples for 6, 8, 10, 12 and 24 hours, when the heat treatment time increases the sizes of the nanoparticles are increasing, this can be understood by the increasing band gap energy values. Not only the size of the nano particles is increasing but also the Urbach energies are decreasing. Urbach energy is related with the quality of the amorphous structure, lower urbach energies indicating improvement quality of the amorphous structure. All the results for band gap energy and Urbach energy can be found in Table 4.7.

Table 4.7. Relation between Urbach Energy and Band gap

CdTe / Glass	Temperature (°C)	Time (h)	Band gap (eV)	Urbach (eV)	Thickness (mm)
As Received	Room Temperature	-	1.73	0.04	0.83
Heat Treated	400	2	2.32	0.21	0.57
Melted			2.27	0.24	0.84
Sample 1	600	6	2.74	0.50	0.46
Sample 2	600	8	2.63	0.63	0.62
Sample 3	600	10	2.77	0.43	0.34
Sample 4	600	12	2.13	0.31	0.67
Sample 5	600	24	1.91	0.22	0.78

The samples were characterized by optical absorption, using Tauc plot [59-61]. The radii of the samples are estimated by employing effective mass model in strong confinement limits from the blue shift of asymptotic absorption edge [62,63].

Table 4.8. Radii of the samples.

CdTe / Glass	Temperature (°C)	Time (h)	Radius (nm)	Thickness (mm)
As Received	Room Temperature	-	2.14	0.83
Heat Treated	400	2	2.08	0.57
Melted			2.14	0.84
Sample 1	600	6	1.70	0.46
Sample 2	600	8	1.78	0.62
Sample 3	600	10	1.68	0.34
Sample 4	600	12	2.35	0.67
Sample 5	600	24	2.86	0.78

Urbach Disorder plot for as received and heat treated sample.

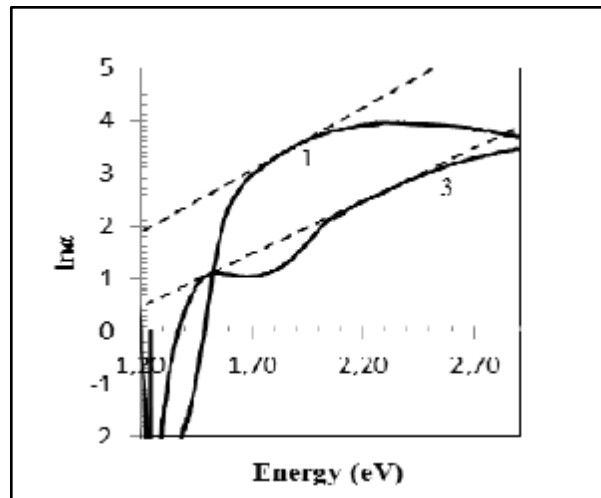


Figure 4.41. $\ln \alpha$ plotted against photon energy for as received sample and heat treated sample. The dashed lines are the linear fits to the straight portion of the data whose slopes give the reciprocal of Urbach energy [36,64].

4.2. DISCUSSION

4.2.1. Phonon Confinement

A typical phonon dispersion graph is shown for a bulk crystal with two atoms per unit cell

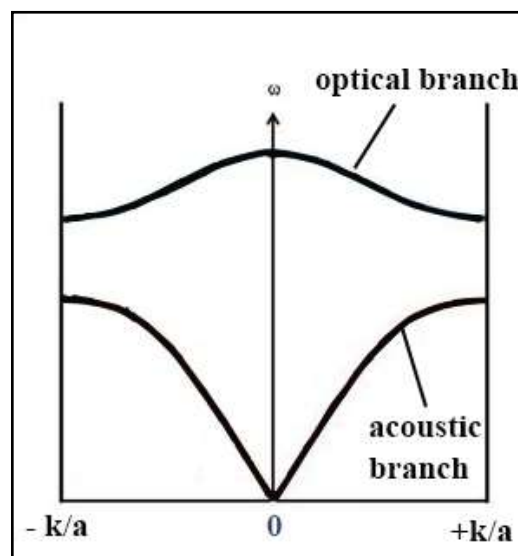


Figure 4.48. phonon dispersion graphic is shown.

The wave number for the laser excitation in the visible frequencies for example for Argon laser $\lambda = 514.5 \text{ nm}$, ($514.5 \times 10^{-7} \text{ cm}$)

$$k_{\text{photon}} \frac{1}{\lambda} = \frac{10^7}{5145} = 20000 \text{ cm}^{-1} = 2 \times 10^4 \text{ cm}^{-1} \quad (4.2)$$

For a zone edge phonon, the wave number

$$k_{\text{phonon}} = \frac{1}{a} = \frac{1}{0.5 \times 10^{-7}} = \frac{10^7}{0.5} = 2 \times 10^7 \text{ cm}^{-1} \quad (4.3)$$

In bulk crystal only zone center phonons are excited since $k_{\text{phonon}} \gg k_{\text{photon}}$, while in nanocrystals

$$\sim R \hbar \Delta k \approx \hbar \quad (4.5)$$

$$\Delta x \cdot \Delta p \approx \hbar \quad (4.4)$$

$$\Delta k = \frac{1}{R} \quad (4.6)$$

For a nanocrystal with radius $R=1 \text{ nm}$, $\Delta k = 1$, $1 \text{ nm} = 10^{-7} \text{ cm}$, $\Delta k \sim k$, $k = 1/10^{-7} = 10^7 \text{ cm}^{-1}$ photon wavenumber becomes comparable to phonon wavenumber. Therefore it is possible to excite zone-edge phonon in a crystal by a laser light in visible region. The fine structure observed in Raman plots at low Raman spectrum values might be due to surface phonons since surface area to volume ratio increases with increasing radius. As the nano crystals mean radius decreases the shift in phonon wave number decreases

$$k = \frac{v}{\lambda} = \frac{v}{v/f} \quad (4.7)$$

4.2.2. Raman Scattering

Raman spectra for melted and quenched to room temperature looks transparent, which means it contains almost no crystalline structure as seen in Figure 4.6 and 4.8. As the heat treatment is initiated a single peak and later a two peak structure reveals as heat treatment goes on. Three representative Raman spectra were chosen to study in detail: i) Figure 4.54 (as received glass), ii) Melted and heat treated at 600 °C for 12 hours in Figure 4.55, iii) Melted and heat treated at 600 °C for 24 hours in Figure 4.56

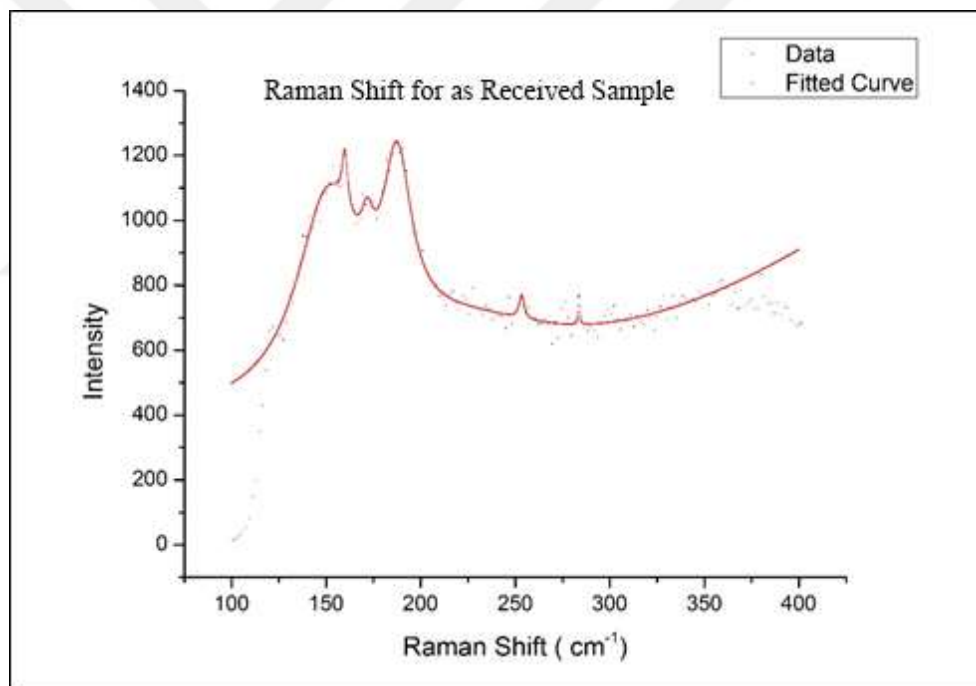


Figure 4.49. Raman shift for as received sample.

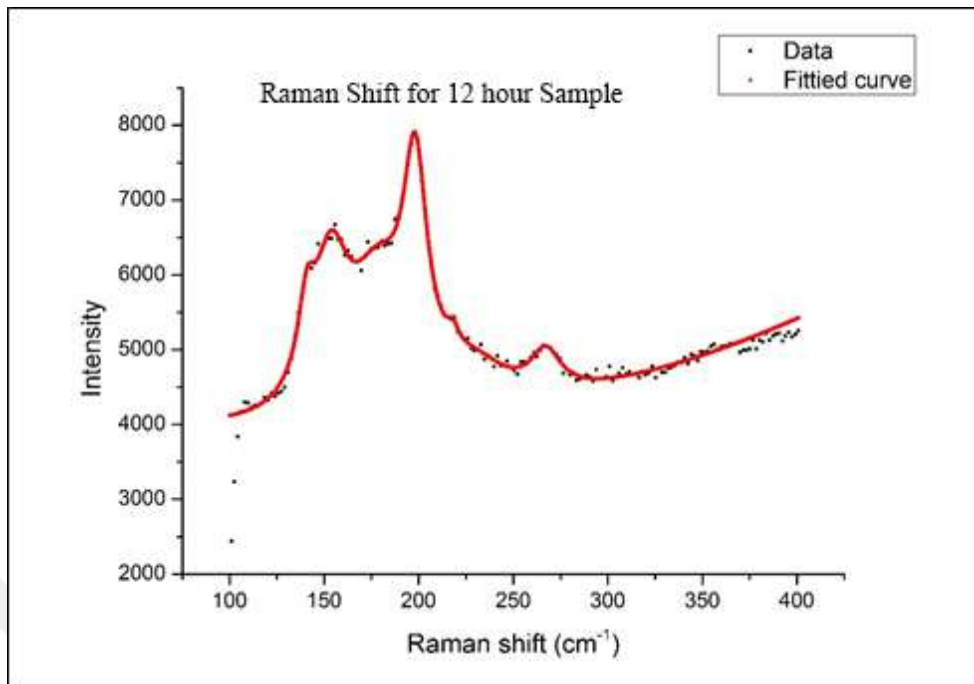


Figure 4.50. Raman Shift for 12 hour sample.

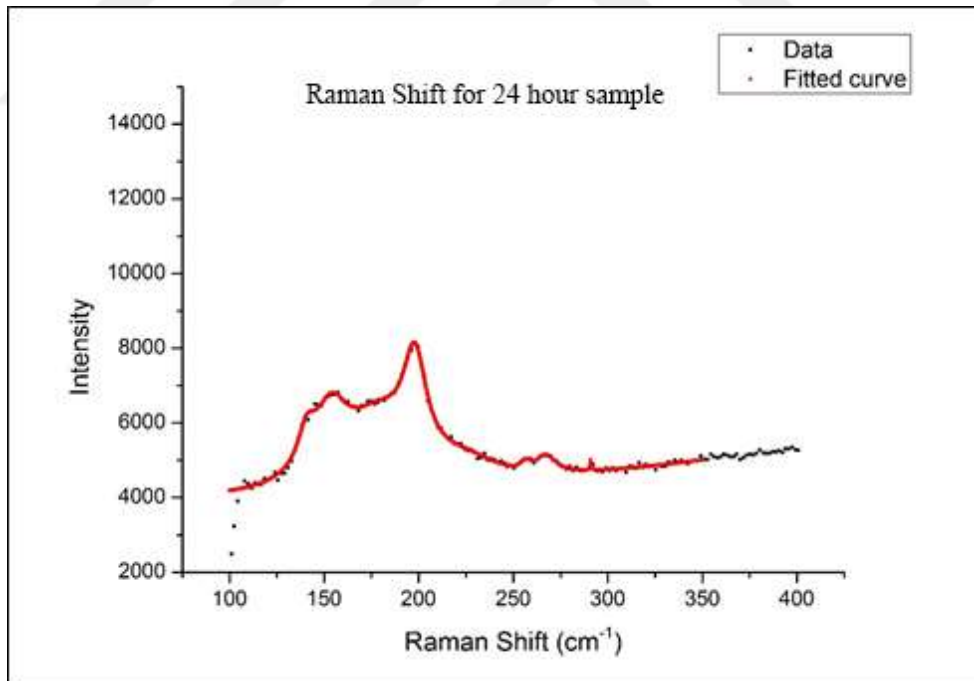


Figure 4.51. Raman shift for 24 hour sample

Fundamental modes in Raman spectra are summarized in Table 4.7 below

Table 4.7. Fundamental modes in Raman spectra

Sample	Raman modes (cm ⁻¹)			
12	140.918	153.638	198.218	267.223
24	140.91	153.698	198.025	267.195
As-received	150.651	159.926	187.596	-

The ternary compound CdTe_{1-x}Se_x displays two mode character in Raman spectra, CdTe like mode at around 160 cm⁻¹ and CdSe like mode at around 190 cm⁻¹. It is proposed in this work that the difference between CdTe and CdSe like modes ($\Delta\omega$) is related to the amount of Se (or Te) in CdTe_{1-x}Se_x nanocrystal as is the case for CdSe_xS_{1-x} which is the well-studied member of ternary group II-VI compounds:

$$X = 0.01944\Delta\omega - 0.25833 \quad (4.8)$$

which was determined by using the data in [65] Table 4.7, assuming linear relation between x and $\Delta\omega$. However the ternary compound Zn_yCd_{1-y}Te displays single mode behavior in Raman spectra: a single peak at around 160 cm⁻¹ for LO₁ mode and around 190 cm⁻¹ for LO₂ mode. The compositional, that is amount of zinc (y) dependence of LO₁ and LO₂ vibrational modes [66].

$$\omega_{LO_1(y)} = -31.322y^2 + 72.169y + 166.73 \quad (4.9)$$

$$\omega_{LO_2(y)} = 13.020y^2 - 25.602y + 166.73 \quad (4.10)$$

It should be noted that CdTe and CdSe like modes for CdTe_{1-x}Se_x crystal and LO₁ and LO₂ modes for Zn_yCd_{1-y}Te overlap. It is not expected that Se content of nanocrystal does change based on previous studies for CdSe_xS_{1-x} [67]. However precipitation of zinc into nanocrystals were observed by other research groups working on Group II-VI nanocrystals. As a result as received filter glass RG 830 contains 35 % Se [52] and according to Equation (4.9) this

gives $\Delta\omega_{\text{expected}} = 31.29 \text{ cm}^{-1}$ for the difference between CdTe and CdSe modes. But the observed value $\Delta\omega_{\text{observed}} = 187.596 - 159.926 = 27.67 \text{ cm}^{-1}$ from table 4.7 for as received sample. The difference between $\Delta\omega_{\text{expected}}$ and $\Delta\omega_{\text{observed}}$ might be due to less Se content in nanocrystals in RG 830. However this figure changes when the as-received glass melted at high temperature and heat treated at around glass transition temperature for 12 and 24 hours. The thermal treatment history of as received glass is unknown but The Raman spectra for these two samples display zinc incorporation into CdTe_{1-x}Se_x nanocrystals during growth because (i) the difference between higher wavenumber and lower wave number modes increases substantially from 27.67 to 44.327 cm⁻¹ and (ii) the Raman intensity of lower wavenumber peak decreases with respect to that of higher wavenumber peak. Equation (4.10) give $y \sim 0.026$, that is $\sim 2.6 \%$ zinc present in nanocrystals. With zinc in it the nanocrystal is to be properly labeled as Zn_yCd_{1-y}Te_{1-x}Se_x.

It is proposed that bulk band gap of Zn_yCd_{1-y}Te_{1-x}Se_x depends on both x and y content of the nanocrystal by the equation

$$E_g (\text{eV}) = 0.35x + 0.75y + 0.27xy + 1.5 \quad (4.11)$$

which gives $E_g = 1.644 \text{ eV}$ for $x = 0.35$ and $y = 0.026$. The optical absorption edge for as received sample is calculated to be 1.74 eV which is 100 meV higher than what is calculated for bulk, yet this is expected due to confinement effect increasing the band gap energy.

5. CONCLUSION

In this thesis work Group II-VI Semiconductor quantum dots were grown in glass matrix by heat treatment at glass transition temperature. The optical transmission and Raman measurements were employed to study the properties of nano crystals. In Raman Spectra vibrational modes are noticed which indicates the precipitation of Zinc into CdTe_{1-x}Se_x nanocrystal during diffusion limited growth. The LO₁ and LO₂ modes at frequencies 150-160cm⁻¹ range shift and their profile are the solid evidence for zinc incorporation into CdTe_{1-x}Se_x nanocrystals. The Raman shifts in LO₁ mode toward lower wave numbers and in LO₂ mode toward upper wave numbers by around 10 cm⁻¹ is clear evidence for the incorporation of Zinc into particles. It should be noted that the shift due to phonon confinement is calculated as 5cm⁻¹ which can not explain alone shifts observed in Raman spectra.

Optical transmission measurements were performed to understand the crystalline disorder through Urbach tail, to estimate size and asymptotic optical absorption edge through the optical absorption. The results indicate that Urbach tail below bandgap is ~23meV for as received sample and it decreases to ~3 meV and ~4 meV for melted and heat treated at 600 °C for 12 hours and 24 hours respectively. The asymptotic absorption edge is calculated as ~1.74 eV for as received sample and it increases to 1.92 eV to 2.13 eV for the samples melted and then heat treated at 600 °C for 12 hours and 24 hours respectively. The increase in bandgap energy is due to both quantum confinement of charged particles and Zinc incorporation to the nano crystals during growth. Optical transmission measurements were performed to estimate average nanocrystal radius, size distribution and to understand the crystalline disorder. The numerical results estimated are summarized below Table 4.8

Table 5.1. Optical transmission measurements

Samples	Raman Scattering Mode (cm ⁻¹)	Asymtotic Absorption	Radius (nm)	Urbach Tail
As Received	150.651	1.73	2.14	1.47
12 hours	153.638	1.91	2.35	1.32
24 hours	153.698	1.85	2.86	1.29

Nanocrystals embedded in glass matrix provide a solid a stable structure up to 250 °C for technological applications in opto-electronics. The results obtained in this work are based on optical studies including optical transmission and Raman scattering measurements. They should be backed by structural measurements such as High Resolution Transmission Electron Microscope and small angle X-ray scattering to asses relative weight of the results and conclusions drown.



REFERENCES

1. Efros A.L. Interband absorption of light in a semiconductor sphere. *Soviet Physical Semiconductor*. 1982; 16: 772-775.
2. Ekimov A.I., Onushchenko A.A.. Quantum size effect in the optical-spectra of semiconductor micro-crystals. *Sov. Phys. Semiconductor*. 1982; 16:775–778.
3. Warnock J., Awschalom D.D., Quantum size effects in simple colored glass *Phys. Rev. B*. 1985; 32 5529(R).
4. Potter B.G., Simmons J.H., Quantum size effects in optical properties of CdS glass composites *Phys Rev. B*. 1988; 37 (18): 10838-10845.
5. Yükselici M.H., Aşıkoğlu Bozkurt A., Allahverdi Ç., Nassar Z., Bulut D., Can Ömür B., Torun M.K., İnce A.T.. Optical and Structural Properties of Quantum Dots, *Low Dimensional and Nanostructured Materials and Devices*, Chapter 14 Springer International Publications, Switzerland, 2016.
6. Taniguchi, N., *On the Basic Concept of 'Nano-Technology*. Proc. Intl. Conf. Prod. London, Part II British Society of Precision Engineering, 1974
7. Drexler, K.E., *Engines of Creation: The Coming Era of Nanotechnology*, Anchor Books, New York 1986
8. S. Iijima. Helical Microtubules of Graphitic Carbon *Nature*. 1991; 354, 56-58.
9. Robert A. Freitas Jr. *Nanomedicine, Volume I: Basic Capabilities* Landes Bioscience Austin Texas, 1999
10. Kumar CSSR editor, Gerion D. Fluorescence imaging in biology using nanoprobe *Nanosystem Characterization Tools in the Life Sciences*. 2006; 1st. Vol. 3: Wiley-VCH; Weinheim, Germany, pp. 1–37.

- 11 Drbohlavova J., Vojtech A., Kizek R., Hubalek J., Quantumdots- Characterization Preparation and Usage in Biological Systems *International Journal of Molecular Sciences*. 2009; 10(2): 656–673.
- 12 Walling MA, Novak J A, Shepard J R E. Quantum dots for live cell and *in vivo* imaging *Int. J. Mol. Sci*. 2009; 10: 441–491.
13. Ekimov A. I., Onushchenko A. A., Quantum size effects in three-dimensional microscopic semiconductor crystals *JETP Lett*. 1981; 34: 345.
14. Flytzanis C., Harbe F., M. Klein C., and Ricard D.. Optics in Complex Systems *The international society for optics and photonics (SPIE)*, 1990 Bellingham.
15. Jain R., Lin R. C. J., Degenerate four-wave mixing in semiconductor-doped glasses *Optical Society America*. 1983; 73: 647.
16. Nozik A. J.. Quantum dot solar cells *Physica E*. 2002; 14: 115-120.
17. Sutherland A. J. Quantum dots as luminescent probes in biological systems *Current Opinion in Solid State and Materials Science*. 2002; 6: 365.
18. Bawendi M. G., Carroll P. J., Wilson W. L., Brus L. E. J. Luminescence properties of CdSe quantum crystallites: Resonance between interior and surface localized states *The Journal of Chemical Physics*. 1992; 96: 946.
19. Hache F., Klein M. C., Ricard D., Flytzanis C., J Photoluminescence study of Schott commercial and experimental CdSSe-doped glasses: observation of surface states *Journal of the Optical Society of America B*. 1991; 8:1802.
20. Ochoa O. R., Colajacomo C., Witkowski E. J., Simmons J. H., Potter B. G. Quantumconfinement effects on the photoluminescence spectra of CdTe nanocrystallites *Solid State Communications*. 1996; 98: 717.

21. Torun M. K., İnce A.T., Yükselici M.H.. The compositional dependence of the structural disorder in $Zn_xCd_{1-x}Te$ quantum dots grown in glass studied through optical transmission and resonant Raman spectroscopies. *10th Nanoscience and Nano Technology Conference* Istanbul, 17-21 June 2014.
22. Gaponenko S.V.. *Optical properties of semiconductor nanocrystals*, Cambridge University Press, Cambridge, 1998.
23. Alivisatos, A.P. Perspectives on the physical chemistry of semiconductor nanocrystals. *The Journal of Physical Chemistry*. 1996; 100:13226–13239.
24. Dow J.D.. Toward a unified theory of Urbach's rule and exponential absorption edges *Physical Review B*. 1972; 5:2.
25. Urbach F.. The long- wavelength edge of photographic sensitivity and of the electronic absorption solids *Physical Review*. 1953; 92:1324.
26. Miller, David A. B. Optical Physics of Quantum Wells, *Quantum Dynamics of Simple Systems*. 1994; pages 239-267, NATO advanced study institute.
27. Brus E. L. Quantum Crystallites and Nonlinear Optics, *Applied Physics A*. 1991; 53: 465-474.
28. Kittel C. *Introduction to solid state physic*, John Wiley & Sons, USA, 2005
29. Yoffe A.D.,. Low-dimensional systems: quantum size effects and electronic properties of semiconductor microcrystallites (zero-dimensional systems) and some quasi-two-dimensional systems. *Advances in Physics*. 1993; 42:173-262.
30. Birşey E. A study of linear and nonlinear refractive index changes and optical absorptions in quantum dots Master thesis Yeditepe University, 2014.

31. Zhang L. and Xie H.J., Electric field effect on the second-order nonlinear optical properties of parabolic and semiparabolic quantum wells, *Mod. Phys lett B*. 2003; 68 235315.
32. Ahn D. and Chuang S.L, Calculation of linear and non linear inter subband optical absorptions in a quantum well model with an applied electric field *IEEE J. Quantum Electron*. 1987; QE-23 2196-2204.
33. Bell W.W., *Special Functions for Scientist and Engineers*, London, princeton; 1968.
34. Arfken H.J., Weber G.B, *Mathematical Methods for physics*, Academic press, elsevier , 2005.
35. Lifshitz V, I M and Slyozov V. The kinetics of precipitation from supersaturated solid solutions. *Journal of Physics and Chemistry of Solids*. 1961; 19:35-50.
36. İnce A. T., Torun M.K., Yükselici M.H.. An Urbach Study of the Degree of Structural Disorder in CdTe Nanocrystals in Glass Matrix. *International Conference on Oxide Materials for Electronic Engineering-Fabrication, properties and application (OMEE)*, Lviv, 2012.
37. Tauc, J. Optical properties and electronic structure of amorphous Ge and Si. *Mater. Res. Bull*. 1968; 3, 37–46.
38. Khan A. F., Mehmood M., Anwar M. R., Taj M. , Effect of annealing on structural, optical and electrical properties of nanostructured Ge thin films, *Applied Surface Science*. 2010; 256, 2031–2037.
39. Jeon J.W, Jeon D. W, Sahoo T., Kim M, Baek J.H , Hoffman J. L. , Kim N. S, Le I.H., Effect of annealing temperature on optical band-gap of amorphous indium zinc oxide film, *Journal of Alloys and Compounds*. 2011; 509 10062–10065.

- 40 Prem Kumar T., Saravanakumar S. , Sankaranarayanan K., Effect of annealing on the surface and band gap alignment of CdZnS thin films, *Applied Surface Science*. 2011; 257, 1923–1927.
- 41 Kazuo Morigaki, *Amorphous Semiconductors Structural, Optical, and Electronic Properties*, John Wiley & Sons, Ltd. West Sussex, 2017.
42. Studenyak I., Kranjčec M., Kurik M. Urbach Rule in Solid State Physics. *International Journal of Optics and Applications*, 2014; 4:76-83.
- 43 Urbach F. *Phys Rev* 92. 1953; 1324
- 44 Cody G D, Tiedje T, Abeles B, Brooks B and Goldstein Y *Phys. Rev. Lett.* 1981; 47 1480–3.
45. Larkin P. *Infrared and Raman Spectroscopy, Principles and Spectral Interpretation*, Elsevier Inc. Stamford, 2011.
46. Smith E., Dent G..*Modern Raman Spectroscopy-A Practical Approach*, John Wiley & Sons, Ltd. The Atrium, Southern Gate West Sussex, 2005
47. Perkampus H. H.. *UV-VIS Spectroscopy and Its Applications*, Springer-Verlag Berlin Heidelberg, 1992.
48. E.C.F. da Silva, D. Strauch. *Landolt-Börnstein Semiconductors Subvolume E*, Springer-Verlag Berlin Heidelberg, April, 2012.
49. Romčević N ,Romčević M. , Kostić R. , Stojanović D., Karczewski B. G., Galazka R. Raman spectra of CdTe/ZnTe self-assembled quantum dots. *Microelectronics Journal*. 2009; 40:830–831.
50. Milekhin A. G., Sveshikova L.L., Repinskiĭ S.M., Gutakovskii A.K.,Friedrich M, Zahn, D.R.T. Optical Vibration Modes in (Cd, Pb, Zn)S Quantum Dots in the Langmuir-Blodgett Matrix. *Physics of Solid State*. 2002; 44:1976-1980.

51. Barron T.H.K. Grüneisen Parameters for the Equation of State Solids. *Annals of Physics*. 1957; 1:77-90
52. Spagnolo V., Scamarcio G., Lugara M., Righini G. C.. Raman scattering in CdTe $_{1-x}$ Se x and CdS $_{1-x}$ Se x nanocrystals embedded in glass. *Superlattices and Microstructures*. 1994; 16:51–54
53. Begum N, Bhatti A.S, Jabeen F, Rubini S, Martelli F, Phonon confinement effect in III-V nanowires, *Nanowires*. 2010
54. Chandra S.. Shooting method in solving quantum structure related problems Master Thesis Jadavpur University 2013.
55. Killingbeck J.. Shooting methods for the Schrödinger equation. *J. Phys A:Math.Gen.* 1986; 20:1411-1417.
56. Hugdal H. G., Berg P. Numerical determination of the eigenenergies of the Schrödinger equation in one dimension. *European Journal of Physics*. 2015; 36:045013.
57. Colomban Ph., Slodczyk A. Raman intensity, An important tool to study the structure and phase transitions of amorphous/crystalline materials *Optical Materials* 2009; 31 1759–1763.
58. Colomban Ph., Romain F., Neiman A., Animitsa I., *Solid State Ionics*. 2001; 145,339,
59. El-Nahass M.M., Youssef G.M., Noby S.Z. Structural and optical characterization of CdTe quantum dots thin films *Journal of Alloys and Compounds*, 2014; 604:253–259.
60. Tauc J.. *Amorphous and Liquid Semiconductors*, Plenum Press, London Newyork, 1974.

61. Ghobadi N. Band gap determination using absorption spectrum fitting procedure *International Nano Letters*.2013; 3:2.
62. Rakhshani A.E., Al-Azab A.S.. Characterization of CdS films prepared by chemical bath deposition *Journal of Physics: Condens. Matter*. 2000; 12:8745-8755.
63. Marple D.T.F., Optical absorption edge in CdTe: Experimental, *Phys. Rev.* 1966;150:728-734.
64. Nozik A.J., Quantum dot solar cells, *Physica E*. 2002; 14:115-120.
65. Gorska M., Nazarewic W. Application of the Random-Element Isodisplacement Model to Long Wavelength Optical Phonons in CdSe_xTe_{1-x} Mixed Crystals. *Physica Status Solidi*. 1974; 65:193-202.
66. Yukselici M.H., Allahverdi C., Athalin H.. Zinc incorporation into CdTe quantum dots in glass. *Materials Chemistry and Physics*. 2010; 119:218–221.
67. Mei G., A photoluminescence study of CdSe_xS_{1-x} semiconductor quantum dots. *J. Phys.*1992; *Condens. Matter* 4: 7521.

APPENDIX A: Matlab Algorithms

```

function varargout = interpolater(varargin)
gui_Singleton = 1;
gui_State = struct('gui_Name',       mfilename, ...
                  'gui_Singleton',  gui_Singleton, ...
                  'gui_OpeningFcn', @interpolater_OpeningFcn, ...
                  'gui_OutputFcn',  @interpolater_OutputFcn, ...
                  ...
                  'gui_LayoutFcn',  [] , ...
                  'gui_Callback',   []);
if nargin && ischar(varargin{1})
    gui_State.gui_Callback = str2func(varargin{1});
end

if nargout
    [varargout{1:nargout}] = gui_mainfcn(gui_State,
varargin{:});
else
    gui_mainfcn(gui_State, varargin{:});
end

function interpolater_OpeningFcn(hObject, eventdata, handles,
varargin)
handles.output = hObject;
guidata(hObject, handles);
global anm_int; global ToplameV1_int; global ToplameV2_int;
global ToplameV3_int; global ToplameV4_int; global
ToplameV5_int; global En_int;
global h1;
load('interpolatedata.mat');
axes(handles.axes1);
h1=plot(anm_int,ToplameV1_int,anm_int,ToplameV2_int,anm_int,T
oplameV3_int, ...

anm_int,ToplameV4_int,anm_int,ToplameV5_int,anm_int,En_int);
set(handles.axes1,'xtick',[0:0.1:5]);
xlim([0 5]); % X eksen sÄ±nÄ±rÄ±nÄ± buradan
degistirebilirsin
grid on;
grid minor;
set(h1(:),'LineWidth',2);
h=legend('TotaleV1','TotaleV2','TotaleV3','TotaleV4','TotaleV
5','En');
xlabel('a (nm)');
ylabel('Energy (eV)');

```

```
function varargout = interpolater_OutputFcn(hObject,  
eventdata, handles)  
varargout{1} = handles.output;
```

```
function edit1_Callback(hObject, eventdata, handles)
```

```
function edit1_CreateFcn(hObject, eventdata, handles)  
if ispc && isequal(get(hObject, 'BackgroundColor'),  
get(0, 'defaultUicontrolBackgroundColor'))  
    set(hObject, 'BackgroundColor', 'white');  
end
```

```
function edit2_Callback(hObject, eventdata, handles)
```

```
function edit2_CreateFcn(hObject, eventdata, handles)  
  
if ispc && isequal(get(hObject, 'BackgroundColor'),  
get(0, 'defaultUicontrolBackgroundColor'))  
    set(hObject, 'BackgroundColor', 'white');  
end
```

```
function edit3_Callback(hObject, eventdata, handles)
```

```
function edit3_CreateFcn(hObject, eventdata, handles)  
if ispc && isequal(get(hObject, 'BackgroundColor'),  
get(0, 'defaultUicontrolBackgroundColor'))  
    set(hObject, 'BackgroundColor', 'white');  
end
```

```
function edit4_Callback(hObject, eventdata, handles)
```

```
function edit4_CreateFcn(hObject, eventdata, handles)  
if ispc && isequal(get(hObject, 'BackgroundColor'),  
get(0, 'defaultUicontrolBackgroundColor'))  
    set(hObject, 'BackgroundColor', 'white');  
end
```

```

function edit5_Callback(hObject, eventdata, handles)

function edit5_CreateFcn(hObject, eventdata, handles)
if ispc && isequal(get(hObject,'BackgroundColor'),
get(0,'defaultUicontrolBackgroundColor'))
    set(hObject,'BackgroundColor','white');
end

function edit6_Callback(hObject, eventdata, handles)

function edit6_CreateFcn(hObject, eventdata, handles)
if ispc && isequal(get(hObject,'BackgroundColor'),
get(0,'defaultUicontrolBackgroundColor'))
    set(hObject,'BackgroundColor','white');
end

function pushbutton1_Callback(hObject, eventdata, handles)
global anm_int; global ToplameV1_int; global ToplameV2_int;
global ToplameV3_int; global ToplameV4_int; global
ToplameV5_int; global En_int;
global h1;
userinput=str2double(get(handles.edit1,'String'));
fark1=abs(anm_int-userinput);
set(handles.edit2,'String',num2str(ToplameV1_int(find(fark1
== min(abs(anm_int-userinput))))));
fark2=abs(anm_int-userinput);
set(handles.edit3,'String',num2str(ToplameV2_int(find(fark2
== min(abs(anm_int-userinput))))));
fark3=abs(anm_int-userinput);
set(handles.edit4,'String',num2str(ToplameV3_int(find(fark3
== min(abs(anm_int-userinput))))));
fark4=abs(anm_int-userinput);
set(handles.edit5,'String',num2str(ToplameV4_int(find(fark4
== min(abs(anm_int-userinput))))));
fark5=abs(anm_int-userinput);
set(handles.edit6,'String',num2str(ToplameV5_int(find(fark5
== min(abs(anm_int-userinput))))));
fark6=abs(anm_int-userinput);
set(handles.edit7,'String',num2str(En_int(find(fark6 ==
min(abs(anm_int-userinput))))));

function edit7_Callback(hObject, eventdata, handles)

function edit7_CreateFcn(hObject, eventdata, handles)
if ispc && isequal(get(hObject,'BackgroundColor'),
get(0,'defaultUicontrolBackgroundColor'))
    set(hObject,'BackgroundColor','white');
end

```

```

function uipushtool1_ClickedCallback(hObject, eventdata, handles)
set(gcf,'Name','Save Image As')
[FileName,PathName] = uiputfile({'*.png'},'Save Image As')
imwrite(F.cdata,[PathName FileName])

function pushbutton2_Callback(hObject, eventdata, handles)
set(handles.edit1,'String','');
set(handles.edit2,'String','');
set(handles.edit3,'String','');
set(handles.edit4,'String','');
set(handles.edit5,'String','');
set(handles.edit6,'String','');
set(handles.edit7,'String','');

function pushbutton3_Callback(hObject, eventdata, handles)
global anm_int; global ToplameV1_int; global ToplameV2_int;
global ToplameV3_int; global ToplameV4_int; global
ToplameV5_int; global En_int;
global h1;
set(handles.edit1,'String','');
set(handles.edit3,'String','');
set(handles.edit4,'String','');
set(handles.edit5,'String','');
set(handles.edit6,'String','');
set(handles.edit7,'String','');
userinput=str2double(get(handles.edit2,'String'));
fark1=abs(ToplameV1_int-userinput);
set(handles.edit1,'String',num2str(anm_int(find(fark1 ==
min(abs(ToplameV1_int-userinput))))));

function pushbutton4_Callback(hObject, eventdata, handles)
global anm_int; global ToplameV1_int; global ToplameV2_int;
global ToplameV3_int; global ToplameV4_int; global
ToplameV5_int; global En_int;
global h1;
set(handles.edit1,'String','');
set(handles.edit2,'String','');
set(handles.edit4,'String','');
set(handles.edit5,'String','');
set(handles.edit6,'String','');
set(handles.edit7,'String','');
userinput=str2double(get(handles.edit3,'String'));
fark1=abs(ToplameV2_int-userinput);
set(handles.edit1,'String',num2str(anm_int(find(fark1 ==
min(abs(ToplameV2_int-userinput))))));

function pushbutton5_Callback(hObject, eventdata, handles)
global anm_int; global ToplameV1_int; global ToplameV2_int;

```

```

global ToplameV3_int; global ToplameV4_int; global
ToplameV5_int; global En_int;
global h1;
set(handles.edit1,'String','');
set(handles.edit2,'String','');
set(handles.edit3,'String','');
set(handles.edit5,'String','');
set(handles.edit6,'String','');
set(handles.edit7,'String','');
userinput=str2double(get(handles.edit4,'String'));
fark1=abs(ToplameV3_int-userinput);
set(handles.edit1,'String',num2str(anm_int(find(fark1 ==
min(abs(ToplameV3_int-userinput))))));

function pushbutton6_Callback(hObject, eventdata, handles)
global anm_int; global ToplameV1_int; global ToplameV2_int;
global ToplameV3_int; global ToplameV4_int; global
ToplameV5_int; global En_int;
global h1;
set(handles.edit1,'String','');
set(handles.edit2,'String','');
set(handles.edit3,'String','');
set(handles.edit4,'String','');
set(handles.edit6,'String','');
set(handles.edit7,'String','');
userinput=str2double(get(handles.edit5,'String'));
fark1=abs(ToplameV4_int-userinput);
set(handles.edit1,'String',num2str(anm_int(find(fark1 ==
min(abs(ToplameV4_int-userinput))))));

function pushbutton7_Callback(hObject, eventdata, handles)
global anm_int; global ToplameV1_int; global ToplameV2_int;
global ToplameV3_int; global ToplameV4_int; global
ToplameV5_int; global En_int;
global h1;
set(handles.edit1,'String','');
set(handles.edit2,'String','');
set(handles.edit3,'String','');
set(handles.edit4,'String','');
set(handles.edit5,'String','');
set(handles.edit7,'String','');
userinput=str2double(get(handles.edit6,'String'));
fark1=abs(ToplameV5_int-userinput);
set(handles.edit1,'String',num2str(anm_int(find(fark1 ==
min(abs(ToplameV5_int-userinput))))));

function pushbutton8_Callback(hObject, eventdata, handles)
global anm_int; global ToplameV1_int; global ToplameV2_int;
global ToplameV3_int; global ToplameV4_int; global
ToplameV5_int; global En_int;

```

```
global h1;
set(handles.edit1,'String','');
set(handles.edit2,'String','');
set(handles.edit3,'String','');
set(handles.edit4,'String','');
set(handles.edit5,'String','');
set(handles.edit6,'String','');
userinput=str2double(get(handles.edit7,'String'));
fark1=abs(En_int-userinput);
set(handles.edit1,'String',num2str(anm_int(find(fark1 ==
min(abs(En_int-userinput))))));
```



APPENDIX B: Schott Data Sheet

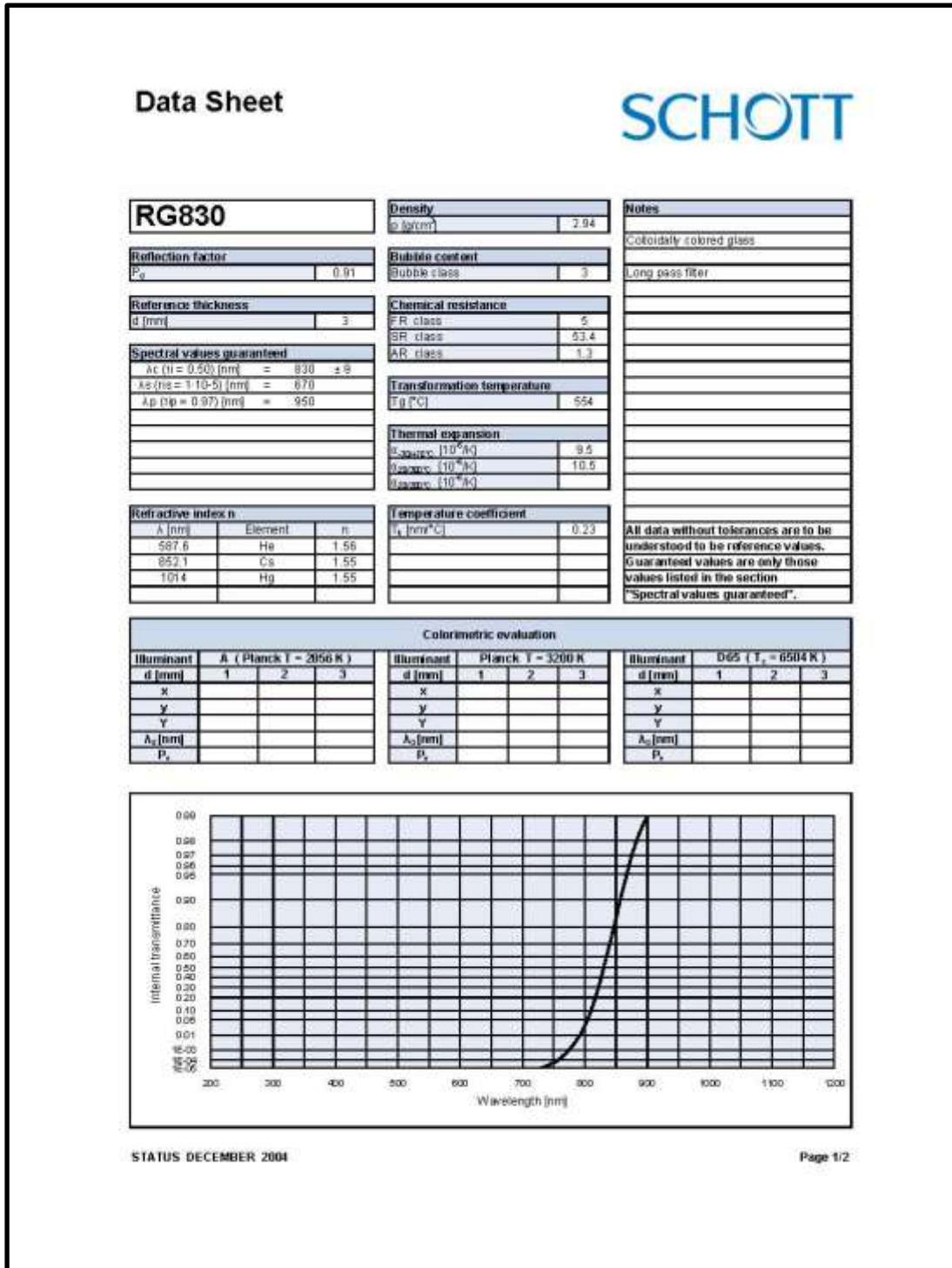


Figure B.1. RG 830 Data Sheet

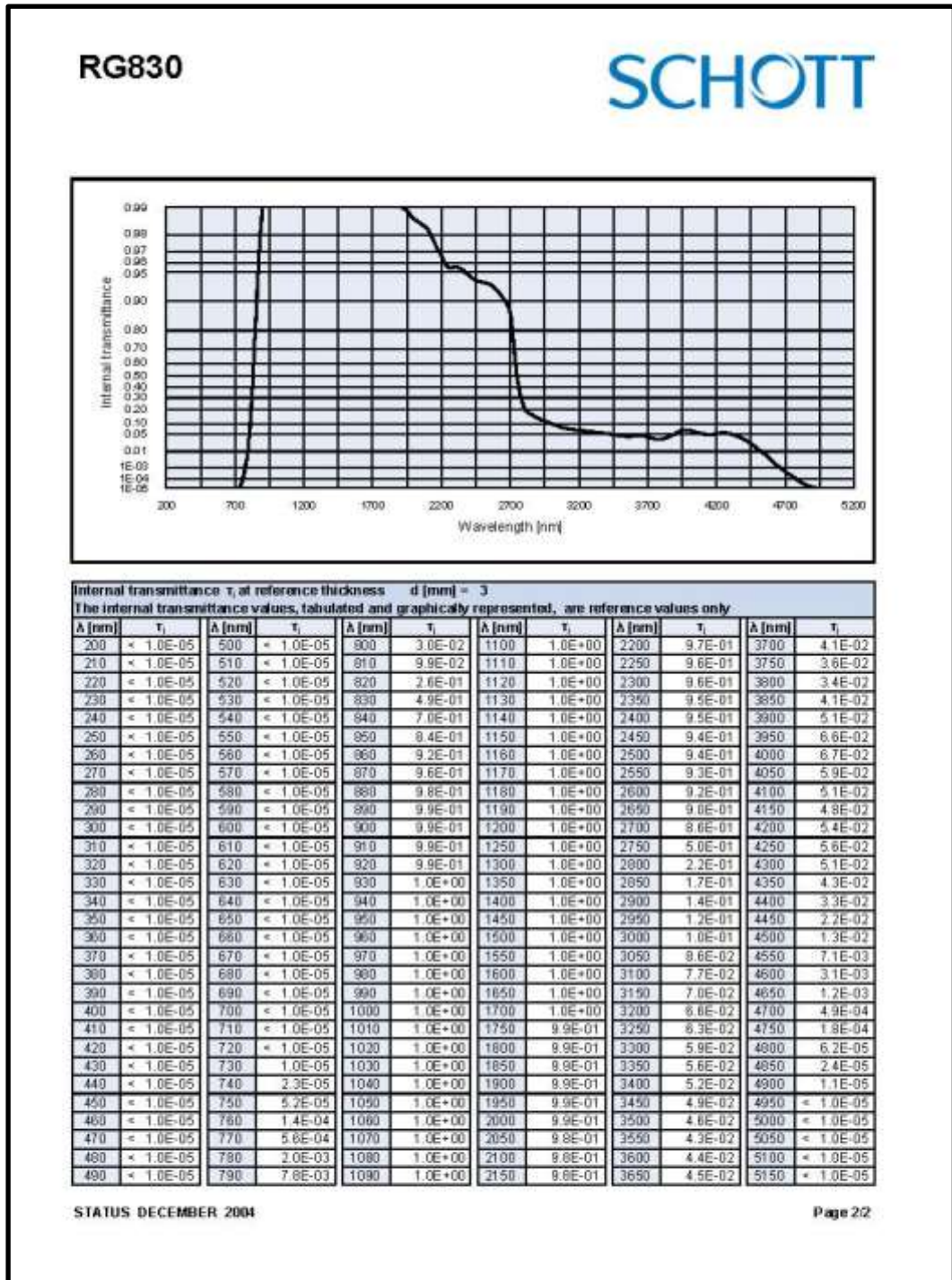


Figure B.2. RG 830 Internal Transmittance vs Wavelength(nm) graph

APPENDIX C: Oriel Monochromator Specifications

MCS130 CORNERSTONE 130 MONOCHROMATORS 42	
13 SPECIFICATIONS	
General Specifications	
Focal Length	130 mm
F/#	F/3.7
Wavelength Selection	Motorized
Usable Wavelength Range	180 to 2500 nm, grating dependent
Spectral Resolution	Grating dispersion and slit width dependent
Wavelength Accuracy	0.50 nm
Wavelength Precision	0.11 nm
Maximum Slew Rate	350 nm/s with 1200 line/mm grating
Stray Light	0.03%
Ports	1 input port, 1 output port
Shutter Control	Software, Hand Controller, low-level commands
Shutter minimum exposure	0.2 s
Shutter maximum repetition	0.5 Hz
Motorized Filter Wheel	Filter Wheel Model 74010, Apex2 Filter Wheel
Utility Software Requirements	Windows 7 32-bit or 64-bit operating system (Windows XP compatible software also available)
TracQ Basic Software Compatible	Yes
74009 Hand Controller Compatible	Yes
100-240 VAC, 47-63 Hz	100-240 VAC, 47-63 Hz
Weight	6.9 lb [3 kg]
Micrometer Adjustable Slit Specifications	
Width Range	4 μm to 3 mm
Height Range	3 mm to 12 mm
Repeatability	$\pm 10 \mu\text{m}$
Accuracy	$\pm 10 \mu\text{m}$ (width from 4 μm to 250 μm) $\pm 5\%$ (width from 250 μm to 3 mm)
<p>Wavelength Accuracy: The capability of the monochromator to output the desired wavelength.</p> <p>Wavelength Precision: The ability of a wavelength to be consistently reproduced and the number of significant digits to which it has been reliably measured.</p>	

Figure C.1. Oriel Monochromator Specifications

APPENDIX D: Monochromator Calibration Process

11.2 SETTING THE WAVELENGTH OFFSET

A wavelength offset is used to shift the wavelength position to either a higher or a lower wavelength. For example, if a HeNe laser operating at 632.8 nm is sent through the monochromator and the output is visible when the monochromator is set to 640 nm, an offset can be introduced.

When performing this procedure, it is necessary to use a light source with a known spectral line appearing within the operating range of the grating. Oriel offers a number of pencil calibration lamps for this purpose, such as the model 6035 Hg lamp. Another line source such as a laser may also be used. Always be sure to follow the appropriate safety precautions when dealing with any light source.

Procedure:

1. Select a radiation source that has at least one narrow spectral line in the wavelength region of interest.
2. Select a detector with an operating range appropriate for the spectral line.
3. Focus the radiation onto the entrance slit (the monochromator is F/3.7). Note that a narrower slit provides greater resolution.
4. Ensure the focused beam is parallel to the monochromator's optical axis.
5. Command the monochromator to select the grating for which the offset is to be applied.
6. Use the STEP command to move the grating position until the spectral line is visible at the output.
7. Use the CALIBRATE command to enter the exact wavelength of the spectral line. The Cornerstone wavelength offset has now been entered into memory. This offset applies to all other wavelength positions when using this grating.
8. Repeat the process for the second grating, if required.

Figure D.1. Monochromator Calibration procedure

APPENDIX E: Calibration Certificate of Thermocouple




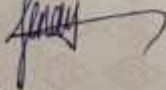
TÜRKAK TÜRK AKREDİTASYON KURUMU TURKISH ACCREDITATION AGENCY tarafından akredite edilmiş TÜRK STANDARLARI ENSTİTÜSÜ KALİBRASYON MERKEZİ BAŞKANLIĞI	
	
Kalibrasyon Sertifikası Calibration Certificate	
 AB-0002-K 1150996 08.11	
Cihazın Sahibi/Adresi <i>Customer/Address</i>	Yeditepe Üniversitesi Fizik Bölümü Yukal Metroloji ve Kal.Lab. Sıcaklık Kalibrasyon Lab. Kayışdağı İnönü Mah. Membap Sok. Yeditepe Üniversitesi Kampüsü
İstek Numarası <i>Order No</i>	1261/1
Makine/Cihaz <i>Instrument/Device</i>	ISILCIFT
İmalatçı <i>Manufacturer</i>	HART SCIENTIFIC
Tip <i>Type</i>	5650
Seri Numarası <i>Serial Number</i>	9294
Kalibrasyon Tarihi <i>Date of Calibration</i>	19.08.2011
Sertifikanın Sayfa Sayısı <i>Number of pages of the Certificate</i>	6
<p>Bu kalibrasyon sertifikası, Uluslararası Birimler Sisteminde (SI) tanımlanmış birimleri realize eden ulusal ölçüm standartlarına idare edilebilirliği belgeleyen belge.</p> <p>This calibration certificate documents the traceability to national standards which realize the unit of measurement according to the International System of Units (SI).</p> <p>Kalibrasyon sertifikalarının tanınması konusunda Türk Akreditasyon Kurumu (TÜRKAK) ile Avrupa Akreditasyon Birliği (EA) ve Uluslararası Laboratuvar Akreditasyon Birliği (ILAC) arasında karşılıklı tanıma anlaşması imzalanmıştır.</p> <p>Turkish Accreditation Agency (TÜRKAK) is signatory to the multilateral agreements of the European co-operation for the Accreditation (EA) and of the International Laboratory Accreditation (ILAC) for the mutual recognition of calibration certificates.</p> <p>Bu sertifikanın tamamlayıcı kısmı olan ölçüm sonuçları, genişletilmiş ölçüm belirlenimleri ve kalibrasyon metodları takip eden sayfalarda verilmiştir.</p> <p>Measurement results, expanded measurement uncertainty and calibration methods which are the complementary parts of this certificate, are given in the following pages.</p>	
Mühür <i>Seal</i>	Tarih <i>Date</i>
	19.08.2011
Kalibrasyonu Yapan <i>Calibrated by</i>	Laboratuvar Müdürü <i>Head of the Calibration Laboratory</i>
	
Şenay KENAR	Aynur DAVUT
<p>Bu sertifika, laboratuvarın yazılı izni olmadan kısmen veya tamamen kopyalanıp çoğaltılamaz. İmza ve mühürsüz sertifikalar geçersizdir.</p> <p>This certificate shall not be reproduced partially or fully without the permission of the laboratory. Calibration certificates without signature and seal are not valid.</p>	
ANKARA KALİBRASYON MÜDÜRLÜĞÜ ERİSNA KALİBRASYON MÜDÜRLÜĞÜ GERZE KALİBRASYON MÜDÜRLÜĞÜ	
Tel: 0 312 414 44 00 / Faks: 0 312 416 64 18 Tel: 0 312 343 90 00 / Faks: 0 312 343 82 21 Tel: 0 312 631 06 00 / Faks: 0 312 631 06 31	

Figure E. 1. Calibration certificate of the thermocouple used to measure furnace temperature.

APPENDIX F: Conversion Table of Thermocouple

TSE TSE KALİBRASYON MERKEZİ BAŞKANLIĞI
GEBZE KALİBRASYON MÜDÜRLÜĞÜ

AB-0002-K
11S0996
08.11

Sayfa (Page) 4 / 6

°C	0	1	2	3	4	5	6	7	8	9
100	0,6458	0,6531	0,6605	0,6679	0,6753	0,6827	0,6901	0,6975	0,7050	0,7124
110	0,7199	0,7274	0,7349	0,7424	0,7499	0,7574	0,7650	0,7726	0,7801	0,7877
120	0,7953	0,8030	0,8106	0,8182	0,8259	0,8336	0,8412	0,8489	0,8566	0,8644
130	0,8721	0,8798	0,8876	0,8954	0,9031	0,9109	0,9187	0,9266	0,9344	0,9422
140	0,9501	0,9579	0,9658	0,9737	0,9816	0,9895	0,9974	1,0054	1,0133	1,0213
150	1,0292	1,0372	1,0452	1,0532	1,0612	1,0692	1,0773	1,0853	1,0934	1,1014
160	1,1095	1,1176	1,1257	1,1338	1,1419	1,1500	1,1582	1,1663	1,1745	1,1826
170	1,1908	1,1990	1,2072	1,2154	1,2236	1,2318	1,2401	1,2483	1,2566	1,2648
180	1,2731	1,2814	1,2897	1,2980	1,3063	1,3146	1,3230	1,3313	1,3396	1,3480
190	1,3564	1,3647	1,3731	1,3815	1,3899	1,3983	1,4068	1,4152	1,4236	1,4321
200	1,4405	1,4490	1,4575	1,4659	1,4744	1,4829	1,4914	1,4999	1,5085	1,5170
210	1,5255	1,5341	1,5426	1,5512	1,5597	1,5683	1,5769	1,5855	1,5941	1,6027
220	1,6113	1,6200	1,6286	1,6372	1,6459	1,6545	1,6632	1,6719	1,6805	1,6892
230	1,6979	1,7066	1,7153	1,7240	1,7327	1,7415	1,7502	1,7589	1,7677	1,7764
240	1,7852	1,7940	1,8028	1,8115	1,8203	1,8291	1,8379	1,8467	1,8556	1,8644
250	1,8732	1,8820	1,8909	1,8997	1,9086	1,9175	1,9263	1,9352	1,9441	1,9530
260	1,9619	1,9708	1,9797	1,9886	1,9975	2,0064	2,0154	2,0243	2,0333	2,0422
270	2,0512	2,0601	2,0691	2,0781	2,0871	2,0960	2,1050	2,1140	2,1230	2,1321
280	2,1411	2,1501	2,1591	2,1682	2,1772	2,1862	2,1953	2,2043	2,2134	2,2225
290	2,2315	2,2406	2,2497	2,2588	2,2679	2,2770	2,2861	2,2952	2,3043	2,3134
300	2,3226	2,3317	2,3408	2,3500	2,3591	2,3683	2,3774	2,3866	2,3958	2,4049
310	2,4141	2,4233	2,4325	2,4417	2,4509	2,4601	2,4693	2,4785	2,4877	2,4969
320	2,5062	2,5154	2,5246	2,5339	2,5431	2,5524	2,5616	2,5709	2,5802	2,5894
330	2,5987	2,6080	2,6173	2,6266	2,6359	2,6452	2,6545	2,6638	2,6731	2,6824
340	2,6917	2,7010	2,7104	2,7197	2,7290	2,7384	2,7477	2,7571	2,7664	2,7758
350	2,7852	2,7945	2,8039	2,8133	2,8227	2,8321	2,8415	2,8508	2,8602	2,8696
360	2,8791	2,8885	2,8979	2,9073	2,9167	2,9262	2,9356	2,9450	2,9545	2,9639
370	2,9734	2,9828	2,9923	3,0017	3,0112	3,0207	3,0301	3,0396	3,0491	3,0586
380	3,0681	3,0775	3,0870	3,0965	3,1060	3,1155	3,1251	3,1346	3,1441	3,1536
390	3,1631	3,1727	3,1822	3,1917	3,2013	3,2108	3,2204	3,2299	3,2395	3,2490
400	3,2586	3,2682	3,2777	3,2873	3,2969	3,3065	3,3161	3,3257	3,3353	3,3448
410	3,3544	3,3640	3,3737	3,3833	3,3929	3,4025	3,4121	3,4217	3,4314	3,4410
420	3,4506	3,4603	3,4699	3,4796	3,4892	3,4989	3,5085	3,5182	3,5278	3,5375
430	3,5472	3,5568	3,5665	3,5762	3,5859	3,5956	3,6053	3,6150	3,6247	3,6344
440	3,6441	3,6538	3,6635	3,6732	3,6829	3,6926	3,7023	3,7121	3,7218	3,7315
450	3,7413	3,7510	3,7608	3,7705	3,7803	3,7900	3,7998	3,8095	3,8193	3,8291
460	3,8388	3,8486	3,8584	3,8681	3,8779	3,8877	3,8975	3,9073	3,9171	3,9269
470	3,9367	3,9465	3,9563	3,9661	3,9759	3,9857	3,9956	4,0054	4,0152	4,0250
480	4,0349	4,0447	4,0546	4,0644	4,0742	4,0841	4,0939	4,1038	4,1137	4,1235
490	4,1334	4,1432	4,1531	4,1630	4,1729	4,1827	4,1926	4,2025	4,2124	4,2223
500	4,2322	4,2421	4,2520	4,2619	4,2718	4,2817	4,2916	4,3015	4,3115	4,3214
510	4,3313	4,3412	4,3512	4,3611	4,3710	4,3810	4,3909	4,4009	4,4108	4,4208
520	4,4307	4,4407	4,4507	4,4606	4,4706	4,4806	4,4905	4,5005	4,5105	4,5205
530	4,5305	4,5405	4,5505	4,5605	4,5705	4,5805	4,5905	4,6005	4,6105	4,6205
540	4,6305	4,6405	4,6506	4,6606	4,6706	4,6806	4,6907	4,7007	4,7108	4,7208
550	4,7309	4,7409	4,7510	4,7610	4,7711	4,7811	4,7912	4,8013	4,8114	4,8214
560	4,8315	4,8416	4,8517	4,8618	4,8718	4,8819	4,8920	4,9021	4,9122	4,9223
570	4,9325	4,9426	4,9527	4,9628	4,9729	4,9830	4,9932	5,0033	5,0134	5,0236
580	5,0337	5,0439	5,0540	5,0641	5,0743	5,0845	5,0946	5,1048	5,1149	5,1251
590	5,1353	5,1454	5,1556	5,1658	5,1760	5,1862	5,1964	5,2065	5,2167	5,2269
600	5,2371	5,2473	5,2576	5,2678	5,2780	5,2882	5,2984	5,3086	5,3189	5,3291
610	5,3393	5,3496	5,3598	5,3700	5,3803	5,3905	5,4008	5,4110	5,4213	5,4315

34.01.R.001/12.04.2007-0

Figure F.1. Conversion table for changing thermocouple readout as mV to °C degree

APPENDIX G: Proceedings

73

An Urbach Study of the Degree of Structural Disorder in CdTe Nanocrystals in Glass Matrix

A.T. Ince^{1*}, M.K. Torun¹ and M.H. Yükseliç²

Abstract. CdTe nanocrystals embedded in matrices such as, glass, plastic and, aqueous solution have been investigated extensively due to their potential applications in nonlinear optical devices, biotechnology and medicine. When the size of bulk semiconductor is reduced to nanometer scales, the crystal gains new optical and electronic properties. Energy levels are quantized as in atoms and the energy difference between levels widens with the inverse of the size squared. CdTe nanocrystals were grown in glass by solid-state phase precipitation at the above glass transition temperature. A size dependent blue shift in the asymptotic absorption edge was observed in optical absorption spectra. The crystalline composition was studied by Resonant Raman spectroscopy. The width of the optical absorption tail at long wavelengths depends on the spread of electron energy levels within the structure, called the Urbach energy, which was calculated depending on size. We observe that the Urbach tail narrows as the surface to volume ratio of the nanocrystals decreases.

Key words: CdTe nanocrystals, Urbach energy, resonant Raman spectroscopy.

I. INTRODUCTION

Group II-VI semiconductor nanocrystals including CdSe_{1-x}S_x (0 ≤ x ≤ 1), ZnO, ZnS and CdTe having band gap energy ranging from 1.5 to 3.7 eV have been scrutinized for two decades due to their opto-electronic properties which can be modified by varying the average size of the ensemble of nanocrystallites [1-3]. Semiconductors, such as CdTe attracted much attention when employed in solar panels as a low cost alternative to high cost and low yield Si based solar panels [4]. The size selective absorption of light is the most important feature of semiconductor nanocrystals, which have been employed to surpass the Shockley Queisser limit of 32%. However, surface to volume ratio of a crystal increase with decreasing size which, in turn, increases crystalline disorder. In this work, the degree of disorder in nanocrystalline CdTe was calculated by studying the Urbach tail below the fundamental optical absorption edge.

II. EXPERIMENTAL

Commercially available Schott RG830 color glass filter doped with CdTe (labeled as "as-received" Sample No:1) was melted at 1050 °C for fifteen minutes to dissolve CdTe nanocrystals of average radius of around 5 nm and annealed at 400 °C for two hours to relieve stress (Sample No:2). One

sample was heat treated at 600 °C for six hours to grow nanoparticles (Sample No: 3) of smaller radii. Samples studied in this work are listed in Table 1.

Table 1. CdTe nanocrystals studied in this work

No	Thermal history	Radius
1	As-received	5* nm
2	Sample 1 melted at 1050 °C for 15 min. and then quenched and finally annealed at 400 °C for 2 h	—
3	Sample 2 annealed at 600 °C for 6 h	2* nm

* estimated by employing effective mass model in strong confinement limit from the blue shift of asymptotic absorption edge.

The optical absorption spectra are given in Fig. 1.

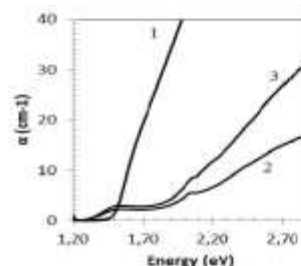


Fig. 1. Optical absorption edge spectra for as-received color glass filter doped with CdTe (1), melted (2) and heat treated (3).

Resonant Raman scattering measurements were carried out at room temperature on a Renishaw 250 mm focal length in Via Reflex Spectrometer System using a Rayleigh line rejection filter allowing Raman spectrum to be recorded up to 100 cm⁻¹ from the laser line.

The Raman spectra for the samples, listed in Table 1, are given in Fig. 2. The as-received sample contains large size nanocrystals and therefore its Raman spectrum displays clear vibrational bands. The LO₁ vibrational mode for bulk CdTe of 166.7 cm⁻¹ is blue shifted by around 24 cm⁻¹. There are three possibilities for this shift: phonon confinement, compressive strain and zinc incorporation into nanocrystals. We exclude the possibility of phonon confinement since it can only produce a red shift. The shift due to the size dependent compressive strain reported so far is 1-3 cm⁻¹[5]. Therefore we expect the observed shift is due to zinc incorporation into particles during growth. The amount of zinc (0 ≤ x ≤ 1) can be estimated by the empirical relationship,

$$\omega_{LO_1}(x) = -31.322x^2 + 72.169x + 166.73 \quad (1)$$

¹ Yeditepe University, Physics Department, Istanbul, Turkey

² Yıldız Technical University, Physics Department, Istanbul, Turkey

* aince@yeditepe.edu.tr

between the LO₁ phonon mode and zinc content [6, 7]. The LO₁ peak position of 191 cm⁻¹ corresponds to 39% zinc incorporated into CdTe nanocrystals.

The well-structured peaks disappear when the glass doped with nanocrystals was melted. The Raman peaks reappear when the sample 2 is heat treated above the glass transition temperature. This is an indication of the growth of CdTe nanocrystals.

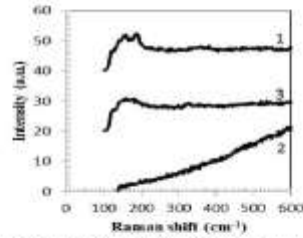


Fig. 2. Raman spectra for glass doped with CdTe samples listed in Table I. Spectra are excited at 514.5 nm with 30 mW Ar⁺ laser.

III. DISCUSSION

The width of the optical absorption tail at long wavelengths depends on the spread of electron energy levels within the structure, called the Urbach energy. The Urbach energy (E_u) is proportional to the reciprocal of the slope of the straight portion of the $\ln\alpha$ against Energy (E) curve according to,

$$\alpha = \alpha_0 e^{-(E - E_g)/E_u} \tag{2}$$

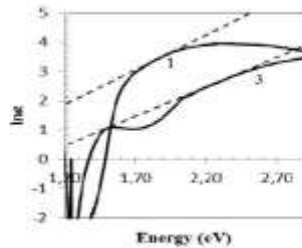


Fig. 3. $\ln\alpha$ plotted against photon energy for sample 1 and sample 3. The dashed lines are the linear fits to the straight portion of the data whose slopes give the reciprocal of Urbach energy.

where E_g is the bulk band gap energy of CdTe. The natural logarithm of Eq. (2) is plotted against energy in Fig. 3. The Urbach energy of 420 meV is calculated for as received glass, which is doped with CdTe nanocrystals of 5 nm, in radius (sample 1) and 530 meV for heat-treated glass embedded with CdTe nanocrystals of 2 nm in radius (sample 3). The Urbach energy is related to structural disorder (X) by the relationship,

$$E_u = \frac{E_p}{2\sigma_0} \left[X + \coth \left(\frac{E_p}{2k_B T} \right) \right] \tag{3}$$

where $E_p = 21$ meV is the phonon energy and $\sigma_0 = 1.19$ is a material-dependent parameter [8, 9]. At room temperature, a structural disorder of $X = 45\%$ was calculated for as-received glass, doped with CdTe nanocrystals of 5 nm in radius, and 58% for heat-treated glass doped with CdTe nanocrystals of 2 nm in radius.

IV. CONCLUSION

Optical absorption spectra for glass samples doped with CdTe nanocrystals display long tails with a defect band superimposed upon them at approximately 1.45 eV. Its origin is unknown and is presently under investigation. The Urbach energy increases from 420 meV to 530 meV, with decreasing size of CdTe nanoparticles from 5 nm to 2 nm in radius. Structural disorder increases from 45% to 58% with decreasing size.

REFERENCES

- [1] C. Flytzanis, F. Harbe, M.C. Klein and D. Ricard, in: *Optics in Complex Systems*, SPIE, Bellingham, WA, 1990.
- [2] A.J. Nozik, "Quantum dot solar cells", *Physica E*, vol. 34, pp. 115-120, 2002.
- [3] A.J. Sutherland, "Quantum dots in luminescent probes in biological systems", *Cor. Opt. Solid St. M.*, vol. 6, pp. 365-370, 2002.
- [4] P.V. Kamat, "Quantum Dot Solar Cells. Semiconductor Nanocrystals as Light Harvesters", *J. Phys. Chem. C*, vol. 112, no. 48, pp. 18737-18753, 2008.
- [5] M. Born and K. Huang, *Dynamical Theory of Crystal Lattices*, Clarendon, Oxford, 1996.
- [6] O. Madelung, U. Rössler, M. Schulz (Ed.) in: *11B: II-VI and I-VII Compounds, Semimagnetic Compounds, Cadmium telluride (CdTe) phonon dispersion, phonon frequencies and wavevectors, local modes, mean square displacements*, Landolt-Börnstein Database, Springer, Berlin, 1982.
- [7] M.H. Yekselci and Ç. Allahverdi, "Size dependent photo-induced shift of the first exciton band in CdTe quantum dots in glass prepared by a two stage heat treatment process", *J. Lumin.*, vol. 128, pp. 537-545, 2008.
- [8] A.E. Rakhshani and A.S. Al-Azab, "Characterization of CdS films prepared by chemical-bath deposition", *J. Phys.: Condens. Matter*, vol. 12, no. 40, pp. 8745-8755, 2000.
- [9] D.T.F. Marple, "Optical absorption edge in CdTe: Experimental", *Phys. Rev.*, vol. 150, no. 2, pp. 728-734, 1966.

Figure G.2. International Conference on Oxide Materials for Electronic Engineering
OMEE-2012 proceeding

APPENDIX H : Poster

YEDİTEPE UNIVERSITY
PHYSICS DEPARTMENT

The compositional dependence of the structural disorder in ZnxCd1-xTe quantum dots grown in glass studied through optical transmission and resonant Raman spectroscopies

M. K. Torun¹, A. T. Ince¹, M. H. Yükseliçi²
¹ Physics Department, Yeditepe University, Istanbul 34755, Turkey
² Physics Department, Yıldız Technical University, Istanbul 34220, Turkey

Abstract

Experimental Different size CdTe nanocrystals were grown in borosilicate glass by heat-treatment at above glass transition temperature through diffusion limited growth by solid phase precipitation. Their size were determined with the help of quantized state effective mass theory under strong confinement regime. The samples were characterized by optical absorption and Raman spectroscopies. The defect levels below band gap is discussed by Urbach method. We evaluate the effect of zinc on structural disorder.

Introduction

CdTe nanocrystals embedded in glass, plastics, aqueous solution, etc. have been investigated extensively due to their potential applications in nonlinear optical devices, biotechnology and medicine. When the size of bulk semiconductor is reduced to nanometer scales, the crystal gains new optical and electronic properties. Energy levels are quantized as in atoms and the energy difference between levels widens with the inverse of the size squared [1-8].

Experimental

In this work, different size CdTe nanocrystals were grown in borosilicate glass by heat-treatment at above glass transition temperature through diffusion limited growth by solid phase precipitation. The samples under investigation are listed in Table 1. Their size were determined with the help of quantized state effective mass theory under strong confinement regime. The samples were characterized by optical absorption and Raman spectroscopies. The vibrational phonon modes at between 140-160 cm⁻¹ in Raman spectra show that Zn precipitates into CdTe nanoparticles during growth. The blue shift in Raman lines relative to the bulk phonon mode is observed. The defect levels below band gap is discussed by Urbach method. The reciprocal of the slope of the straight line fit to the linear portion of the natural logarithm against photon energy is related to the Urbach energy which is a measure of structural disorder. We evaluate the effect of zinc on structural disorder.

Table 1 Summary of the sample properties studied.

CdTe / Glass	Temperature (°C)	Time (h)	Radius (nm)	Thickness (mm)
Sample 1	400	12	2.17	0.07
Sample 2	400	12	2.14	0.09
Sample 3	400	24	2.12	0.09
Sample 4	400	24	1.43	0.09

Results for present optical absorption spectra in Figure 1 and Line Energy graph in Figure 2.

Figure 3: Raman spectra for glass doped with CdTe samples listed in Table 1. Spectra are recorded at 514.5nm with 10 mW Ar laser. The plot shows Intensity (a.u.) vs Raman Shift (cm⁻¹). All spectra show a prominent peak at approximately 145 cm⁻¹ and a smaller peak at approximately 200 cm⁻¹. The peak at 145 cm⁻¹ shifts slightly to lower wavenumbers from Sample 1 to Sample 4.

References

- [1] A. I. Ekimov and A. A. Onushchenko, JETP Lett. 34 345 (1981)
- [2] C. Flytzanis, F. Harbe, M. C. Klein, and D. Ricard, in Optics in Complex Systems, SPIE, Bellingham, WA (1990).
- [3] R. Jain and R. C. Lin, J. Opt. Soc. Am. 73 647(1985).
- [4] A. J. Nozik, Physica E 14 115 (2002).
- [5] A. J. Sutherland, Curr. Opin. Solid State Mater. Sci. 6 365 (2002).
- [6] M. G. Bawendi, P. J. Carroll, W. L. Wilson, L. E. Brus J. Chem Phys. 96 946 (1992).
- [7] F. Hache, M. C. Klein, D. Ricard, C. Flytzanis, J Opt Soc Am B 8 1802 (1991)
- [8] O. R. Ochoa, C. Colajacomo, E. J. Witkowski, J. H. Simmons, B. G. Potter, Solid State Commun. 98 717 (1996)

Figure H.1. Nanoscience and Nanotechnology Conference Poster

APPENDIX I: Chapter

Chapter 14 Optical and Structural Properties of Quantum Dots

M.H. Yükselci, A. Aşkoğlu Bozkurt, Ç. Allahverdi, Z. Nassar,
D. Bulut, B. Can Ömür, M.K. Torun and A.T. İnce

Abstract We report (i) thickness dependent evolution of structural disorder, strain on crystalline planes and grain size in chemical bath deposited (CBD) CdS thin films studied through a combinative evaluation of the results of optical absorption, Raman spectroscopies, X-Ray diffraction (XRD) and Scanning Electron Microscopy (SEM). (ii) refer briefly to CdSe_xS_{1-x} nanocrystals in liquid and (iii) address quantum size effect in CdSe_xS_{1-x} quantum dots embedded in glass studied through steady state photoluminescence spectroscopy. The asymptotic optical absorption edge is red shifted while the long wavelength tail narrows with increasing thickness which is proportional to deposition time. We employ effective mass theory under quantum size effect to estimate average grain size from the energetic position of asymptotic optical absorption edge. The long wavelength tail optical absorption is due presumably to the micro-electric field induced by crystalline defects. The transmission probability through the potential energy barrier created by micro-electric field is calculated with the help of WKB (Wentzel, Kramers, Brillouin) approximation. We conclude that as the deposition time increases from 10 to 150 min, the average grain radius changes by 2 nm, Urbach energy and the electric micro-field decrease from 600 to 400 meV and 2240–820 kV/mm respectively. The shift in XRD pattern shows that the compressive strain decreases with growth. The Raman LO₁ vibrational mode display an increase up to 22 min of deposition time and then a decrease.

M.H. Yükselci (✉) · A. Aşkoğlu Bozkurt · Z. Nassar · B. Can Ömür
Faculty of Science and Letters, Department of Physics, Yıldız Technical University,
Davutpaşa Campus, Esenler, Davutpaşa Mah., Davutpaşa Caddesi, 34220 Istanbul, Turkey
e-mail: mhyukselci@gmail.com

Ç. Allahverdi
Electrical-Electronics Engineering Department, Faculty of Engineering,
Toros University, 45 Evler Campus/Bahçelievler Mahallesi,
16. Street, No: 1/7 Yenisehir, 33140 Mersin, Turkey

D. Bulut · M.K. Torun · A.T. İnce
Department of Physics, İnönüMah. Kayışdağı Cad., Yeditepe University, 26
AğustosYerleşimi, 34755 Ataşehir, İstanbul, Turkey

© Springer International Publishing Switzerland 2016
H. Ünlü et al. (eds.), *Low-Dimensional and Nanostructured
Materials and Devices*, NanoScience and Technology,
DOI 10.1007/978-3-319-25340-4_14

327

Figure I.1. Optical and Structural Properties of Quantum Dots Book Chapter